COMPUTER ALGORITHMS TO SIMULATE NATURE-BASED RESTORATION OF
URBAN RIVER AND STORMWATER SYSTEMS

by
Reza Abdi

A dissertation
submitted in partial fulfillment
of the requirements for the
Doctor of Philosophy Degree
State University of New York
College of Environmental Science and Forestry
Syracuse, New York
July 2019

Department of Environmental Resources Engineering

Approved by:
Theodore Endreny, Major Professor
Melissa K. Fierke, Chair, Examining Committee
Lindi Quackenbush, Department Chair
S. Scott Shannon, Dean, The Graduate School

Acknowledgments

Table of Contents

List of Tables

List of Figures

xiv

Abstract

R. Abdi. Computer Algorithms to Simulate Nature-Based Restoration of Urban River and Stormwater Systems, 190 pages, 16 tables, 42 figures, 2019 (APA style).

The United Nations is calling for the use of nature-based solutions to restore urban water resources and improve human wellbeing and biodiversity. Water quality and quantity are degraded by mismanaged urban systems where impervious cover decreases infiltration, warms runoff, and increases flooding. Riparian trees providing shade and green infrastructure devices providing infiltration can restore water quality and quantity. Management of these problems can be approached with computer algorithms to simulate and design potential solutions. This research involved development of computer algorithms to simulate nature-based restoration of urban river and stormwater systems by: 1) developing a new mechanistic model, i-Tree Cool River, as a tool for simulating how natural processes of riparian shade, stormwater infiltration, and mixing of river water and groundwater as hyporheic exchange reduce thermal pollution in an urban; and 2) developing new mechanistic algorithms of green infrastructure devices in the i-Tree Hydro model to link stormwater management with a catchment hydrology model linking atmospheric, vegetation, and subsurface transfer of water. The research first developed the river algorithms, and demonstrated how infiltration of stormwater to groundwater, rather than allowing for overland flow on warm impervious surfaces, could reduce the thermal loading. The research then developed the green infrastructure algorithms to simulate how bioretention basins, rain gardens, infiltration trenches, swales, and permeable pavement can recharge groundwater and increase subsurface flows to the catchment outlet, such as the river. The newly developed i-Tree Cool River and updated i-Tree Hydro models were designed to bring nature-based restoration designs to planners and managers involved with urban systems.

Key Terms: Urbanization, River thermal pollution, Urban stormwater reduction, Green infrastructure, Mechanistic model, i-Tree Cool River, i-Tree Hydro.

R. Abdi
Candidate for the degree of Doctor of Philosophy, June 2019
Theodore Endreny, Ph.D.
Department of Environmental Resources Engineering
State University of New York College of Environmental Science and Forestry, Syracuse, New York

1 Introduction

1.1 Overview

This dissertation research addresses urban sustainability through nature-based solutions to obtaining ecosystem benefits from the urban forest and related water and energy balances.

The first problem this research addresses, in chapters 2 and 3, is thermal pollution in urban rivers, which occurs due to properties and processes in the urban terrestrial area, such as impervious surfaces generating warm stormwater. Thermal pollution is defined as an artificially elevated temperature of the water, which adversely degrades chemical and biological indicators of water quality (Herb et al., 2008). Thermal pollution has often been associated with discharges of coolant water used by industry and in energy production by power plants, but it is also associated with land-use change, including urbanization, river impoundment, channelization, and regulation (Langan et al., 2001). Urbanization can generate thermal pollution through changes in water shading, channel geometry, groundwater input, and inflows of storm water, and wastewater (Herb et al., 2009).

River water temperature is a critical water quality parameter for riverine systems which controls the concentration of dissolved oxygen needed for aquatic ecosystems (Sand-Jensen and Pedersen 2005) and the reactions and concentrations of riverine pollutants (Ficke et al., 2007; Segura et al., 2015). Water temperature can be one of the factors limiting the potential fish habitat in a river (Bovee 1982). Changes in the river thermal regime can significantly impact fish distribution, growth, mortality, production,

1

habitat use and community dynamics (Elliott et al., 1995; Ahmadi-Nedushan et al., 2007). This is a particular concern in receiving waters which have thermally sensitive water uses (Van Buren et al., 2000). Thermal pollution from such sources can actually lower power plant efficiency, reducing its coolant benefit; it can also require power plant shutdowns when river temperatures approach environmental regulation thresholds (Miara et al., 2013).

A national regulation limiting thermal pollution is Section 316(b) of the Clean Water Act (CWA). It requires the EPA to ensure that the location, design, construction, and capacity of cooling water intake structures reflect the best technology available for minimizing adverse environmental impacts, including thermal pollution (EPA, 2014). Urban development can also be regulated for thermal pollution. The Energy Independence and Security Act (EPA, 2014) requires the restoration of storm water temperature to predevelopment conditions on all federally funded construction projects (Jones et al., 2012). This research examines how the nature-based solutions of riparian forests and subsurface inflows can restore thermal pollution problems.

The second problem this research addresses, in chapters 4 and 5, is stormwater runoff hydrology in grey infrastructure, which disrupts the natural hydrologic cycle of infiltration and evapotranspiration. The grey infrastructure associated with urbanization typically modified natural hydrology in order to reduce local flooding, and this has often resulted in degradation of physical, chemical, and biological indicators of water quality (Brilly et al., 2006; Elosegi et al., 2010; Miserendino et al., 2011; Holt et al., 2012). Stormwater is more quickly removed from urban areas by replacing natural surface and

subsurface runoff flow paths with artificial flow paths in storm sewer and road networks (Palmer et al., 2010; Waltham and Connolly 2011). Once delivered to riverine receiving waters by storm sewers, the stormwater is more quickly conveyed out of the urban area by removing natural channel vegetation, sinuosity, and active-floodplain connectivity in the river corridors and installing straightened and incised flood conveyance channels (Bledsoe and Watson 2001; Stover and Montgomery 2001; Brilly et al., 2006; Miguez et al., 2009).

Physical impacts to the riverine ecosystem of this grey infrastructure include increased thermal pollution (Perry et al., 2011), higher velocity river flows, greater scour forces on riverine features, decreased woody debris, decreased substrate roughness elements, and decreased in-channel habitat (Deng et al., 2016). Chemical impacts to the riverine ecosystem include lower dissolved oxygen in the water column, greater turbidity in the water column, and higher concentrations of dissolved pollutants (Preston et al., 2003). Biological impacts to the riverine ecosystem include decreased the presence of native aquatic species, and an increased presence of invasive and undesirable aquatic species (Violin et al., 2011; Wang et al., 2012). Individually or collectively, these impacts cause riverine waters to be considered impaired relative to their ecosystem services and target use, which includes being drinkable, swimmable, and fishable (citation Clean Water Act, EPA impaired waters). This research examines how the nature-based solutions of green infrastructure can restore these stormwater problems.

1.2 References

Abdi, R.; Yasi, M. (2015). Evaluation of environmental flow requirements using eco-hydrologic-hydraulic methods in perennial rivers. *Water Sci. Technol. 72*, 354–363.

Ahmadi-Nedushan, B., St-Hilaire, A., Quarda, T.B.M.J., Bilodeau, L., Robichaud, E., Thiemonge, N., Bobee, B. (2007). Predicting river water temperatures using stochastic models: Case study of the Moisie River (Quebec, Canada). *Hydrol. Process. 21*, 21–34.

Bovee, K.D., (1982). A guide to stream habitat analysis using the instream incremental flow methodology. *US Fish and Wildlife service*.

Brilly, M., Rusjan, S. Vidmar, A. (2006). Monitoring the impact of urbanisation on the Glinscica stream. *Physics and Chemistry of the Earth*, 31(17), 1089–1096.

Bledsoe, B.P., Watson, C.C. (2001). Effects of urbanization on channel instability. Journal of the American Water Resources Association. 37(2), 255-270.

Deng, X. et al., 2016. Spatial-temporal evolution of the distribution pattern of river systems in the plain river network region of the Taihu Basin, China. *Quaternary International*. 392, 178–186.

Elliott, J.M., Hurley, M.A. Fryer, R.J. (1995). A New, Improved Growth Model for Brown Trout, Salmo trutta. *Functional ecology*, 9(2), 290–298.

Elosegi, A., Díez, J. Mutz, M. (2010). Effects of hydromorphological integrity on biodiversity and functioning of river ecosystems. *Hydrobiologia*, 657(1), 199–215.

Ficke, A.D., Myrick, C.A., Hansen, L.J. (2007). Potential impacts of global climate change on freshwater fisheries. *Rev. Fish Biol. Fish*. 17, 581–613.

Herb, W.R., Janke, B., Mohseni, O., Stefan, H.G. (2008). Thermal pollution of streams by runoff from paved surfaces. *Hydrol. Process. 22*, 987–999.

Herb, W.R., Janke, B., Mohseni, O., Stefan, H.G. (2009). Runoff temperature model for paved surfaces. *J. Hydrol. Eng.* 14, 1146–1155.

Hester, E.T. & Bauman, K.S., 2013. Stream and Retention Pond Thermal Response to Heated Summer Runoff From Urban Impervious Surfaces. *Journal of the American Water Resources Association*, 49(2), 328–342.

Holt, A.R., Moug, P. Lerner, D.N. (2012). The network Governance of urban river corridors. *Ecology and Society*, 17(4), 25.

Jones, M.P., Hunt, W.F., Winston, R.J. (2012). Effect of Urban Catchment Composition on Runoff Temperature. *Journal of Environmental Engineering*, 138(12), 1231–1236.

Langan, S.J., Johnston, L., Donaghy, M.J., Youngson, F., Hay, D.W., Soulsby, C. (2001). Variation in river water temperatures in an upland stream over a 30-years period. Sci. Total Environ. 265, 195–207.

Miara, A., Vörösmarty, C.J., Stewart, R.J., Wollheim, W., Mand Rosenzweig, B. (2013). Riverine ecosystem services and the thermoelectric sector: strategic issues facing the Northeastern United States. *Environ. Res. Lett.* 8, 025017.

Miguez, M.G., Mascarenhas, F.C.B. (2009). Planning and Design of Urban Flood Control Measures: Assessing Effects Combination. *Journal of Urban Planning and Development.*135, 100-109.

Miserendino, M.L. et al. (2011). Assessing land-use effects on water quality, in-stream habitat, riparian ecosystems and biodiversity in Patagonian northwest streams. *Science of the Total Environment*, 409(3), 612–624.

Palmer, M.A., Menninger, H.L., Bernhardt, E.S. (2010). River Restoration, Habitat Heterogenity and Biodiversity: A Failure of Theory or Practice. *Freshwater Biology.* 55(1), 202-222.

Perry, R., Risley, J., Brewer, S., (2011). Simulating daily water temperatures of the Klamath River under dam removal and climate change scenarios. US Geological Survey Open-File Report.

Preston, C.D., et al., (2003). The long-term impact of urbanisation on aquatic plants: Cambridge and the River Cam. *Science of the Total Environment.* 316(3), 67–87.

Sand-Jensen, K. Pedersen, N.L., (2005). Differences in temperature, organic carbon and oxygen consumption among lowland streams. *Freshwater Biology*, 50(12), 1927–1937.

Stover, S.C., Montgomery, D.R. (2001). Channel change and flooding, Skokomish River, Washington. *Journal of Hydrology.* 243, 277-286.

US Environmental Protection Agency (EPA). (2010). Economic Analysis for the Final Section 316(b) Existing Facilities Rule. *US Environmental Protection Agency.*

Violin, C.R. et al., (2011). Effects of urbanization and urban stream restoration on the physical and biological structure of stream ecosystems. *Ecological Applications*, 21(6), 1932–1949.

Van Buren, M., Watt, W.E., Marsalek, J., Anderson, B.C. 2000. Thermal enhancement of stormwater runoff by paved surfaces. *Water Res. 34*, 1359–1371.

Waltham, N.L., Connolly, R.M. (2011). Global extent and distribution of artificial, residential waterways in estuaries. *Estuarine, Coastal and Shelf Science*. 94, 192-197.

Wang, B. et al., (2012). Impacts of urbanization on stream habitats and macroinvertebrate communities in the tributaries of Qiangtang River, China. *Hydrobiologia*, 680(1), 39–51.

2 A River Temperature Model to Assist Managers in Identifying Thermal Pollution Causes and Solutions

Abstract: Thermal pollution of rivers degrades water quality and ecosystem health, and cities can protect rivers by decreasing warmer impervious surface stormwater inflows and increasing cooler subsurface inflows and shading from riparian vegetation. This study develops the mechanistic i-Tree Cool River Model and tests if it can be used to identify likely causes and mitigation of thermal pollution. The model represents the impacts of external loads including solar radiation in the absence of riparian shade, multiple lateral storm sewer inflows, tributaries draining reservoirs, groundwater flow, and hyporheic exchange flow in dry weather steady flows and wet weather unsteady flows. The i-Tree Cool River Model estimates the shading effects of the riparian vegetation and other features as a function of heights and distances as well as solar geometry. The model was tested along 1500 m of a New York mountain river with a riparian forest and urban areas during 30 h with two summer storm events in 2007. The simulations were sensitive to the inflows of storm sewers, subsurface inflows, as well as riparian shading, and upstream boundary temperature inflows for steady and unsteady conditions. The model simulated hourly river temperature with an R^2 of 0.98; when shading was removed from the simulation the R^2 decreased 0.88, indicating the importance of riparian shading in river thermal modeling. When stormwater inflows were removed from the simulation, the R^2 decreased from 0.98 to 0.92, and when subsurface inflows were removed, the R^2 decreased to 0.94. The simulation of thermal loading is important to manage against pollution of rivers.

Key Terms: River thermal pollution; Mechanistic model; Urban hydrology; Riparian shading; Heat balance

2.1 Introduction

Excessive river temperatures are detrimental to water quality and ecosystem health (Herb et al., 2008). River warming can result from increased inflows of warm point and non-point source discharges, decreased inflows of cool sub-surface waters, removal of riparian shade, increased air temperatures, and changes in channel substrate and depth that increase absorption, conduction, and convection in heat transfer (Parker and Krenkel, 1969; Wunderlich, 1972; Pournasiri Poshtiri and Pal, 2016). River thermal pollution is often associated with discharges of coolant water used by industry, but it is also associated with land-use change, including urbanization, river impoundment, channel management, and regulation (Deas and Orlob, 1999; Langan et al., 2001). River temperature is a critical water quality parameter for riverine systems, that affects the saturation of dissolved oxygen (Abdi and Yasi, 2015; Sand-Jensen and Pedersen, 2005), kinetic reactions and resulting pollutant concentrations (Ficke et al., 2007; Segura et al., 2015), and fish distribution, metabolism, growth, reproduction, and mortality (Elliott et al., 1995; Ahmadi-Nedushan et al., 2007). Urbanization can elevate river temperatures through changes in riparian land cover which affects shade on the water surface, through river morphology which affects water depth, surface area, and velocity, and through flow connectivity with groundwater, stormwater, and other point and non-point source inflows (LeBlanc et al., 1997; Chen et al., 1998; Van Buren et al., 2000; Sridhar et al., 2004; Herb et al., 2009; Sun et al., 2015). When precipitation

strikes hot impervious surfaces of urban areas, this generates warmer stormwater relative to the temperature of river water (Jones et al., 2012; Hester and Bauman, 2013; Guzy et al., 2015).

River temperature management and mitigation of thermal pollution are best planned with simulation models that enable scenario evaluation, to explore relationships between river temperature response and drivers that vary in space and time (Edinger et al., 1968; Aboelnour and Engel, 2018). Caissie (2006) provides a review of research into the spatial and temporal drivers of river temperature, and the evolution of modeling approaches, including statistical models and cause-effect deterministic models, which we call mechanistic models. An illustration of field observed spatial and temporal variation is provided by Webb and Zhang, (1997) who monitored 11 reaches in south-west England, through July 1992 to February 1993, noting a correspondence between variations in hourly river temperature and variation in discharge and drainage area (180 km2 to 0.4 km2), channel surface area (17 m2 to 439 m2), depth (0.1 m to 0.5 m), slope (0.002 to 0.05), orientation (north-south to east-west), and riparian cover (pasture to dense woodland). They found drainage basin land cover, especially riparian vegetation, overwhelmed other drivers of temperature. In two separate studies of more than16 rivers in the Washington, DC area, it was determined that runoff from impervious land uses entering rivers through urban storm sewers was the major thermal stressor, causing rapid (< 3 h) surges in temperature greater than 3 °C (Herb et al., 2008; Nelson and Palmer, 2007).

A comprehensive mechanistic model developed for river managers is Heat Source (Boyd and Kasper, 2003), which allows the user to specify local climatology, hydrology, morphology, and land use into Microsoft Excel and ESRI Arc View software, to simulate spatial and temporal variation in river temperature as a function of shortwave and longwave radiation, sensible and latent heat, riverbed conduction, and inflows from tributaries, groundwater, and hyporheic exchange. Data and algorithm limitations can constrain utilization of input-intensive mechanistic models, but these limitations can sometimes be overcome with innovations. Yearsly (2009) developed a semi-Lagrangian scheme to advect river heat within a large river network when channel morphology data needed by Heat Source (Boyd and Kasper, 2003) and similar models (e.g., HSPF, CE-QUAL-W2, and QUAL2K) were not measured. To better capture abrupt changes in velocity and riparian shading, Crispell (2008) created a retention time alternative to the advection-dispersion routing algorithm used in Heat Source (Boyd and Kasper, 2003), which maintains numerical stability at very fine spatial but coarse temporal discretization. For cases when observed boundary condition data are not available, Sun et al. (2015) modified the DHSVM–RBM mechanistic model of river temperature to use Mohseni et al.'s (1998) non-linear regression between weekly air temperature and river temperature to generate the upstream river temperature time series needed as a boundary condition.

The portability and accessibility of river temperature models are significant limitations for users interested in river management, pollution mitigation and restoration scenarios. The Heat Source model provides a balance between scenario simulation

options and model parsimoniousness that made it our choice as the base code for developing a free, open-source, lower-complexity river temperature model useful in river pollution mitigation and restoration. The complexity of HSPF, CE-QUAL-W2, and QUAL2K is high, each containing many non-temperature routines, and CE-QUAL-W2 representing a 2-dimensional (2D) domain. These three models do not simulate ecological processes important in scenario analysis, including hyporheic exchange and temporal variation in the riparian shade; HSPF does have a pre-processor to provide temporal variation in riparian shade, which we use in our code development (Chen, 1998). Glose et al., (2017) noted that the major limitation of Heat Source (Boyd and Kasper, 2003) is lack of automation in making multiple simulations for parameter calibration and sensitivity analysis, given it is written in the Visual Basic for Applications language within Microsoft Excel. Glose et al., (2017) addressed this limitation by using Matlab, a well-supported scientific programming language, to create the steady state model HFLUX, which represents many of the mechanistic processes in Heat Source. The HFLUX model (Glose et al., 2017) does not include the shade factor estimation and unsteady state routing algorithms of Heat Source (Boyd and Kapser, 2003), which are important in cases of temporal variation in shading and storm flow dynamics. Unfortunately, neither Heat Source (Boyd and Kapser, 2003) nor HFLUX (Glose et al., 2017) can be compiled into an executable, and therefore cannot be deployed outside of the VBA or Matlab environment.

This study created the i-Tree Cool River Model to address limitations of the Heat Source (Boyd and Kapser, 2003) and HFLUX (Glose et al., 2017) models and advance

mechanistic model simulation of river management, pollution mitigation, and restoration scenarios in a parsimonious manner. The i-Tree Cool River Model is designed to allow for flexible shading factor algorithms, steady and unsteady flow, as well as other heat and mass transfer processes. The i-Tree Cool River Model is an open-source tool written in C++, and its package contains the routines and an executable file for running the code, which can be downloaded from http://www.itreetools.org/research_suite/coolriver. The model executable is called at the command line along with a configuration extensible markup language (XML) file, which includes the required initial information. The i-Tree Cool River Model C++ algorithms can be edited and recompiled with Visual Studio 2017 Community Edition or later, which is freeware. The simulation output includes the simulated river temperature and the heat fluxes.

The objectives of this paper are to present the theory of the i-Tree Cool River Model, to apply the model in a case study with unsteady stormwater inflows, and to evaluate the importance of the heat and mass transfer processes. To that end, following the model development, the manuscript provides a model testing to address the application of the model. The science questions are: When analyzing sources of thermal pollution, and possible mitigation scenarios, what is the relative contribution of (a) storm sewer inflows, (b) subsurface inflows of groundwater and hyporheic exchange, (c) riparian shading and weather, on the accuracy of simulated river temperature?

2.2 Methods

2.2.1 Heat Flux Formulation

The i-Tree Cool River Model simulates an advection-dispersion equation with inflows and heat fluxes following Martin and McCutcheon (1999):

$$\frac{\partial T_w}{\partial t} = -U\,\frac{\partial T_w}{\partial x} + D_L\,\frac{\partial^2 T_w}{\partial x^2} + R_h + R_i \qquad (1)$$

where T_w is the cross-sectional averaged river temperature (°C), t is time (s), U is the reach average flow velocity (m/s), x is river distance (m), D_L is the dispersion coefficient (m²/s), R_h is the heat flux reaction term, also known as heat transfer (Wunderlich, 1972; Boyd and Kasper 2003), and R_i is the reaction term of the external inflows. When R_i is combined with the advection and dispersion terms in equation (1), they are collectively referred to as mass transfer (Wunderlich, 1972; Boyd and Kasper 2003). The R_h and R_i are defined as

$$R_h = \frac{\Phi_{net}}{\rho C_p D} \qquad (2)$$

$$R_i = \frac{Q_i T_i + Q_{GW} T_{GW} + Q_{Hyp} T_{Hyp} + Q_{SS} T_{SS}}{Q_i + Q_{GW} + Q_{Hyp} + Q_{SS}} - T_{i-1} \qquad (3)$$

where Φ_{net} is the net exchange of thermal energy (W/m²), ρ is the water density (kg/m³), C_p is the specific heat capacity of water (J/kg °C), D is the average water column depth (m), Q is discharge (m³/s), T is water temperature (°C), and subscripts i is the river flow, GW is groundwater flow, Hyp is hyporheic exchange, and SS is stormwater inflow. River velocities, dispersion, and inflows are calculated using standard methods,

described in Supplementary Materials Section S1. The subsurface inflows distinguish between hyporheic and groundwater inflows due to their different environmental processes and use a separate mathematical formulation for each term. For surface inflows, users can include tributaries in place of storm sewers, and assign an unlimited number of surface inflows for each cross section.

The net exchange of thermal energy is defined as in Boyd and Kasper (2003) as

$$\Phi_{net} = \Phi_{longwave} + \Phi_{shortwave} + \Phi_{latent} + \Phi_{sensible} + \Phi_{sediment} \tag{4}$$

where the Φ is the heat flux (W/m^2), and subscripts $_{net}$ is the net heat flux at the water surface, $_{longwave}$ is the longwave radiation flux at the water surface, $_{shortwave}$ is the shortwave radiation at the water surface, $_{latent}$ is the latent heat flux from evaporation, $_{sensible}$ is the sensible heat flux representing the convective thermal flux from the water surface, and $_{sediment}$ is the bed sediment heat flux representing conduction forcing at the water column interface.

The longwave radiation flux in Equation (4) is composed of positive downward fluxes from the atmosphere and land cover over the water surface, and a negative upward flux from the waterbody to the air, following the approach of Boyd and Kasper (2003):

$$\Phi_{longwave} = \Phi_{longwave}^{atmospheric} + \Phi_{longwave}^{land\ cover} + \Phi_{longwave}^{back} \tag{5}$$

where $\Phi_{longwave}^{atmospheric}$ is the atmospheric flux (W/m^2), $\Phi_{longwave}^{land\ cover}$ is the land cover flux (W/m^2), and $\Phi_{longwave}^{back}$ is the back-to-air flux (W/m^2). Atmospheric longwave radiation is a

15

function of air temperature and exposure from the river surface to the atmosphere, called the view-to-sky factor (f), calculated using Boyd and Kasper (2003)

$$\Phi_{longwave}^{atmospheric} = 0.96\varepsilon_{atm}\sigma(T_{air} + 273.2)^4 \min(f_1, f_2, f_3)$$ (6)

where T_{air} is air temperature (°C), the ε_{atm} is the emissivity of the atmosphere (0 to 1), σ is the Stefan-Boltzmann constant (5.6696×10^{-8}, W/m^{2}K^4), and min(f_1, f_2, f_3) is the minimum of the three view-to-sky factors (0 to 1), where f_1 represents building effects, f_2 represents vegetation effects, and f_3 represents topographic effects (Figure 1). The emissivity of the atmosphere ε_{atm} is calculated using (Kustas et al., 1994)

the building shading angle, VSA is the vegetation shading angle, and TSA is the topographic shading angle. h$_{building}$, h$_{tree}$, and h$_{bank}$ are building, vegetation, and bank heights respectively. D$_{building}$, D$_{canopy}$, and D$_{bank}$ are building to the bank, canopy to the bank, and bank distances (modified from Chen et al. 1998; Sun et al. 2015).

$$\varepsilon_{atm} = 1.72(\frac{0.1e_a}{T_{air} + 273.2})^{\frac{1}{7}}(1 + 0.22C_L^2)$$ (7)

where e_a is the actual vapor pressure (mbar), and C_L is the cloudiness, which ranges from 0 for a clear sky to 1 for full cloud cover (Dingman, 1994).

The view-to-sky factors value of 1 indicates a full unobstructed sky view (Boyd and Kasper, 2003; Westhoff et al., 2007; Benyahya et al., 2010). The general sky-view-factor formula for f_i is computed for each cross-section based on Chen et al., (1998)

16

$$f_i = 1 - \frac{2}{\pi} SA_i \qquad (8)$$

where i indicates the object at that cross-section, where 1 = building, 2 = vegetation, or 3 = topography; and SA is the shade angle (radians), computed as and h_c is the combined height of the objects above the water (e.g., if a tree is set on a hill, $h_c = h_{tree} + h_{bank}$), and max (D_i) is the maximum distance from all objects at that cross-section to the edge of the water.

$$SA_i = \tan^{-1}\left(\frac{h_c}{\max(D_{i,1-3})}\right) \qquad (9)$$

The land cover longwave radiation in Equation (5) also uses the view-to-sky factors. The land cover radiation represents the land cover, e.g., vegetation such as trees' influence on water temperature, and the model by default sets land cover temperature equal to atmospheric temperature, following the approach of Boyd and Kasper (2003)

$$\Phi_{longwave}^{land\ cover} = 0.96(1 - \min(f_1, f_2, f_3))0.96\sigma(T_{air} + 273.2)^4 \qquad (10)$$

The waterbody to air radiation term in Equation (5) is a function of water temperature, representing heat flux emitted from the water surface, following the approach of Boyd and Kasper (2003)

$$\Phi_{longwave}^{back} = -0.96\sigma(T_w + 273.2)^4 \qquad (11)$$

where the T_W is the river temperature (°C).

17

See the Supplementary Materials, Section S2 for the methods used to find the remaining right-hand side terms in Equation (4), which are short wave radiation, latent heat flux, sensible heat flux, and bed sediment heat flux. Table S1 and Table S2 lists the 10 input files required by i-Tree Cool River, and names and describes the parameters in each of the files.

2.2.2 Study Area and Model Inputs

The i-Tree Cool River Model's accuracy in representing thermal loading was tested in unsteady state (i.e., wet weather) using unpublished data from 11 to 12 June 2007 for a 1500 m reach of Sawmill Creek, in Tannersville, New York (42.1955 N, 74.1339 W, WGS84). Sawmill Creek is a second-order mountainous river with varying watershed land use, starting in forests and transitioning to urban land. At the end of the Sawmill Creek study reach, the time of travel was approximately 30 min and the upstream watershed area is 8.16 km2, which includes a nested urban watershed of 1.8 km2 draining to the river in storm sewers (Figure 2a,b). Sawmill Creek flow at the upstream boundary was estimated using stage-discharge relations, monitoring stage with pressure transducers (manufactured by Global Water Instruments) at the upstream and downstream stations (0 m and 1500 m respectively) and in storm sewers. Stage was converted to discharge using the Manning equation, with stage converted to channel area and hydraulic radius using geometry relations, and the Manning roughness coefficients estimated from pebble counts Wolman (1954) at each cross section by Crispell (2008). We installed compound weir plates in the sewers and used the weir plate manufacturer equations to convert stage to discharge for the storm sewer

inflows. Observed storm flows were corroborated with simulated flows by the i-Tree Hydro model (Yang, et al. 2011), calibrated to match the estimated baseflow.

Rainfall occurred twice during 12 June 2007 the first time with a 2 h duration totaling 3.3 mm and the second time with a 3 h duration totaling 8.4 mm. The storm sewer inflows were active during dry and wet weather, in dry weather due to illicit connections draining buildings, and in wet weather due to storm runoff. Crispell (2008) monitored river temperatures and storm sewer drainage temperatures at 12 river stations in the Sawmill Creek reach and the two inflow locations at 10-minute intervals using ibutton temperature data loggers, which were used to set boundary conditions. The temperature monitoring ibuttons in Sawmill Creek reach were strategically placed and considered representative of the reach temperature, capturing the influence of stormwater inflows after they had distance to mix with the channel water (Crispell, 2008). In the upstream section of the reach, between the cross section at station 0 m and a station at 600 m, the observed average river temperature increased by 0.03 °C per 100 m (3.3%), and between the cross section at station 900 m and a station 1500 m, temperature increased by 0.008 °C per 100 m (1%). In the middle section of the reach, between the cross section at station 600 m and station 900 m, the temperature increased by 0.1 °C per 100 m, three times the rate of the upstream reach, an increase attributed to the warming effect of the Tannersville's storm sewer inflow (Table S3).

The i-Tree Cool River was also tested in steady state mode, e.g., no rainfall events, for a 475 m reach of Meadowbrook Creek (43.0306 N, 76.0680 W, WGS84), a first order and urbanized river in the city of Syracuse, New York (Figure 3a,b). Flow at

the upstream boundary, cross section survey data, and river temperature at 30

monitoring locations at 5-minute intervals were provided by Glose et al. (2017), who

used these data to develop HFlux. We simulated the 5-day period of 13–19 June 2012.

The i-Tree Cool River Model simulated Sawmill Creek using input data from

multiple sources. Specification of hourly weather data, including air temperature T¬air,

dew point temperature Tdew, shortwave radiation Sin, fraction cloudiness C, and wind

speed Uwind were obtained from the National Solar Radiation Data Base (NSRDB)

station ID#1227776, located 23 km from the study site. The NSRDB provides satellite

estimated surface radiation at 30 min intervals. The shading factor, SF, in Equation (S2)

and view-to-sky coefficients, f in equation (S4) were estimated at 1 m intervals along

Sawmill Creek using the TTools algorithm from observations of riparian vegetation and

aerial images of the study area (Crispell, 2008). The river base width and bank slope

were obtained from field surveys at each cross section (Crispell, 2008), which defined

the irregular pattern of river widening and narrowing. The simulated Sawmill Creek

reach was delineated into 15 segments considering the locations where the temperature

was observed, with segment lengths no greater than 100 m, which resulted in a

simulation timestep of 0.5 seconds to satisfy the i-Tree Cool River Model stability

criteria. The simulations represented the observed conditions, as well as alternative

scenarios to determine model sensitivity to shading, subsurface inflow, and the

calculated upstream boundary condition, which are sometimes difficult to obtain. Our

calculated upstream boundary condition was derived with Mohseni et al., (1998)

Equation (122), a non-linear regression between air temperature and river temperature.

$$T_w = \mu + \frac{\alpha - \mu}{1 + e^{\gamma(\beta - T_{air})}}.$$ (12)

In the equation, the coefficient α is the estimated maximum stream temperature, γ is a measure of the steepest slope of the function, and β represents the air temperature at the inflection point.

Our observed upstream boundary condition was obtained from ibutton thermistor measurements. We analyzed the simulated and observed river temperatures for each of the cross sections averaged with respect to time to obtain a 30-hour average at each of the 12 cross sections. Simulations were written hourly for each cross sections, which can be written at any timesteps for each meter of the river. We ran this simulation using Equations (5) to (11) for longwave radiation, Equation (S2) for shortwave radiation, Equation (S11) for latent heat, Equation (S12) for sensible heat, and Equation (S15) for the sediment heat.

2.3   Results

2.3.1   Model Evaluation

A scatterplot of the 30-hours of simulated and observed river temperatures for each of the 12 cross sections along the 1500 m of Sawmill Creek reach provides insights on the relative goodness of fit for each cross section and associated drivers of i-Tree Cool River Model accuracy (Figure 4). At cross section 1, along the upstream boundary, as expected, the observed boundary condition, resulted in a model fit with an R^2 of 1.0. Downstream, the fit degraded. Initial conditions of 14.7 °C for all cross sections caused the largest deviations between simulated and observed temperatures

for most scatterplots. The model underestimated observed temperatures at cross sections 4 to 12 by approximately 1 °C, while upstream cross section temperatures were cooler and closer to the initial condition. The falling limb of storm event hydrograph corresponded with deviations in simulations at 22:00 hours of day 1 and 02:00 h of day 2 for cross sections 9 to 12, overestimating temperatures by approximately 0.3 °C and 0.5 °C, respectively.

The i-Tree Cool River model simulated hourly water temperatures were not significantly different than the observed, for reach averaged data, based on the p-values calculated using a paired-samples t-test and the α = 0.05 (See Table S3 for more details). The 30-hour average simulated and observed river temperature, along the entire 1500 m Sawmill Creek reach, increased by 0.4 °C at a slope of approximately 0.02 °C per 100 m, but with longitudinal variation in that slope. For the 1500 m reach, the model had a root-mean-square error (RMSE) of 0.03 °C and a coefficient of determination (R^2) of 0.98 with a p-value of 0.87 which was greater than the α of 0.05. The model simulated the relatively rapid increase in water temperature recorded by the sensors, between cross section 600 m and 900 m, corresponding to the reach with storm sewer inflow. This relatively rapid increase in temperature leveled at station 900 m, which is the first station downstream of the last storm sewer outfall. Relatively warm water in the Tannersville storm sewer entering Sawmill Creek between cross sections at station 600 m and at station 900 m was a major driver of the i-Tree Cool River Model forecasting a rise in river temperature during both wet and dry weather conditions (Figure S1a). During the wet weather, a total of 7 hours, the rate that simulated river

temperature increased from station 600 m to station 900 m at a rate of 0.32 °C per 100 m (Figure S1b), much steeper than during dry weather. During dry weather, the simulated river temperature from station 600 m to station 900 m increased at a rate of 0.04 °C per 100 m (Figure S1c), approximately 12% of the wet weather slope. The i-Tree Cool River algorithms for shading, net groundwater discharge, hyporheic exchange, and upstream boundary condition temperature influenced the simulation of longitudinal river temperature and the model goodness of fit. In all of the scenarios, the calculated paired t-test p-values were smaller than the $\alpha = 0.05$, rejecting the null hypothesis, H_0 of a significant difference between the means of the simulated and observed reach averaged river temperatures (See Table S5 for more details). When the shading algorithm was disabled, i.e., no shade was simulated, the i-Tree Cool River Model overestimated the river temperature for all cross sections by 0.34 °C, at a rate of 0.02 °C per 100 m, for the 30-hour period, 11 to 12 June 2007 (Figure S2), and the model RMSE increased to 0.36 °C and the R^2 decreased to 0.88.

Diurnal sinusoidal patterns of simulated and observed river warming and cooling were driven by the heat balance but disrupted by abrupt pulses of inflow due to warm runoff during the two storm events on 11 and 12 June 2007. The Sawmill Creek mean temperature, the average of measurements at the 12 cross sections, diurnally peaked at 15.8 °C by 15:00 h June 11, 2007 (Figure 5a), two hours after the peak in shortwave radiation (Figure 5b). By 20:00 hours, shortwave radiation has declined to 0, net radiation became negative, and river temperature has decreased from the peak of 15.8 °C to 15.1 °C. A storm event at 21:00 h 11 June 2007, and then again at 01:00 h of 12

June 2007, generates inflow of warmer water from the upstream and storm sewer, creating a temporary increase in temperature, which disrupts the sinusoidal pattern in cooling toward the diurnal minimum temperature at 05:00 h of 12 June 2007. Dry weather extends through the remainder of the simulation, and at 06:00 h of 12 June 2007, the increasing shortwave and thus net radiation reestablish heat flux as the main driver of the increasing river temperature, which peaks at 16.4 °C at 14:00 h. There was no significant difference between the simulated and observed time averaged river temperature datasets based on the paired-samples t-test and $\alpha = 0.05$ (See Table S6 for more details). The model simulations of the abrupt pulses in river temperature during the wet weather, extending from hour 20 of day 1 to hour 3 of day 2, had a Nash-Sutcliffe Efficiency (NSE) coefficient of 0.9 and a p-value of 0.80 (Figure 5a). The magnitude of the simulated river temperature changes due to the inflow of stormwater from the Tannersville storm sewer system was 0.3 °C during the first storm and 0.4 °C during the second storm. The model simulations had their poorest fit with observed river temperatures during a 6 h period on 12 June 2007, between 03:00 and 09:00 h, centered at sunrise, when it overestimated the river temperature by an average of 0.13 °C.

The river temperature simulated by the i-Tree Cool River Model was a function of spatially and temporally varying contributions of groundwater, hyporheic exchange, and storm sewer inflow. Analysis of these components to thermal loading can assist in developing pollution mitigation or river restoration scenarios. In cross sections without storm sewer inflow and in the absence of rain events, the river temperature was

24

predominantly determined by river flow from the upstream reach, and groundwater only contributed approximately 1%, while hyporheic exchange contributed approximately 10% (Figure 6a; 350 m, and 1100 m). In cross sections with storm sewers, even in the absence of rain events, when the storm sewers discharged flow from illicit connections, they contributed approximately 25% of the flow influencing the cross section river temperature (Figure 6a; 800 m), which warmed the river water (see Table S4 reflecting warmer average temperature of the storm sewer in the dry weather). During wet weather, there was inflow from the storm sewer due to the flows from impervious areas, and this inflow contributed approximately 50% of the flow thereby influencing the river temperature (Figure 6b, 800 m) and provided the thermal load to the river system. Integrated along the 1500 m of Sawmill Creek reach, the contribution of groundwater summed to 15% of the total river volume, while the hyporheic exchange, which flows in and out within each sub-reach associated with a cross section, averaged approximately 10% of inflow in each sub-reach.

In addition to the analysis of unsteady simulations in Sawmill Creek, the i-Tree Cool River Model performance was analyzed for the steady state condition in Meadowbrook Creek for 13–19 June 2012. The i-Tree Cool River Model simulated the time averaged river temperatures at 30 cross sections with an RMSE of 0.2 °C. We combined these 30 cross sections into reach averaged river temperature data to examine the diurnal pattern driven by the heat balance (Figure 7a). There was no significant difference between the simulated and observed reach averaged river temperatures based on a paired-samples t-test and α = 0.05 (See Table S6 for more

25

details). The model simulations of the temperature for steady state in the Meadowbrook

Creek study reach for 13–19 June 2012 had a NSE coefficient of 0.9 and a p-value of

0.72. The model captures how Meadowbrook Creek cools by 0.25 °C as it flows along

the 475 m reach (Figure 7b), driven by the constant inflow of cooler groundwater.

2.3.2 Sensitivity Analysis

A sensitivity analysis of the i-Tree Cool River Model examined the fluctuation in

simulated temperature with changes in input data to identify the most sensitive

parameters, which is useful when considering impacts of environmental change. The

sensitivity analysis was performed for steady and unsteady simulations. We used global

sensitivity analysis to identify the most important parameters and coordinated this

analysis with that for the Meadowbrook Creek reach in summertime, by Glose et al.

[31], noting both models are based on Heat Source [27]. Glose et al. [31] used an

observed boundary conditions and our Equations (1), (2), (4), (5), (6), (10), (11), (S2),

(S11), and (S12), and varied discharge by ±10%, groundwater temperature ±15%,

varied shading factor and view-to-sky factor by ±20%. They identified groundwater as

the most sensitive parameter, with a ±0.2 °C change on average stream temperature.

We replicated this sensitivity analysis to the 1500 m Sawmill Creek reach, confirming

these sensitivities. We then extended the analysis in the 1500 m Sawmill Creek reach to

consider varying parameters of storm sewer temperature, sediment temperature, and

recorded boundary conditions temperature by ±15% (Figure S3) and varying

parameters of substrate hydraulic conductivity (SHC), cloudiness factor (Cl), and

groundwater discharge (GW) by ±20% (Figure S4). When storm sewer temperature was

varied by ±15%, the reach-averaged temperature changed by 1.65% (0.27 °C). When

sediment temperature was varied by ±15%, the reach-averaged temperature changed

by 0.3%. When upstream boundary conditions temperature was varied by ±15%, the

reach-averaged temperature changed by 9.5%. When substrate hydraulic conductivity

was varied by ±20%, the reach-averaged temperature changed by 0.15%. When

cloudiness factor was varied by ±20%, the reach-averaged temperature changes by

0.02%. When groundwater discharge factor was varied by ±20%, the reach-averaged

temperature changes by 0.03% (Table S7). Based on this analysis, the most sensitive

model parameters, ranked in order of importance, are upstream boundary conditions,

storm sewer temperature, sediment temperature, substrate hydraulic conductivity,

groundwater discharge, and cloudiness (additional sensitivity analysis is presented in

supplementary materials Figures S3–S6).

2.4   Discussion

The i-Tree Cool River Model simulated the warming effects of the many potential

sources of thermal pollution, including radiation fluxes and urban runoff, both dry

weather illicit connections and wet weather stormwater. The model also shows how

groundwater and hyporheic exchange inflows can provide a cooling effect, providing a

comprehensive approach to assessing and perhaps mitigating thermal loading. To

determine which factors are most effective in such management, this discussion

provides some perspective on the effects of each warming and cooling effect.

The impact of urban runoff on the average temperature was rapid, within 1 hour

of the onset of precipitation, and caused a temperature increase of 0.3 °C for the first

storm, and 0.4 °C for the second storm of 12 June 2007. The rapid and large change in river temperature can be attributed to the short duration event, which Herb et al. (2008) suggest when rainfalls only last 2 to 3 h will make the largest impact on raising stormwater and water temperature. The urban storm sewer area was approximately 21% of the watershed drainage area and had 35% impervious cover, which contributed to a relatively large volume of flashy, warm, stormwater response. Relative differences between air and water temperatures contribute to the warming, as noted by Herb et al., (2008); for the Sawmill Creek reach the average air temperature was 21.2 °C and average dew point temperature was 18.0 °C, both warmer than the average river temperature which was 15.2 °C. Even though the two rainfall events occurred at night during 12 June 2007, when solar radiation was not present, the prior day averaged 20% cloud coverage, allowing 80% of summer shortwave radiation to reach the small albedo impervious surface.

Simulation of the effects of the nighttime stormwater thermal load in riverine receiving waters on Sawmill Creek contributes additional data and tools to the investigation and management of the urban heat island. A common signature of the urban heat island is elevated nighttime air temperatures in urban areas relative to rural areas, due to physical differences affecting solar heating, such as albedo and thermal capacity, and anthropogenic heat sources (Memon et al., 2011). Daytime insulation is a common driver of thermal loading of receiving waters (Hathaway et al., 2016), but for 12 June in Tannersville, the daytime solar heating of impervious area did not cause thermal loading of the river until the nighttime wet weather event. The nighttime

precipitation landed on warm impervious surfaces, retaining much of their daytime

elevated surface temperatures due to high capacitance, and this surface warmth was

conducted into the stormwater entering the relatively cool, rural origin, receiving water.

The effect of urban heat islands on rivers was studied by Somers et al., (2013), who

noted a 1.6 °C higher warm season temperature in urban rivers than forested rivers,

and 8 °C greater spatial variation in urban rivers than in rural river temperatures along a

1 km transect. During a daytime storm event affecting all rivers, the temperatures in

urban rivers rose as much as 4 °C, compared with a negligible rise in temperature in the

forested rivers (Somers et al., 2013). Nelson and Palmer (2007) forecasted the thermal

impact of individual storm events and found storm-induced river temperature surged by

3.5 °C for the warm season in urban watersheds near Washington, DC, USA; with

drainage areas averaging 8 km^2.

Proper simulation with the i-Tree Cool River Model of unsteady flows and their

thermal pollution of receiving waters requires consideration of model goals and

limitations. Typical model goals are either model inter-comparison for contrasting

scenarios, such as varying impervious or tree cover, or model simulation for hindcasting

or forecasting. In cases of model inter-comparison, the model has fewer limitations and

the model physics will allow users to consider changes in river temperature for changes

in study site conditions; model simulation has accuracy constrained by the accuracy of

inputs as well as a model epistemic error (Beven, 2013; Glose et al., 2017). This project

attempted to improve accuracy of model simulations in Sawmill Creek by obtaining

accurate data of the storm volumes and temperatures entering at the upstream and

storm sewer locations along the boundary, using ibutton sensors, which are widely used for river temperature monitoring (Crispell and Endreny, 2009; Hester et al., 2009; Glose et al., 2017). In cases where point or diffuse sources enter at multiple, unspecified locations along the river channel, such as with groundwater seeps, ibuttons may be inefficient and a better monitoring approach may involve using distributed temperature sensing system (Sand-Jensen and Pedersen, 2005; Westhoff et al., 2007) for high-frequency time series, or from forward-looking infrared radar (Loheide and Gorelick, 2006) temporally coarser data. An alternative to monitoring storm sewer inflow temperatures is estimating those temperatures using models of impervious runoff (Herb et al., 2009; Kim et al., 2008), and upstream boundary conditions can be estimated using air temperature records with the Mohseni et al., (1998) non-linear regression.

Groundwater and hyporheic exchange were significant factors of temperature regulation during wet and dry weather. The section of Sawmill Creek simulated by the i-Tree Cool River Model had groundwater flow rates of approximately 0.0024 m^3/s per 100 m, or 1% of flow, and riverbed longitudinal slopes that generated 10% contributions of hyporheic exchange (Figure 6). This combined subsurface flow, through the model inflow routines, contributed a cooling effect for the simulated summer period in 11–12 June 2007. Removing these inflows from the simulation caused the model to achieve RMSE of 0.18 °C and R^2 of 0.94, less important than the cooling through shading and the heat flux routines, when removed generated a RMSE of 0.36 °C and R^2 of 0.88. In winter, when river temperature is typically below subsurface water temperatures, this inflow would likely contribute a warming effect, as observed in other rivers by Risley et

al., (2010) and Kurylyk et al., (2016). From a survey of other studies, the relative contribution of groundwater and hyporheic exchange inflow with river water varies by site conditions and time. Poole and Berman, (2001) working in mountain rivers, with bed slopes above 2%, also found the surface water received a larger volumetric inflow from hyporheic exchange than from groundwater, while Glose et al., (2017) working in valleys with approximately 1% slopes did not identify significant hyporheic exchange and set groundwater as the only subsurface source of inflow.

Riparian shading from tree canopy, hillslope, and buildings provided the only land-based reduction in shortwave radiation and the view to the sky for the river, which influenced the longwave radiation. We used model inter-comparison simulations to contrast a scenario with and without shading and determined shading cooled river temperatures by an average of 0.34 °C during the 30 hours period. The landscape contribution to shading varied longitudinally along the reach, and at cross-section 9 was primarily from building shade, while upstream at cross sections 1 to 5 was primarily forest; hillslope topography provided minimal shading at this site. Shading is a concern in river thermal loading, and shallow and slow moving water is more vulnerable to such warming, and others have modeled this effect. Sun et al. (2015) simulated 6 years along 6 separate reaches ranging in length from 85 to 1185 m of Mercer Creek in Washington State, and determined that tree and hillslope shading reduced the annual maximum temperatures by 4 °C. Roth et al. (2010) simulated three cloud-free summer days in August 2007 along a 1260 m section of the Boiron de Morges River in southwest Switzerland, and determined riparian shading, by decreasing shortwave radiation,

decreased daily average water temperatures by 0.7 °C. Guoyuan et al. (2012) demonstrated predictions of shade from riparian vegetation (e.g., the Chen et al. (1998) method used in i-Tree Cool River) were sensitive to the interaction of river azimuth and latitude, with E-W rivers in low latitudes benefiting least from riparian shade. Lee et al. (2012) recommended for effective reduction in shortwave radiation, riparian areas utilize shading angles of 70° (1.22 radian) and view-to-sky factors smaller than or equal to 0.22. In the 1500 m Sawmill Creek reach, less than 10% of the view-to-sky factors were smaller or equal to 0.22 and shading angles averaged 50°, and therefore additional thermal management opportunities are present.

The i-Tree Cool River Model was designed to assist river managers assess mechanistic causes of thermal pollution using free, open source, relatively simple algorithms in order to negotiate the balance between complexity and accuracy. While the model requires several input files, many of these can be obtained from publicly available data, site surveys, or estimation approaches; for model inter-comparison studies the accuracy of input data become less critical than in forecast simulations. The number of input files required by the model is comparable to other mechanistic models simulating river temperature, such as HFlux, HSPF, and QUAL2K, which require approximately 25 to 40 parameters, spatial data of river geometry and riparian features, and time series data describing the weather and discharge. Obtaining these inputs is a potential limitation of the i-Tree Cool River Model, and methods to obtain or estimate these input files are discussed above.

2.5 Conclusions

In this study, we developed the one-dimensional mechanistic i-Tree Cool River Model to simulate river temperature considering a combination of advection, dispersion, heat flux, and inflow processes. The i-Tree Cool River Model has the ability to analyze the impacts of external loads including multiple lateral storm sewer inflows, groundwater flow, and hyporheic exchange flow in steady and unsteady flows. The i-Tree Cool River Model estimates the shading effects of the riparian vegetation and other features as a function of heights and distances as well as solar geometry. The model performance was tested in steady and unsteady modes for the Meadowbrook reach in Syracuse, New York and Sawmill Creek in Tannersville, New York, respectively. The i-Tree Cool River Model performed satisfactorily in both simulations. The model can be used to conduct thermal pollution analysis of urban areas and investigate land cover and hydrology-based mitigation methods. The simulated river temperature of the i-Tree Cool River Model can be used for other environmental models, such as urban development models, atmospheric models, climate change models, and hydrology models.

2.6 Acknowledgments

2.7 References

Abdi, R., Yasi, M. (2015). Evaluation of environmental flow requirements using eco-hydrologic-hydraulic methods in perennial rivers. *Water Sci. Technol. 72*, 354–363.

Aboelnour, M., Engel, B.A. (2018). Application of remote sensing techniques and geographic information systems to analyze land surface temperature in response to land use/land cover change in greater Cairo region, Egypt. *J. Geogr. Inf. Syst. 10*, 57–88.

Ahmadi-Nedushan, B., St-Hilaire, A., Quarda, T.B.M.J., Bilodeau, L., Robichaud, E., Thiemonge, N., Bobee, B. (2007). Predicting river water temperatures using stochastic models: Case study of the Moisie River (Quebec, Canada). *Hydrol. Process. 21*, 21–34.

Benyahya, L., Caissie, D., El-jabi, N., Satish, M.G. (2010). Comparison of microclimate vs. remote meteorological data and results applied to a water temperature model (Miramichi River, Canada). *J. Hydrol. 380*, 247–259.

Beven, K. (2013). So how much of your error is epistemic? Lessons from Japan and Italy. *Hydrol. Process. 27*, 1677–1680.

Boyd, M., Kasper, B. (2003). Analytical Methods for Dynamic Open Channel Heat and Mass Transfer: Methodology for Heat Source Model Version 7.0.

Caissie, D. (2006). The thermal regime of rivers: A review. *Freshw. Biol. 51*, 1389–1406.

Caissie, D., Kurylyk, B.L., St-Hilaire, A., El-Jabi, N., MacQuarrie, K.T.B. (2014). Streambed temperature dynamics and corresponding heat fluxes in small streams experiencing seasonal ice cover. *J. Hydrol. 519*, 1441–1452.

Caissie, D., Satish, M.G., El-Jabi, N. (2007). Predicting water temperatures using a deterministic model: Application on Miramichi River catchments (New Brunswick, Canada). *J. Hydrol. 336*, 303–315.

Chen, Y.D., Carsel, R.F., McCutcheon, S.C., Nutter, W.L. (1998). Stream temperature simulation of forested riparian areas: I. Watershed-Scale model development. *J. Environ. Eng. 124*, 304–315.

Crispell, J.K. (2008). Hyporheic Exchange Flow around Stream Restoration Structures and the Effect of Hyporheic Exchange Flow on Stream Temperature. Master' Thesis, College of Environmental Science and Forestry, State University of New York, New York, NY, USA, 63p.

Crispell, J.K., Endreny, T.A. (2009). Hyporheic exchange flow around constructed in-channel structures and implications for restoration design. *Hydrol. Process. 23*, 2267–2274.

DeWalle, D.R. (2010). Modeling stream shade: Riparian buffer height and density as important as buffer width. *J. Am. Water Resour. Assoc. 46*, 323–333.

Dingman, S.L. (1994). *Physical Hydrology*; Prentice-Hall Inc.: Upper Saddle River, NJ, USA.

Deas, M.L., Orlob, G.T. (1999). *Klamath River Modeling Project and Appendices*; University of California: Davis, CA, USA, 376p.

Domenico, P.A., Scwartz, F.W. (1990). *Physical and Chemical Hydrogeology*; John
Wiley and Sons, Inc.: New York, NY, USA.

Edinger, J.E., Duttweil, D., Geyer, J.C. (1968). Response of water temperatures to
meteorological conditions. *Water Resour. Res. 4*, 1137–1143.

Elliott, J.M., Hurley, M.A., Fryer, R.J. (1995). A new, improved growth model for brown
trout, Salmo trutta. *Funct. Ecol. 9*, 290–298.

Ficke, A.D., Myrick, C.A., Hansen, L.J. (2007). Potential impacts of global climate
change on freshwater fisheries. *Rev. Fish Biol. Fish. 17*, 581–613.

Glose, A., Lautz, L.K., Baker, E.A. (2017). Stream heat budget modeling with HFLUX:
Model development, evaluation, and applications across contrasting sites and
seasons. *Environ. Model. Softw. 92*, 213–228.

Guoyuan, L., Jackson, C., Kraseski, K. (2012). Modeled riparian stream shading:
Agreement with field measurements and sensitivity to riparian conditions. *J. Hydrol.
428*, 142–151.

Guzy, M., Richardson, K., Lambrinos, J.G. (2015). A tool for assisting municipalities in
developing riparian shade inventories. *Urban For. Urban Green. 14*, 345–353.

Hathaway, J.M., Winston, R.J., Brown, R.A., Hunt, W.F., McCarthy, D.T. (2016).
Temperature dynamics of stormwater runoff in Australia and the USA. *Sci. Total
Environ. 559*, 141–150.

Herb, W.R., Janke, B., Mohseni, O., Stefan, H.G. (2008). Thermal pollution of streams by runoff from paved surfaces. *Hydrol. Process. 22*, 987–999.

Herb, W.R., Janke, B., Mohseni, O., Stefan, H.G. (2009). Runoff temperature model for paved surfaces. *J. Hydrol. Eng. 14*, 1146–1155.

Hester, E.T., Bauman, K.S. (2013). Stream and retention pond thermal response to heated summer Runoff from urban impervious surfaces. *J. Am. Water Resour. Assoc. 49*, 328–342.

Hester, E.T., Doyle, M.W., Poole, G.C. (2009). The influence of in-stream structures on summer water temperatures via induced hyporheic exchange. *Limnol. Oceanogr. 54*, 355–367.

Jones, M.P., Hunt, W.F., Winston, R.J. (2012). Effect of urban catchment composition on runoff temperature. *J. Environ. Eng. 138*, 1231–1236.

Kim, K., Thompson, A.M., Botter, G. (2008). Modeling of thermal runoff response from an asphalt-paved plot in the framework of the mass response functions. *Water Resour. Res. 44*, W11405.

Kurylyk, B.L., Moore, R.D., Macquarrie, K.T.B. (2016). Scientific briefing: Quantifying streambed heat advection associated with groundwater-surface water interactions. *Hydrol. Process. 30*, 987–992.

Kustas, W.P., Rango, A., Uijlenhoet, R. (1994). A simple energy budget algorithm for the snowmelt runoff model. *Water Resour. Res. 30*, 1515–1527.

Langan, S.J., Johnston, L., Donaghy, M.J., Youngson, F., Hay, D.W., Soulsby, C. (2001). Variation in river water temperatures in an upland stream over a 30-years period. *Sci. Total Environ. 265*, 195–207.

Leach, J.A., Moore, R.D. (2014). Winter stream temperature in the rain-on-snow zone of the Pacific Northwest: Influences of hillslope runoff and transient snow cover. *Hydrol. Earth Syst. Sci. 18*, 819–838.

LeBlanc, R.T., Brown, R.D., FitzGibbon, J.E. (1997). Modeling the effects of land use change on the water temperature in unregulated urban streams. *Environ. Manag. 49*, 445–469.

Lee, T.Y., Huang, J.C., Kao, S.J., Liao, L.Y., Tzeng, C.S., Yang, C.H., Kalita, P.K., Tung, C.P. (2012). Modeling the effects of riparian planting strategies on stream temperature: Increasing suitable habitat for endangered Formosan Landlocked Salmon in Shei-Pa National Park, Taiwan. *Hydrol. Process. 26*, 3635–3644.

Loheide, S.P., Gorelick, S.M. (2006). Quantifying stream−Aquifer interactions through the analysis of remotely sensed thermographic profiles and in situ temperature histories. *Environ. Sci. Technol. 40*, 3336–3341.

Long, D.L., Dymond, R.L. (2014). Thermal pollution mitigation in cold water stream watersheds using bioretention. *J. Am. Water Resour. Assoc. 50*, 977–987.

Martin, J.L., McCutcheon, S.C. (1999). *Hydrodynamics and Transport for Water Quality Modeling*; Lewis Publishers: New York, NY, USA.

Memon, R.A., Leung, D.Y.C., Liu, C.H., Leung, M.K.H. (2011). Urban heat island and its effect on the cooling and heating demands in urban and suburban areas of Hong Kong. *Theor. Appl. Climatol. 103*, 441–450.

Mohseni, O., Stefan, H.G., Erickson, T.R. (1998). A nonlinear regression model for weekly stream temperatures. *Water Resour. Res. 34*, 2685–2692.

Nash, J.E., Sutcliffe, J.V. (1970). River flow forecasting through conceptual models part I—A discussion of principles. *J. Hydrol. 10*, 282–290.

Nelson, K., Palmer, M.A. (2007). Stream temperature surges under urbanization and climate change: Data, models, and responses. *J. Am. Water Resour. Assoc. 43*, 440–452.

Ouellet, V., Secretan, Y., St-hilaire, A., Morin, J. (2014). Water temperature modelling in a controlled environment: Comparative study of heat budget equations. *Hydrol. Process. 28*, 279–292.

Parker, F.L., Krenkel, P.A. (1969). *Thermal Pollution: Status of the Art*; Report 3; Department of Environmental and Resource Engineering, Vanderbilt University: Nashville, TN, USA.

Poole, G.C., Berman, C.H. (2001). An ecological perspective on in-stream temperature: Natural heat dynamics and mechanisms of human-caused thermal degradation. *Environ. Manag. 27*, 787–802.

Pournasiri Poshtiri, M., Pal., I. (2016). Patterns of hydrological drought indicators in

    major U.S. River basins. *Clim. Chang. 134*, 549–563.

Risley, J.C., Constantz, J., Essaid, H., Rounds, S. (2010). Effects of upstream dams

    versus groundwater pumping on stream temperature under varying climate

    conditions. *Water Resour. Res. 46*, W06517.

Roth, T.R., Westhoff, M.C., Huwald, H., Huff, J.A., Rubin, J.F., Barrenetxea, G., Vetterli,

    M., Parriaux, A., Selker, S., Parlange, M.B. (2010). Stream temperature response to

    three riparian vegetation scenarios by use of a distributed temperature validated

    model. *Environ. Sci. Technol. 44*, 2072–2078.

Sand-Jensen, K., Pedersen, N.L. (2005). Differences in temperature, organic carbon

    and oxygen consumption among lowland streams. *Freshw. Biol. 50*, 1927–1937.

Segura, C., Caldwell, P., Sun, G., Mcnulty, S., Zhang, Y. (2015). A model to predict

    stream water temperature across the conterminous USA. *Hydrol. Process. 29*,

    2178–2195.

Somers, K.A., Bernhardt, E.S., Grace, J.B., Hassett, B.A., Sudduth, E.B., Wang, S.,

    Urban, D.L. (2013). Streams in the urban heat island: Spatial and temporal variability

    in temperature. *Freshw. Sci. 32*, 309–326.

Sridhar, V., Sansone, A.L., LaMarche, J., Dubin, T., Lettenmaier, D.P. (2004).

    Prediction of stream temperature in forested watersheds. *J. Am. Water Resour.*

    Assoc. 40, 197–213.

Sun, N., Yearsley, J., Voisin, N., Lettenmaier, D.P. (2015). A spatially distributed model for the assessment of land use impacts on stream temperature in small urban watersheds. *Hydrol. Process. 29*, 2331–2345.

Van Buren, M., Watt, W.E., Marsalek, J., Anderson, B.C. (2000). Thermal enhancement of stormwater runoff by paved surfaces. *Water Res. 34*, 1359–1371.

Van Vliet, M.T.H., Yearsley, J.R., Franssen, W.H.P., Ludwig, F., Haddeland, I., Lettenmaier, D.P., Kabat, P. (2012). Coupled daily streamflow and water temperature modelling in large river basins. *Hydrol. Earth Syst. Sci. 16*, 4303–4321.

Wolman, M.G. (1954). A method of sampling coarse bed material. *Trans. Am. Geophys. Union. 35*, 951–956.

Webb, B., Zhang, Y. (1997). Spatial and seasonal variability in the components of the river heat budget. *Hydrol. Process. 11*, 79–101.

Westhoff, M.C., Savenije, H.H.G., Luxemburg, W.M.J., Stelling, G.S., Giesen, N.C., Van De, Selker, J.S. (2007). Sciences A distributed stream temperature model using high-resolution temperature observations. *Hydrol. Earth Syst. Sci. 11*, 1469–1480.

Wunderlich, T.E. (1972). *Heat and Mass Transfer between a Water Surface and the Atmosphere*; Report No. 14; Water Resources Research Laboratory, Tennessee Valley Authority: Norris Tennessee, TN, USA.

Yang, Y., Endreny, T.A., Nowak, D.J. (2011). iTree-Hydro: Snow hydrology update for the urban forest hydrology model. *J. Am. Water Resour. Assoc. 47*, 1211–1218.

Yearsley, J.R. (2009). A semi-Lagrangian water temperature model for advection-dominated river systems. *Water Resour. Res. 45*, W12405.

Zheng, C., Bennett, G.D. (1995). *Applied Contaminant Transport Modeling*; Van Nostrand Reinhold: New York, NY, USA.

2.8 Supplementary Materials

2.8.1 River Velocity, Dispersion, and Inflows (Section S1)

The i-Tree Cool River Model uses inputs of river discharge to solve for the advection and dispersion terms in equation (1) as well as solve for the inflow reaction term, R_i in equation (1 and 3). In unsteady conditions, such as during a storm, the model determines river velocity and dispersion using the one-dimensional St. Venant equation, which is solved numerically using the finite difference method given in equations (3-25) to (3-29) by Boyd and Kasper (2003). This St. Venant finite difference method uses the Manning equation to relate velocity with river water depth, wetted perimeter, and cross-sectional area. The Manning equation operates in trapezoidal, triangular, or square channels with prescribed width, roughness, and side slope. The i-Tree Cool River Model uses a version of the Manning equation provided by Boyd and Kasper (2003) in equation (3-11). The Newton-Raphson root finding iterative method is used to solve the Manning equation and determine the adjusted wetted depth, hydraulic radius, wetted perimeter, cross-sectional area, and bottom width (Boyd and Kasper, 2003). The i-Tree Cool River model uses the estimated velocity with the MacCormick method to determine the rate at which river water temperature travels between cross sections, using equations (2-119) to (2-122) from Boyd and Kasper (2003). The St. Venant finite difference method requires compliance with Courant and frictional stability conditions for each node every timestep, using equations (3-30) and (3-31) of Boyd and Kasper (2003). In steady state conditions, the model can determine velocity and dispersion using the St. Venant method, as done by Boyd and Kasper (2003), or the

user can select the Crank-Nicolson numerical method to solve a coupled set of velocity and temperature equations, following the approach of Zheng and Bennett, (1995).

Inflows are composed of surface and subsurface sources. The surface inflow terms, Q_{ss} and T_{ss} of equation (3) are input as a time series of flow rate (m^3/s) and temperature (°C), respectively, for any node receiving storm sewer, tributary, or other surface inflows. The flow and temperature values are either provided through measured observation or through estimation; we used observation in our study below.

The subsurface terms for groundwater inflow, Q_{GW} and T_{GW} of equation (3) are input as a time series of groundwater flow rate (m^3/s) and temperature (°C) for each node and can be based on observation or estimation. The groundwater temperature was set to a constant 14.4 °C for the simulation period which was based on a function of annual average air temperature warming slightly in the summertime. Groundwater inflow was determined from observation, measuring baseflow at the upstream (station at the 0 m) and downstream (station at the 1500 m) sections of the Sawmill Creek during dry weather, and computing the inflow rate per unit length of the reach.

The subsurface hyporheic flow rate (m^3/s), $Q_{Hyp,}$ and hyporheic flow temperature (°C), T_{Hyp} terms of equation (3) for each node can be based on observation or estimation. Similar to groundwater flow, the hyporheic temperature was set to the constant 14.4 °C and hyporheic inflow was calculated in the i-Tree Cool River Model based on the Darcy's Law (Domenico and Schwartz, 1990) as

$$Q_{Hyp} = A_S K_S \frac{dh_D}{dx}$$ (S1)

where A_S is cross-sectional across seepage face (m^2), K_S is dominant substrate hydraulic conductivity (m/s), h_D is hydraulic head for Darcy calculation (m), and x is the model distance step (m).

2.8.2 Heat Flux Calculations (Section S2)

2.8.2.1 Shortwave Radiation (First Method; Section S2.1a)

The model provides two methods for calculating shortwave radiation. The first method calculates the total shortwave radiation in equation (4) is a function of the incoming solar radiation observed at the edge of the atmosphere (Ouellet et al., 2014), which i-Tree Cool River can calculate with two methods. The first method is based on the albedo and a shading factor, which is based on the riparian vegetation condition along the river reach (Chen et al., 1998)

$$\Phi_{shortwave} = S_{in}(1-a)(1-SF)$$ (S2)

where S_{in} is incoming shortwave radiation, the sum of direct and diffuse shortwave radiation, a is the albedo (0 to 1), and SF is the estimated shading factor (0 to 1, with 1 for complete shade).

2.8.2.2 Shortwave Radiation (Second Method; Section S2.1b)

The second method for evaluating the shortwave radiation combines the adjusted direct and diffuse shortwave radiation, and uses sky view factors and shading width in place of a shading factor (Sun et al., 2015)

$$\Phi_{shortwave} = \Phi^{''direct}_{shortwave} + \Phi^{'diffuse}_{shortwave} \tag{S3}$$

The view-to-sky factor is applied to compute the topographic shading effect on diffuse solar radiation ($S^{diffuse}_{shortwave}$) (Chen et al., 1998)

$$\Phi^{'diffuse}_{shortwave} = S^{diffuse}_{shortwave}(1-a)\min(f_1, f_2, f_3) \tag{S4}$$

Direct shortwave radiation is computed using two steps, accounting for the width of shade across the river surface, and the river slope and aspect, as well as solar azimuth and altitude (Sun et al., 2015)

$$\Phi^{''direct}_{shortwave} = \Phi^{'direct}_{shortwave}\left(1 - \frac{W'_{eff}}{W_{river}}\right) \tag{S5}$$

where W'_{eff} is the width of the effective shading and W_{river} is the river section wetted width, and are explained in the next paragraph, and $\Phi^{'direct}_{shortwave}$ is

$$\Phi^{'direct}_{shortwave} = S^{direct}_{shortwave}(1-a)[\sin\alpha\cos\varphi\cos(\beta - \theta_{sun}) + \cos\alpha\sin\varphi] \tag{S6}$$

where $S^{direct}_{shortwave}$ is the incoming direct shortwave radiation, α is the longitudinal water surface slope (radians), β is the aspect with 0 set to true north (radians), θ_{sun} is solar azimuth angle (radians), indicating the angle of the position of the sun relative to true north, and φ is solar altitude (radians). The second method for calculating shortwave radiation, can reduce to the first method, in cases of full shade and full sun. For the case of full sun, the shade angle, $SA = 0$ and $f_i = 1$, resulting in $\Phi^{'diffuse}_{shortwave} = S^{diffuse}_{shortwave}(1-a)$ for equation (S4), and the complementary term $\Phi^{''direct}_{shortwave}$, becomes $\Phi^{'direct}_{shortwave} =$

$S_{shortwave}^{direct}(1-a)$ when $\varphi = \pi/2$ in equation (S6) and $W'_{eff} = 0$ in equation (S5). For the

case of full shade, the corollary occurs, with $SA = 1$ and $f_i = 0$, and $W'_{eff} = W_{river}$ in

equation (S6), resulting in no solar radiation on the river.

The total shadow width, W_{shade}, of near river objects, is calculated at each time

step as a function of solar azimuth, altitude, and river azimuth (θ_{river}), in addition to

object height at each node (Sun et al., 2015)

$$W_{shade} = (h_i)\left|\frac{\sin(\theta_{sun} - \theta_{river})}{\tan\varphi}\right| \tag{S7}$$

where the h_i is the combined height of the topography ($i = 3$) and building or vegetation

bordering the river. When building and vegetation are present, the object is selected

based on which has the largest shade angle SA from equation (9) of the main text. The

river width and distance from river to the shading object is compared with W_{shade} to

determine the distances across the river surface covered in shade, and to determine the

width of river effectively shaded, W_{eff} and the width of river directly under an

overhanging object, $W_{overhang}$ such as tree canopy (Chen et al., 1998). The model

estimates the tree canopy width protruding from the tree trunk midpoint as 10% of the

tree height (Chen et al., 1998). The overhang is computed for either left or right banks

(Chen et al., 1998) as

$$W_{overhang} = \begin{cases} (0.1h_{tree} - D_{canopy})\rho_{veg} & \text{if } \left[(0.1h_{tree} - D_{canopy}) < W_{stream}\right] \\ W_{stream}\rho_{veg} & \text{if } \left[(0.1h_{tree} - D_{canopy}) \geq W_{stream}\right] \end{cases} \tag{S8}$$

where ρ_{veg} is the average density of the vegetation canopy, which ranges from 0 to 1 (unitless). The effective shading width is computed using Beer's Law as (Chen et al., 1998)

$$W_{eff} = \begin{cases} (W_{shade} - D_i - W_{overhang})(1-e^{-\lambda L_{avg}}) & \text{if } SA_{veg} > SA_{i=1or3} \\ (W_{shade} - D_i - W_{overhang}) & \text{if } SA_{i=1or3} > SA_{veg} \end{cases} \tag{S9}$$

where λ, the radiation extinction coefficient, is calculated as a function of the leaf area index, *LAI* from the equation 2 of DeWalle (2010) and L_{avg} is the average path length of direct solar radiation through the shaded zone around the river (m) (Sun et al., 2015). When canopy overhangs the river surface, the model uses an adjusted effective width $W_{eff}^{'}$ computed as

$$W_{eff}^{'} = W_{eff} + W_{overhang} \tag{S10}$$

Using the adjusted direct radiation affected by topographic shading ($\Phi_{shortwave}^{'direct}$) and the calculated adjusted effective width, the net direct solar radiation affected by the topographic and shading barriers reaching to the surface, $\Phi_{shortwave}^{"direct}$ can be calculated as shown in equation (S5) (Sun et al., 2015).

2.8.2.3 *Latent Heat Flux (Section S2.2)*

The latent heat flux in equation (4) of the main text is a negative upward flux representing evaporative cooling (Webb and Zhang, 1997; Westhoff et al., 2007). The latent heat flux is computed as (Boyd and Kasper, 2003)

$$\Phi_{latent} = -\rho L_e E \qquad \text{(S11)}$$

where L_e is the latent heat of vaporization (J/kg), and E is the evaporation rate (m/s).

The i-Tree Cool River Model provides two methods for calculation of E from open water,

the Penman-Monteith combination method using equation (30) of Westhoff et al. (2007),

and a mass transfer method using equation (2-96) of Boyd and Kasper (2003).

2.8.2.4 Sensible Heat Flux (Section S2.3)

Sensible convection of heat in equation (4) of the main text represents the heat

exchange between the surface of the water and the air (Webb and Zhang, 1997). The i-

Tree Cool River Model provides three flexible methods to calculate the sensible heat

flux, first and second methods (equations 13 and 14) based on the Bowen ratio of

sensible to latent heat, and the third method (equation 15) based on the sensible heat.

The simpler of the two Bowen ratio methods is based on Boyd and Kasper (2003)

$$\Phi_{sensible} = B_r \Phi_{latent} \qquad \text{(S12)}$$

where Br is the Bowen ratio. The more complex of the Bowen ratio methods is based on

Yearsley (2009)

$$\Phi_{sensible} = B_r \rho_w \gamma N U_{wind} (T_{air} - T_w) \qquad \text{(S13)}$$

where γ is the latent heat of vaporization (2.4995×10^6 J/kg), N is an empirical constant

(1.59×10^{-9} s/m.mb) and U_{wind} is wind speed (m/s). The sensible-heat-based method

considers wind speed as a driver of the convective flux, based on Dingman (1994),

given by Boyd and Kasper (2003) as

$$\Phi_{sensible} = -K_H U_{wind} (T_w - T_{air})$$ (S14)

where K_H is the heat exchange coefficient for sensible heat (J/ m^3 ^{o}C).

2.8.2.5 Bed Sediment Heat Flux (Section S2.4)

The bed sediment heat flux in equation (4) of the main text is due to the heat conduction between the bed sediment and the water column and is rate limited by the size and conductance properties of the substrate. The approach modifies equation (2-90) of Boyd and Kasper (2003) as

$$\Phi_{se\,diment} = 2K_{CL} \frac{T_{bed} - T_w}{\frac{d_w}{2}}$$ (S15)

where K_{CL} is the volumetric weighted thermal conductivity (J/ms ^{o}C), T_{bed} is the bed temperature (^{o}C), and d_w is the average river depth in the cross section (m). The sediment interface with the river water is the T_{bed} in equation (S15); some applications prescribe T_{bed} to a depth below the interface. The sediment substrate in Sawmill Creek includes bedrock, boulders, cobbles, and gravels. Some boulders protrude above the water column, which is relatively shallow, and the unsubmerged sections of the sediment reach relatively high temperatures due to absorption of shortwave radiation. The mid-depth of the river, $d_W/2$, is used in equation (S15) to represent a mid-point of the river water temperature reservoir. By solving for the heat fluxes of equation (1) of the main text, the i-Tree Cool River Model can solve equation (2) and provide the heat flux reaction term, R_e, for the governing advection-dispersion-reaction equation (1) used to simulate river temperatures.

2.8.3   Additional Sensitivity Analysis for Shading and Boundary Conditions (Section S3)

Shading along the riparian corridor modifies shortwave radiation, and patchiness in land cover then influences the land cover longwave radiation and longitudinal pattern in river warming when heat flux is the main driver of temperature. The NSRDB satellite estimated surface shortwave radiation was adjusted for each cross section based on the shading factor corresponding with that cross section (Figure S5). The shading factor along the 1500 m of Sawmill Creek reach was primarily a function of riparian tree shade from the canopy but was also a function of riparian topography and riparian building shade, which does include bridges crossing the river. When the shading factor was relatively small the shortwave radiation reaching the surface of Sawmill Creek was relatively large; for example values of radiation above 400 W/m^2 were associated with shade factors below 0.4. The shading factor used for each model node is observed at each cross sections, and between cross sections, there can be a considerable fluctuation between the minimum and maximum shading factors (see Figure S5). The upstream riparian corridors were more densely forested, while the downstream urbanized sections had intermittent coverage of buildings in the riparian corridors, and as a result, the shading factor tended to decrease from upstream to downstream. The river cross sections between the station 600 m and the station 900 m, where storm sewers contributed runoff from impervious areas, coincided with the large variation in the shade factor (Figure S5). Initially, the shading factors at cross section monitoring stations increased from 0.1 at 810 m to 1.0, the bridge, at 870 m, and then decreased to

approximately 0.15 downstream of the urban section, at 1100 m. This increase in the shade factor from 0.1 to 1 about the bridge in the urban section of the reach reduced incoming shortwave radiation, which contributed to a mitigation of the thermal load delivered by urban runoff in this sub-reach.

The utilization of observed, i.e., recorded by a data logger, versus calculated upstream boundary conditions for water temperatures impacted simulation accuracy, which was a function of distance downstream and time of day (Figure S6). We examined the impact to our model simulation of changing the upstream boundary conditions from the recorded to the calculated upstream temperature. Impact was computed as delta temperature, $\Delta T_{i,} = T_{observed} - T_{simulated}$, where the ΔT_i refers to $\Delta T_{recorded}$ when the boundary was recorded, and ΔT_{calc} when the boundary was calculated using the non-linear regression equation (Mohseni et al., 1998), and $T_{observed}$ is the observed temperature at each cross section, and $T_{simulated}$ is the simulated temperature at each cross section. We obtained $\Delta T_{recorded}$ and ΔT_{calc} for: a) 01:00 hours on 11 June 2007, selected as the mid-point between sunset to sunrise; and b) 12:00 hours on 12 June 2007, selected as the mid-point between sunrise to sunset. In nighttime, $\Delta T_{recorded}$ varies about 0 °C throughout the reach, while ΔT_{calc} has a positive slope, trending from 1.0 °C upstream to 0.1 °C downstream in nighttime and trending from 0.9 °C upstream to 0.6 °C downstream. Comparison of the upstream cross section and downstream cross section differences indicated that running the model using the non-linear regression equation as the upstream boundary condition generated better simulations with distance downstream reach, more so during nighttime than daytime.

2.9 Tables

Table 1 (Table S1): List of the input files required for the simulation process of the i-Tree Cool River Model

Input file	The parameter name	Description
BedData.dat	Number	The number of the observations indicates the locations of the observed streambed data.
	Distance (m)	Distances through the river reach where the streambed observations are recorded.
	Depth of Measurement (m)	Depth at which groundwater temperatures are recorded in each cross section
	GW_Temp (°C)	Groundwater temperature in downstream.
	Type	Bed-sediment type which can be clay, silt, sand, or gravel.
	Horizontal Bed Conductivity (mm/s)	Horizontal effective thermal conductivity in each observed cross-section.
	Bed Particle Size (mm)	Bed particle size (Bedient and Huber, 1992, Rosgen, 1996) in the observed location.
	Embeddedness (fraction)	Embeddedness in each considered cross section.
DEM.txt	Elevation data for calculating slope and aspect for calculating the hillslope effect on energy flux which can be converted from raster file to ASCII in Arc Map. The raw DEM data can be downloaded from the National Map Viewer.	
Discharge.dat	Number	The number of the observations indicates the locations of the observed groundwater data.
	Distance (m)	Distances through the river reach where the magnitude of groundwater flow is recorded
	Q_GW (cms)	Groundwater discharge.
Inflow.dat*	Number	The number of the observations which indicates the number of the time steps for the hydrographs of the river and lateral inflows.
	Inflow Rate Storm (cms)	Discharge rates of the river in upstream at each timestep defining the hydrograph in steady or unsteady mode.

	Inflow Temp Storm (°C)	Observed stream temperatures corresponding to the river hydrograph timesteps in upstream.
	Inflow Rate 1 (cms)	Discharge rates of the lateral storm sewer inflow at each timestep for the first location defining the hydrograph in steady or unsteady mode.
	Inflow Temp 1 (°C)	Observed stream temperatures corresponding to the first lateral storm sewer inflow hydrograph timesteps.
	Inflow Rate 2 (cms)	Discharge rates of the lateral storm sewer inflow at each timestep for the second location defining the hydrograph in steady or unsteady mode.
	Inflow Temp 2 (°C)**	Observed stream temperatures corresponding to the second lateral storm sewer inflow hydrograph timesteps.
	* The First row of the input file below the headings should be considered as the location of each hydrograph. The river's hydrograph gets 1 m indicating the upstream and other lateral inflows receive their own location from the upstream.	
	** The number of lateral inflows can be changed in the code by the user.	
Morphology.dat	Number	The number of the observations indicates the locations of the measured geomorphic data.
	Distance (m)	Distances through the river reach corresponding with the cross sections where the geomorphic data are recorded.
	Area (m^2)	Initial cross-sectional wetted area of the river channel; dummy variable.
	Width (m)	Channel bottom width.
	Depth (m)	Initial channel water depth.
	Discharge (cms)	River discharge magnitude at the location where the geometric data are measured.
	Slope	Channel longitudinal slope
	Row#**	The row number in the DEM file where the cross-section is located.
	Column#**	The column number in the DEM file where the cross-section is located.
	Longitude (deg)**	Longitude of the cross-section in the geographic coordinate system.

	Latitude (deg)**	Latitude of the cross-section in the geographic coordinate system.
	Z (H:V)	The side slope of the trapezoidal channel, equivalent to horizontal distance to vertical distance ratio. Same value for both channel sides.
	** These input data are required for calculating the slope and aspect of each cell to apply the values on hillslope effect and the shortwave radiation. In case of using fixed magnitudes for the shade factor and view-to-sky values, these values are not effective in the simulation process.	
Shading.dat*	Number	The number of the observations reflecting the locations of the measured shading information.
	Distance (m)	Distances through the river reach corresponding with the cross sections where the shading information are recorded.
	EastBankH (m)	The height of the bankfull[1] at the measured cross section on the Eastside.
	EastTreeH (m)	The height of the canopy at the measured cross section on the Eastside.
	EastBuildingH (m)	The height of the building at the measured cross section on the Eastside.
	EastBankDist (m)	Distance from the bankfull to the edge of the water at the measured cross section on the Eastside.
	EastCanDist (m)	Distance from the canopy to the edge of the water at the measured cross section on the Eastside.
	EastBuildingDist (m)	Distance from the building to edge of the water at the measured cross section on the Eastside.
	EastBufferW (m)	The magnitude of the canopy buffer at the location of the measured cross section on the Westside
	WestBankH (m)	The height of the bankfull at the measured cross section in the Westside.
	WestTreeH (m)	The height of the canopy at the measured cross section on the Westside.

---

[1] The water level, or stage, at which a stream, river or lake is at the top of its banks and any further rise would result in water moving into the flood plain.

	WestBuildingH (m)	The height of the building at the measured cross section on the Westside.
	WestBankDist (m)	Distance from the bankfull to the edge of the water at the measured cross section on the Westside.
	WestCanDist (m)	Distance from the canopy to the edge of the water at the measured cross section on the Westside.
	WestBuildingDist (m)	Distance from the building to edge of the water at the measured cross section on the Westside.
	WestBufferW (m)	The magnitude of the canopy buffer at the location of the measured cross section on the Westside
	Elevation (m)	The elevation of the cross-section.
	StreamAzimuth (deg)	The stream azimuth at the location of the measured cross section.
	* These input data are required for calculating the topographic, canopy (tree), and building shade angle and view-to-sky factor to apply the values to hillslope effect and the shortwave radiation. In case of using fixed magnitudes for the shading factor and view-to-sky values, these values are not effective in the simulation process.	
ShadingPercent.dat*	Number	The number of the observations reflecting the locations of the shading factors.
	Distance (m)	Distances through the river reach corresponding with the cross sections where the shading factor and the view-to-sky values are calculated.
	ShadeFactor	The value of cross-section shade factor for daily average, with 0 for no shading, and 1 for full shading. This is representative of entire channel, and can be the average for right and left banks. It can be estimated using site visit, aerial photos, or best estimates.
	View-to-Sky	The value of View-to-Sky in the desired cross-section which is 1-ShadeFactor
	* In case the topographic, canopy, and building heights and distances are considered for shading calculations, the magnitude of ShadeFactor and View-to-Sky are not effective in the simulation process.	
SolarRadiation.dat*	yyyymmdd	The date of the simulation period.
	Hr: Min: Sec	The time of the simulation period.
The number of entries in this file should match	DirSW (W/m^2)	Direct shortwave radiation at the edge of the atmosphere.

the attribute value of totTime in the config file (see Table 2)	DiffSW (W/m^2)	Diffuse shortwave radiation at the edge of the atmosphere.
	* Source: National Solar Radiation Database (NSRDB)	
Time.dat	Number	The number of the time steps.
	Time (s)	The desired time step for the output intervals.
Weather.dat* The number of entries in this file should match the attribute value of totTime in the config file (see Table 2)	yyyymmdd	The date of the simulation period.
	Hr: Min: Sec	The time of the simulation period.
	Tair (F)	Air temperature.
	WndSpd (m/s)	Wind speed.
	Precip (m/h)	Precipitation rate.
	Cloudiness	The magnitude of the cloudiness.
	Humidity	Relative humidity.
	obsT_x0 (℃)	Observed river temperature in the upstream.
	sedT (℃)	Riverbed temperature.
	* National Center for Environmental Information	

Table 2 (Table S2): The alternative methods to for obtaining the input data for the i-Tree Cool River model input data.

Input file	Parameter	Explanation / Obtaining method	Alternative Obtaining method/website
BedData.dat	Depth of Measurement (m)	Typically set to 2 m below the bed for measurement of groundwater temperature.	
	GW_Temp (°C)	At 2 m depth is estimated as average annual air temperature, possibly with seasonal adjustment.	NOAA's NCDC database: https://gis.ncdc.noaa.gov/maps/ncei/ or National Solar Radiation Database: https://rredc.nrel.gov/solar/old_data/nsrdb/
	Type	Bed substrate material type is based on estimate of site visit, and is selected from range of 4 types within model code: cobble, gravel, sand, clay	
	Horizontal Bed Conductivity (mm/s)	Values are associated with bed substrate material type, and can be set based on hydrology reference materials or site testing. Boyd and Kasper (2003) has values for these.	
	Bed Particle Size (mm)	Values are associated with bed substrate material type, and can be set based on hydrology reference materials or site testing. Boyd and Kasper (2003) has values for these.	
	Embeddedness (fraction)	Values are associated with bed substrate material type, and can be set based on morphology reference materials or site testing. Boyd and Kasper (2003) has values for these.	
DEM.txt		Extent of DEM can extend out to entire watershed or be limited to river corridor, and used tp compute hillslope effect on energy flux.	National Map Viewer: https://viewer.nationalmap.gov/advanced-viewer/ Google Engine: https://earthengine.google.com/
Discharge.dat	Q_GW (cms)	Estimated as the difference in discharge at the downstream and upstream section of the reach. The discharge at each end of the reach could be from i-Tree Hydro simulations, observation, or USGS StreamStats.	USGS's Stream stats: https://streamstats.usgs.gov/ss/
Inflow.dat	Inflow Rate (cms)	Lateral flow from steady or unsteady state, and is either estimated or observed. Estimates could come from i-Tree Hydro model simulation.	SWMM: https://www.epa.gov/water-research/storm-water-management-model-swmm
	Inflow Temp (°C)	Estimate or observation, for steady or unsteady state. Anticipate a new algorithm could be added to Unified Hydro (w/ Cool Air) to simulate this value.	A non-linear regression equation based on air temperature: Mohseni et al., (1998) https://agupubs.onlinelibrary.wiley.com/doi/abs/10.1029/98WR01877
Morphology.dat used for 3 model options: Crank Nicholson,	Distance (m)	Distances to downstream channel cross sections. Estimated based on map or site analysis such as NHD, or based on systematic intervals.	National Hydrography Data: https://www.usgs.gov/core-science-systems/ngp/national-hydrography National Map Viewer: https://viewer.nationalmap.gov/advanced-viewer/ Google Engine:

| Runge Cutta, or Explicit Finite Difference. Not used in model option: HEC-RAS.

Alternatively use:

HecRasData.dat, which contains: downstream distance (between cross-sections); discharge; minimum channel elevation; water surface elevation; velocity; area; top width; water surface slope; wetted perimeter. All of these outputs are generated by HEC-RAS as SI units.			
	Area (m^2)	Initial value of cross-sectional area, dummy variable not used by model.	
	Width (m)	Cross-sectional bottom width for trapezoidal channel (0 value for triangular). Could be estimated: a) using field surveys; or b) using modification of hydraulic geometry relations to get channel geometry at bankfull based on watershed area, which is provided by some USGS SteamStats sites and NHD - scale values for lower flow.	
	Depth (m)	Initial time step of water depth. Could be estimated: a) using field surveys; or b) using modification of hydraulic geometry relations to get channel geometry at bankfull based on watershed area, which is provided by some USGS SteamStats sites and NHD - scale values for lower flow.	
	Discharge (cms)	Upstream boundary flow from steady or unsteady state, and is either estimated or observed. Estimates could come from i-Tree Hydro model simulation.	
	Slope	Longitudinal bed slope. Could be estimated: a) using field surveys; b) using DEM analysis; or c) USGS SteamStats sites and NHD.	USGS's Stream stats: https://streamstats.usgs.gov/ss/
	Row#	Associated with the DEM.txt input, and is input row number (0 is first row) of each river cross-section. Used to compute slope and aspect for radiation estimates. Could estimate from observation or overlaying NHD image of river on DEM in ArcGIS.	National Map Viewer: https://viewer.nationalmap.gov/advanced-viewer/ Google Engine: https://earthengine.google.com/
	Column#	Associated with the DEM.txt input, and is input column number (0 is first column) of each river cross-section. Used to compute slope and aspect for radiation estimates. Could estimate from observation or overlaying NHD image of river on DEM in ArcGIS.	National Map Viewer: https://viewer.nationalmap.gov/advanced-viewer/ Google Engine: https://earthengine.google.com/
	Longitude (deg)	Associated with each river cross-section. May not vary with short river. Could estimate from observation or map analysis.	National Map Viewer: https://viewer.nationalmap.gov/advanced-viewer/ Google Engine: https://earthengine.google.com/
	Latitude (deg)	Associated with each river cross-section. May not vary with short river. Could estimate from observation or map analysis.	National Map Viewer: https://viewer.nationalmap.gov/advanced-viewer/ Google Engine: https://earthengine.google.com/
	Z (H:V)	Channel side slope for trapezoidal channel banks, same value used on each bank. Could estimate from field	National Map Viewer: https://viewer.nationalmap.gov/advanced-viewer/

		observation, design decision, or image analysis.	Google Engine: https://earthengine.google.com/
Shading.dat	All the parameters	All the parameters for this input data (2nd method of calculating the longwave and shortwave radiations) are based on direct measurements at field site or of maps and images.	Lidar surveying data (if it is available) https://viewer.nationalmap.gov/basic/ https://gisgeography.com/top-6-free-lidar-data-sources/
ShadingPercent.dat	ShadeFactor	The value of cross-section shade factor for daily average, with 0 for no shading, and 1 for full shading. This is representative of entire channel, and can be the average for right and left banks. It can be estimated using: a) site visits; b) aerial photos with manual interpretation or TTools module in Heat Source Model; or c) scenario estimates.	The heat source model's TTools module: https://www.oregon.gov/deq/wq/tmdls/Pages/TMDLs-Tools.aspx
	View-to-Sky	The value of View-to-Sky in the desired cross-section which is 1-ShadeFactor	
SolarRadiation.dat	Direct and Diffuse shortwave radiation data	National Solar Radiation Database: https://rredc.nrel.gov/solar/old_data/nsrdb/	i-Tree Hydro preprocessor:
Time.dat	Time (s)	The desired time step for the output data intervals.	
Weather.dat	Tair (F)	Weather input data of air temperature	NOAA's NCDC database: https://gis.ncdc.noaa.gov/maps/ncei/ National Solar Radiation Database: https://rredc.nrel.gov/solar/old_data/nsrdb/
	WndSpd (m/s)	Weather input data of wind speed	
	Precip (m/h)	Weather input data of precipitation	
	Cloudiness	Weather input data of cloudiness	
	Humidity	Weather input data of humidity	
	obsT_x0 (℃)	Upstream boundary river temperature, for each time step. Estimated with observation or non-linear regression with air temperature.	A non-linear regression equation using air temperature: Mohseni et al., (1998) https://agupubs.onlinelibrary.wiley.com/doi/abs/10.1029/98WR01877
	sedT (℃)	Channel bed substrate temperature, for each time step. Estimated with observation or model prediction based on solar radiation or temperature data.	NOAA's NCDC database: https://gis.ncdc.noaa.gov/maps/ncei/ National Solar Radiation Database: https://rredc.nrel.gov/solar/old_data/nsrdb/

Table 3 (Table S3): Observed water temperatures for three reaches of Sawmill Creek and for the Tannersville storm sewer, during June 11 and 12, 2007, as the average for all time steps during the dry or wet weather conditions.

Reach	Flow type	Average temperature (^{o}C)
Upstream (0 m to 600 m)	Dry weather	15.1
	Wet weather	14.5
Middle (600 m to 900 m)	Dry weather	15.5
	Wet weather	14.8
Downstream (900 m to 1500 m)	Dry weather	15.6
	Wet weather	15.0
Storm sewer	Dry weather	14.9
	Wet weather	16.9

Table 4 (Table S4): Statistical analysis (paired t-test) of the reach averaged observed and simulated river temperature in Sawmill Creek for the (a) original condition including both wet and dry weather (b) wet weather, and (c) dry weather.

Paired t-test	t-value	Degrees of freedom	p-value	95 percent confidence interval		mean of the differences
				Lower tale	Upper Tale	
a	0.1593	11	0.8763	-0.02058636	0.02379879	0.001606213
b	-0.43766	11	0.6701	-0.06951900	0.04645744	-0.01153078
c	1.7253	11	0.1124	-0.01098885	0.09070502	0.03985809

Table 5 (Table S5): Statistical analysis (paired t-test) of the reach averaged observed and simulated river temperatures using the scenarios for the (a) no shading effect, (b) no groundwater and hyporheic exchange inflows, and (c) calculated boundary condition.

Paired t-test	t-value	Degrees of freedom	p-value	95 percent confidence interval		mean of the differences
				Lower tale	Upper Tale	
a	-9.8096	11	8.955e-07	-0.4188181	-0.2653184	-0.3420683
b	-6.6702	11	3.514e-05	-0.19337108	-0.09741817	-0.1453946
c	-11.553	11	1.717e-07	-0.6902328	-0.4693167	-0.5797748

Table 6 (Table S6): Statistical analysis (paired t-test) of the observed and simulated river temperatures in Sawmill Creek, between 12:00 hours of June 11, 2007 to 17:00 hours of June 12, 2007.

Paired t-test	t-value	Degrees of freedom	p-value	95 percent confidence interval		mean of the differences
				Lower tale	Upper Tale	
Sawmill Creek	0.25605	29	0.7997	-0.06101277	0.07847554	0.008731384
Meadowbrook Creek	0.35807	116	0.7209	-0.05020794	0.07236796	0.01108001

Table 7 (Table S7): Sensitivity analysis of the temperature simulations using the i-Tree Cool River model.

Parameter	Parameter Variation (%)	Temperature change (%)
Storm sewer temperature	±15	1.65
Sediment temperature	±15	0.3
Upstream Boundary Condition	±15	9.5
Substrate Hydraulic Conductivity	±20	0.15
Cloudiness	±20	0.02
Groundwater discharge	±20	0.03

2.10 Figures
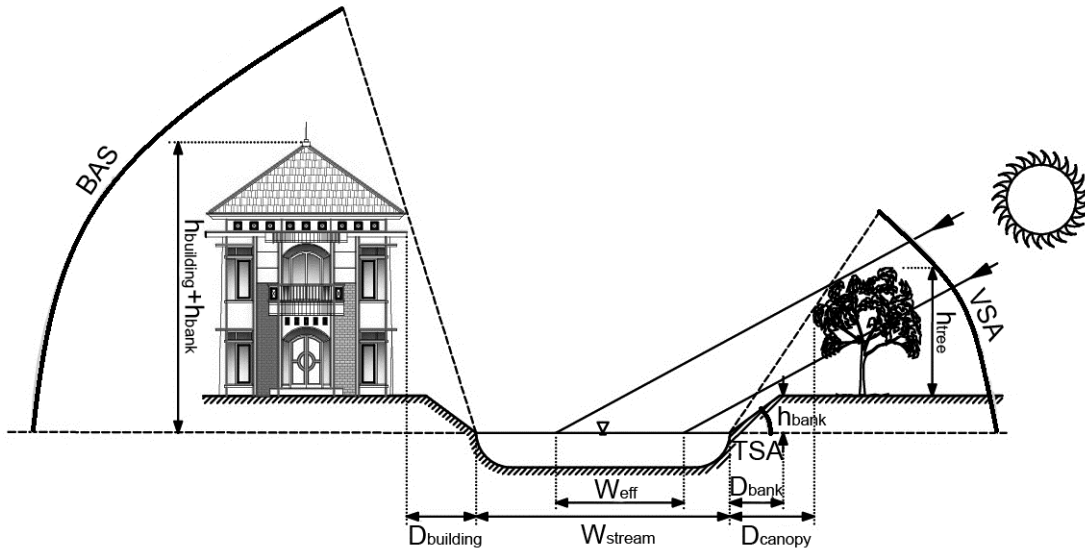
Figure 1 (Figure 1): Shading of the river surface. A cross-sectional view, in which BSA is the building shading angle, VSA is the vegetation shading angle, and TSA is the topographic shading angle. $h_{building}$, h_{tree}, and h_{bank} are building, vegetation, and bank heights respectively. $D_{building}$, D_{canopy}, and D_{bank} are building to the bank, canopy to the bank, and bank.
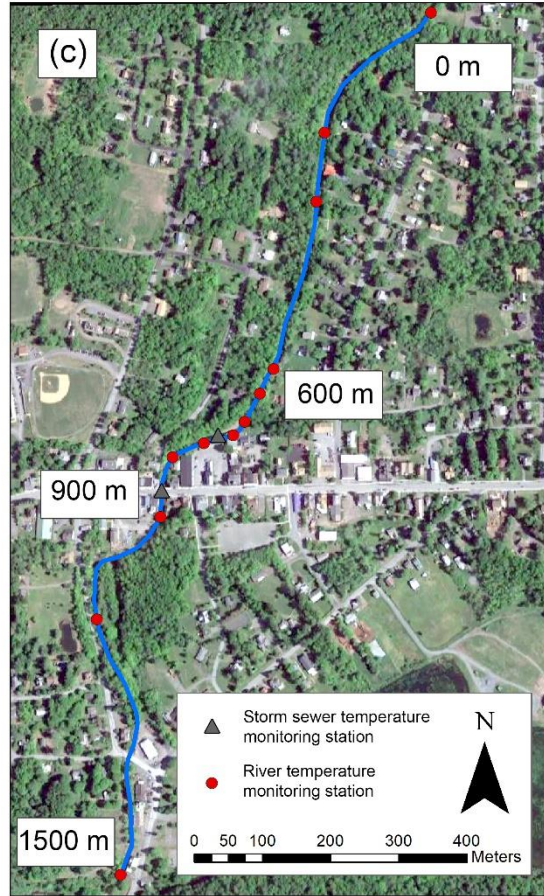
Figure 2 (Figure 2): (**a**) New York State with the Sawmill Creek study area denoted by the star. (**b**) Monitoring stations and reach distances along Sawmill Creek.
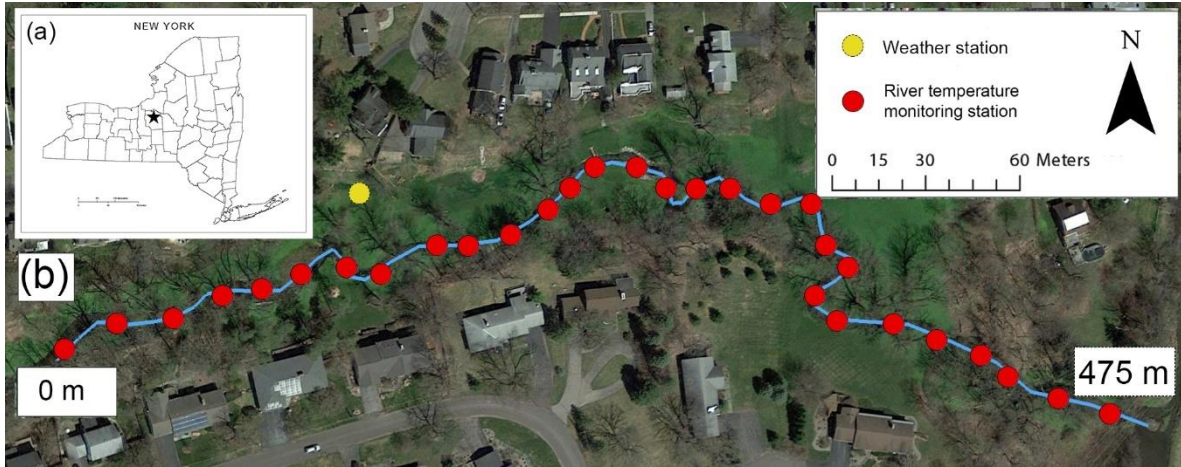
Figure 3 (Figure 3): (**a**) New York State with the Meadowbrook Creek study area denoted by the star. (**b**) Monitoring stations and reach distances along Meadowbrook Creek.
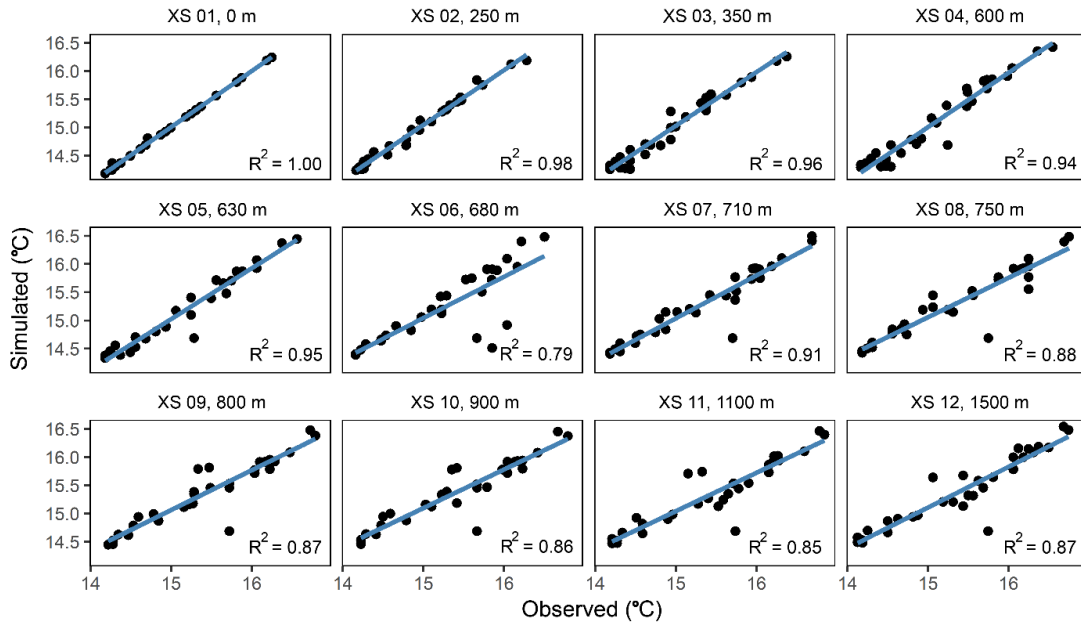
Figure 4 (Figure 4): Observed versus simulated river temperatures for the 12 cross sections (XS) and stations from 0 m to 1500 m in Sawmill Creek. The coefficient of determination, R^2 for each cross section is shown in the plot.
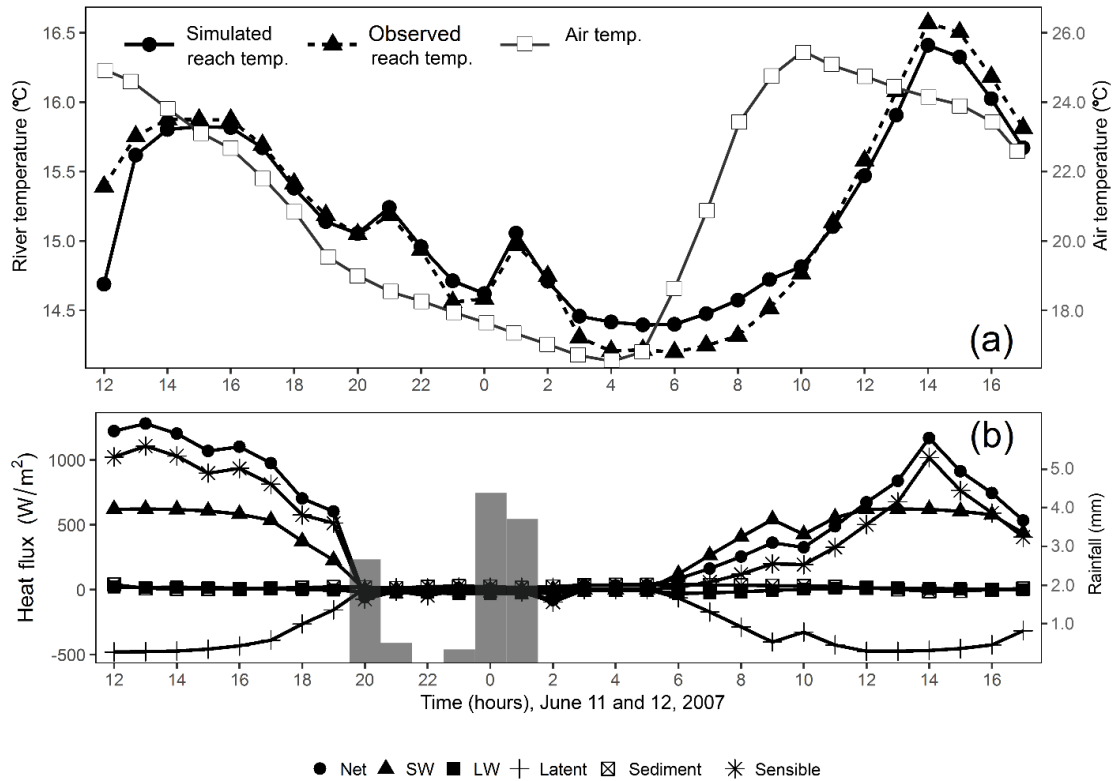
Figure 5 (Figure 5): (**a**) Reach average air temperature and observed and simulated river temperatures in Sawmill Creek, between 12:00 h of 11 June 2007 to 17:00 h of 12 June 2007; (**b**) Simulated reach averaged heat fluxes and precipitation into Sawmill Creek between 12:00 h of 11 June 2007 to 17:00 h of 12 June 2007.
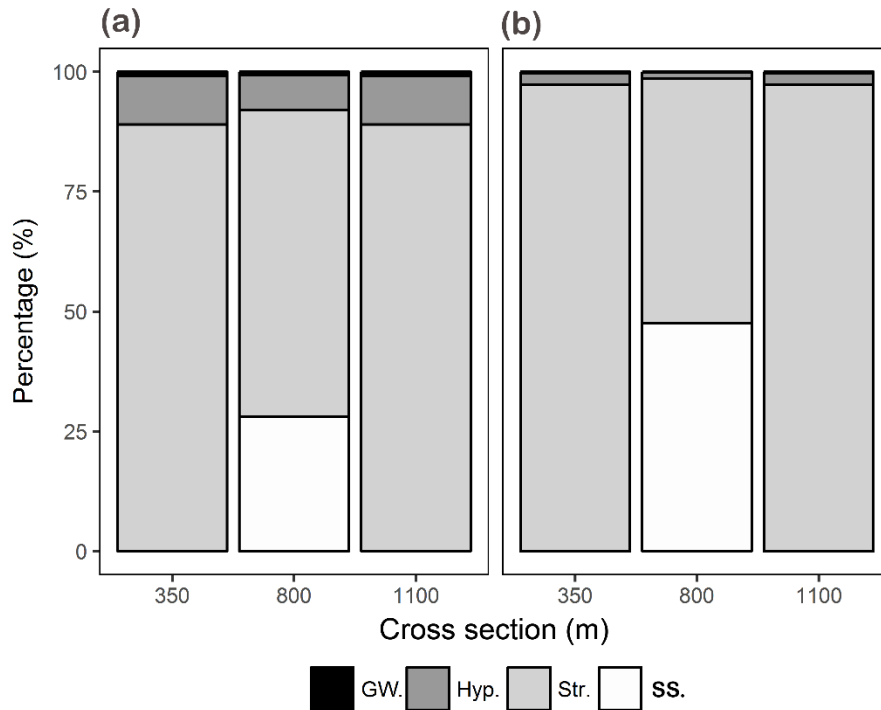
Figure 6 (Figure 6): Simulated contribution to river temperature of the river flow (Str.), storm sewer (SS.), hyporheic exchange (Hyp.), and groundwater flow (GW.) in two timesteps including (**a**) before storm and (**b**) during the storm at three representative cross sections from the upper reaches (between cross sections at station 0 m and 600 m), middle reach (between cross sections at station 600 m and 900 m), and downstream reach (between cross sections at station 900 m and 1500 m).
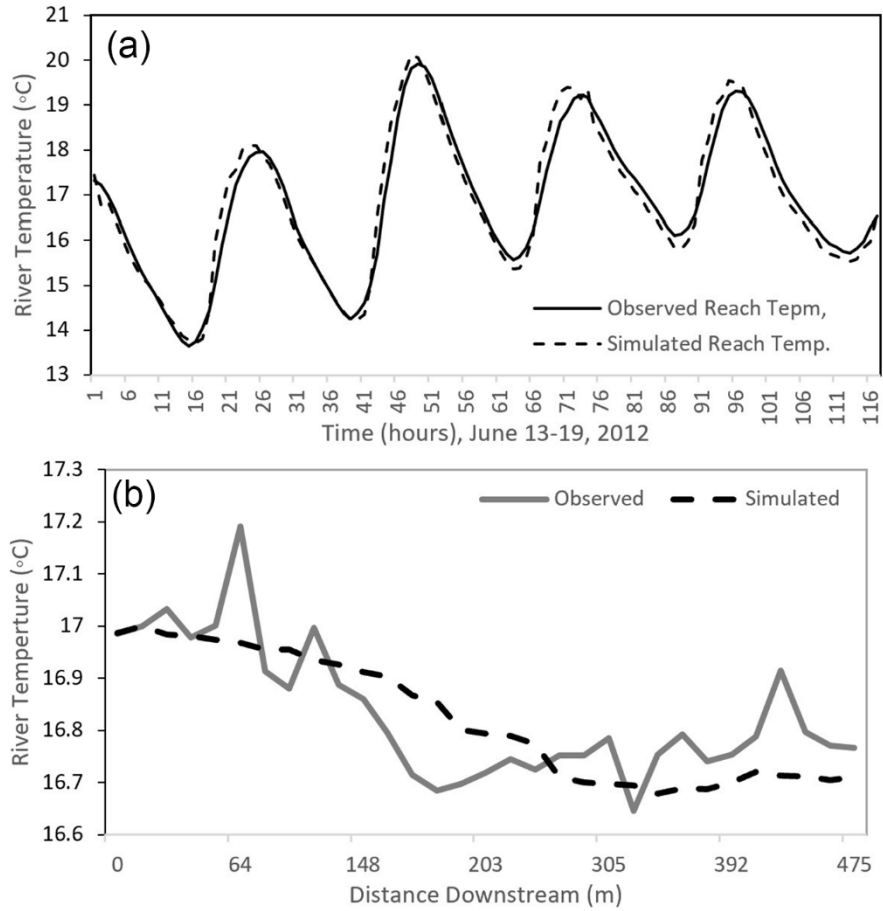
Figure 7 (Figure 7): (**a**) Reach average observed and simulated river temperatures in Meadowbrook Creek, for 13–19 June 2012; (**b**) Time averaged observed and simulated river temperatures for 475 m reach of the Meadowbrook Creek.
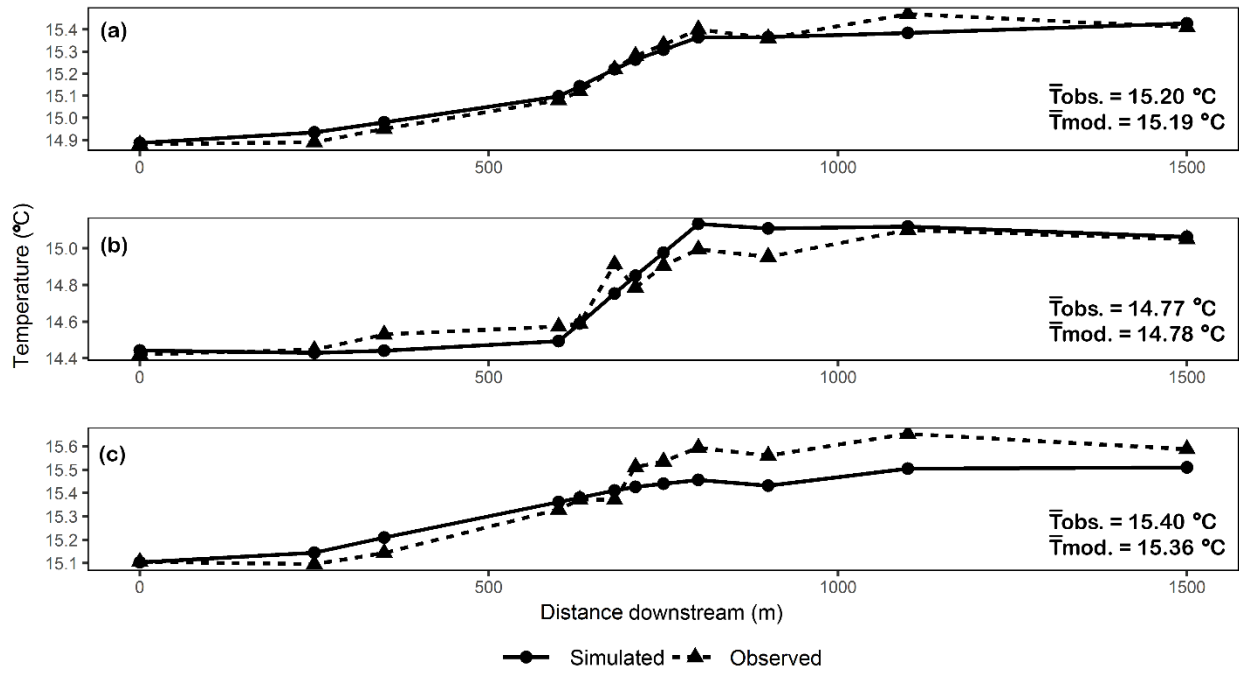
Figure 8 (Figure S1): Time averaged observed and simulated river temperature in Sawmill Creek for the (a) original condition including both wet and dry weather (b) wet weather, and (c) dry weather.
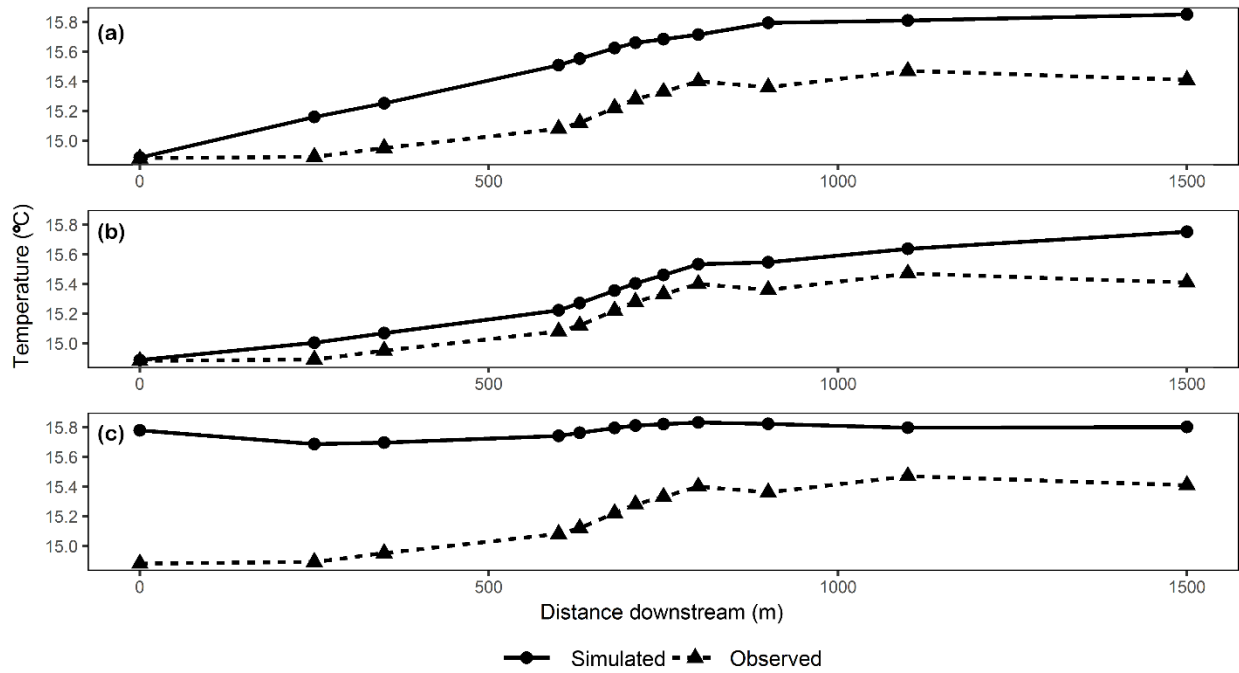
Figure 9 (Figure S2): Time averaged observed and simulated river temperatures using the scenarios for the (a) no shading effect, (b) no groundwater and hyporheic exchange inflows, and (c) calculated boundary condition.
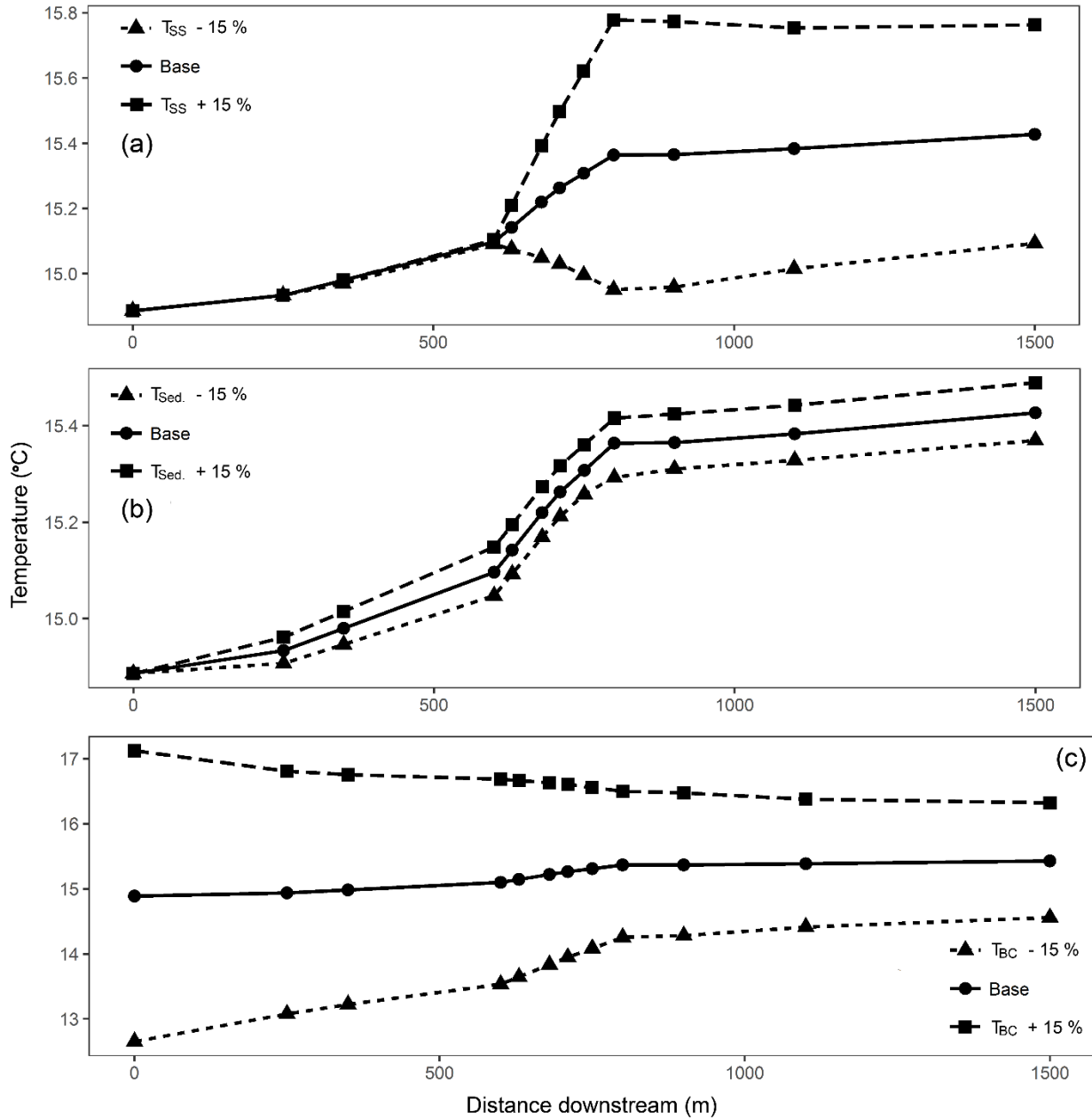
Figure 10 (Figure S3): Simulated time averaged river temperatures along the 1500 m Sawmill Creek reach for the original condition (Base) and for conditions with ±15 % changes in (a) storm sewer temperature (T_{SS}), (b) sediment temperature, and (c) boundary conditions temperature.
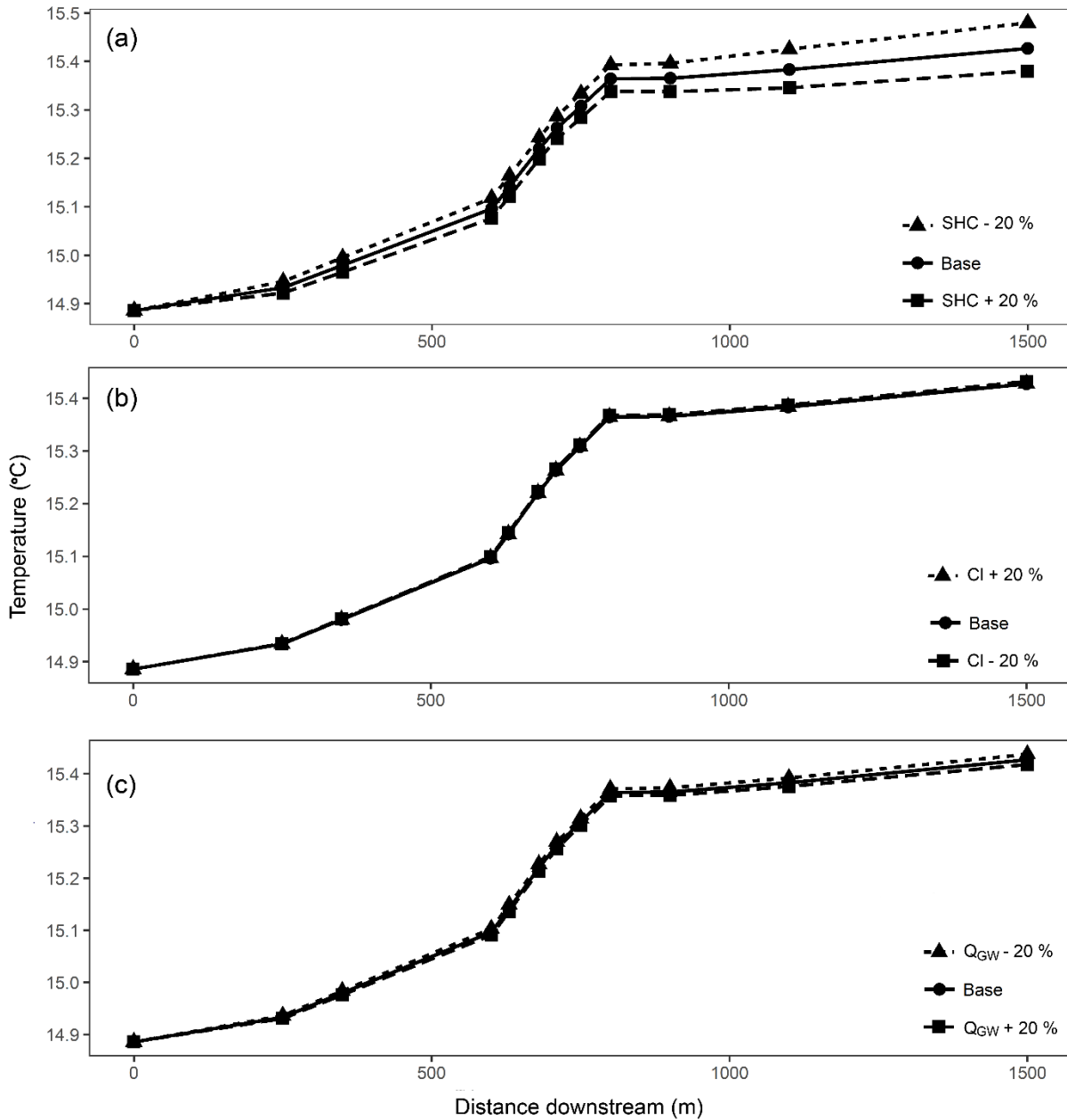
Figure 11 (Figure S4): Simulated time averaged river temperature along the 1500 m Sawmill Creek reach for the original condition (Base) and for conditions with ±20 % changes in (a) substrate hydraulic conductivity (SHC), (b) cloudiness factor (Cl), and (c) groundwater discharge (GW).
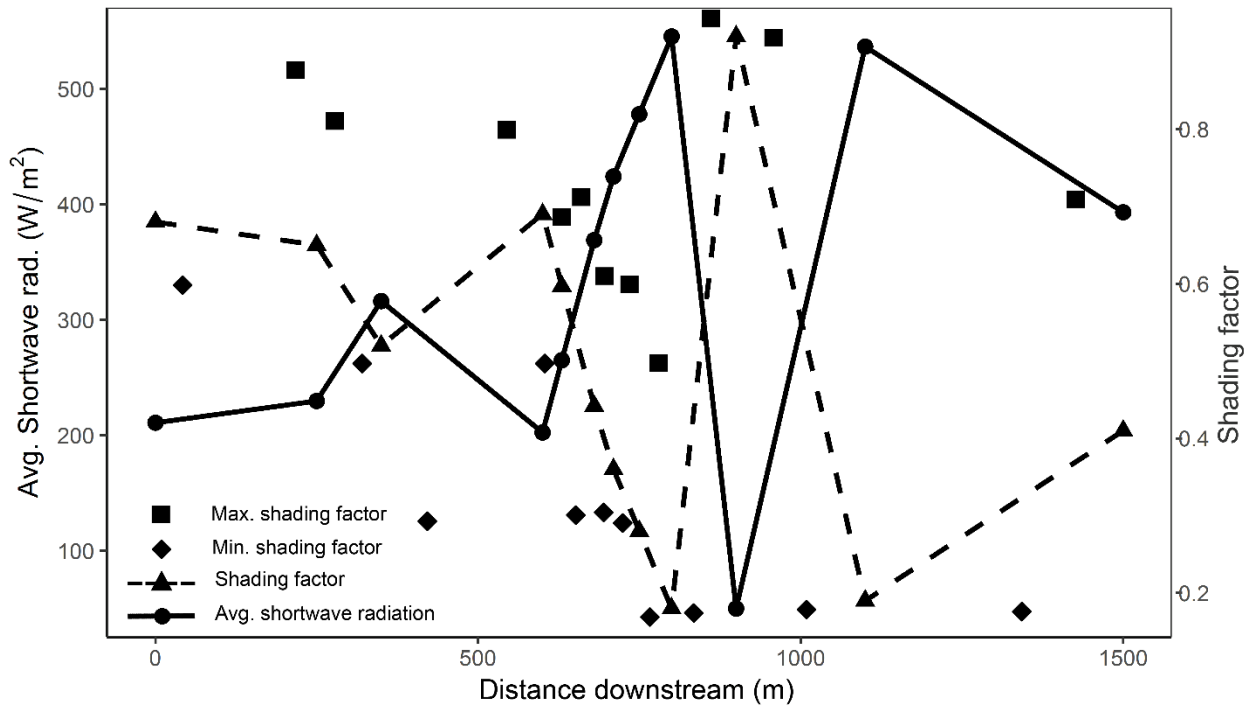
Figure 12 (Figure S5): Fluctuations of shading factors and daily average shortwave radiation along the 1500 m Sawmill Creek reach. The shading factors denoted by a triangle are measured at each of the 12 monitoring stations, and the minimum and maximum shading factors were selected from the 5 m interval set of shading factors measured between each station.
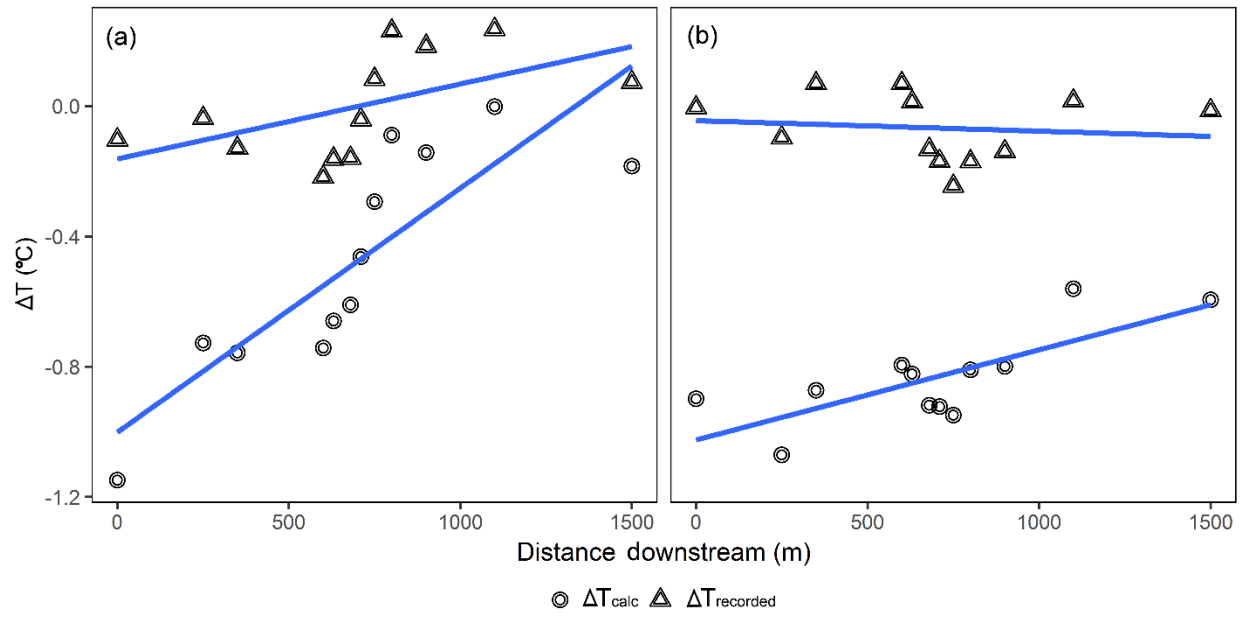
Figure 13 (Figure S6): Temperature differences between the observed and simulated river temperature when using Mohsni et al. (1998), $ΔT_{calc,}$ versus recorded, $ΔT_{recorded,}$ boundary conditions, for (a) nighttime and (b) daytime.

3 A model to Integrate Analysis of Urban River Thermal Cooling and Flood Risk in River Restoration

Abstract: River water quality and habitats are degraded by thermal pollution from urban areas caused by warm surface runoff, lack of riparian forests, and impervious channels that transfer heat and block cool subsurface flows. This study updates the i-Tree Cool River model to simulate restoration of these processes to reverse the urban river syndrome, while using the HEC-RAS model water surface profiles needed for flood hazard analysis in restoration planning. The new model was tested in a mountain river within the New York City drinking water supply area, and then used for base case and restoration scenarios on the 17.5 km reach of the Los Angeles (LA) River where a multi-million dollar riverine restoration project is planned. The model simulated the LA River average temperature in the base case decreased from 29.5°C by 0.3℃ when warm surface inflows were converted to cooler groundwater inflows by green infrastructure; by 0.7°C when subsurface hyporheic exchange was increased by removal of armoring and installation of riffle-pool bedforms; by 3.6℃ when riparian forests shaded the river; and by 6.4°C when floodplain forests were added to riparian forests to cool surface reservoirs and local air temperatures. The simulated decreases in river temperature lead to increased saturated dissolved oxygen levels, reaching 8.7 mg/L, up from the 7.6 mg/L in the base case scenario, providing improved fish habitat and reducing eutrophication and hypoxic zones.

Key Terms: Los Angeles River, urban river, thermal pollution, riparian shading, green infrastructure

3.1   Introduction

The "urban stream syndrome" describes the ecological degradation of waters draining urban lands and is characterized by a rapid oscillation in water flows (i.e., flashy hydrographs; Mazrooei et al., 2017), increased nutrient and metal concentrations, straightened and flattened channel banks and bed (i.e., channelized), reduced biotic richness (Walsh et al., 2005; Abdi and Yasi, 2015), and thermal pollution, characterized by hot urban surfaces (i.e., urban heat island) generating water temperatures above the tolerance of native fauna (Somers et al., 2013). To remediate the urban stream syndrome, urban areas could naturalize stormwater management (Walsh et al., 2005) and reduce the urban heat island, which typically involves the restoration of floodplain and riverine urban areas (Somers et al., 2013, Shafiei Shiva et al., 2019), which typically require flood hazard area development permits (Ohio EPA, 2019).

The ecological impacts of urban river degradation, overall, are extensive and have been the focus of work by scientists, city planners, and policymakers (Somers et al., 2013). There are large economic benefits in reducing river temperature (Seedang et al., 2008), which stem from increasing riverine dissolved oxygen (DO), reducing harmful algal blooms (Anderson et al., 2000), and slowing accelerated eutrophication from nutrient loading (Pretty et al., 2003). Riverine thermal pollution changes riverine ecology by directly and indirectly affecting the metabolism of living organisms, their food webs, and their habitat suitability (Gitay et al., 2002; Stefan and Sinokrot, 1993). Dodds et al. (2009) estimated the damage costs of accelerated eutrophication in the freshwater of the USA at approximately $2.2 billion per year, while Pretty et al., (2003) estimated the

cost in England and Wales at $105-160 million per year. Total maximum daily loads as quantitative thresholds for thermal pollutant sources (Seedang et al. 2008) are established to address river degradation due to thermal pollution (US EPA 2013).

Naturalization of stormwater management and reduction of the urban heat island can be part of holistic plan replacing terrestrial and aquatic grey infrastructure with green infrastructure. Terrestrial grey infrastructure, such as buildings, parking lots, and roads, warms air temperatures and conveys stormwater to gutters and sewers (Somers et al., 2013), and aquatic grey infrastructure, such as bridges and concrete embankments, channelizes and removes nature form the rivers. Terrestrial green infrastructure, such as bioretention basins and bioswales, increase canopy interception and storage of precipitation, soil infiltration rates, plant and soil evapotranspiration, solar shading of runoff, and surface roughness thereby slowing runoff and reducing riverine flooding (US EPA, 2016; Mosleh and Zamani-Miandashti, 2013).

Aquatic green infrastructure, such as riparian vegetation, permeable riverbeds and banks, and in-channel bedform morphology, increases habitat and shading in the aquatic ecosystem, reduces erosion, and induces cooling groundwater inflow and hyporheic exchange (Bernhardt et al., 2005; USDA, 2007). Hyporheic exchange is the natural flux of river water into the near-surface aquifer and groundwater into the river. Eco-hydrologists encourage the restoration of hyporheic exchange through the removal of impervious channels and reshaping bedform morphology with riffle-pool and meander sequences (Hester and Gooseff, 2010). River basin restoration can be managed for the

multiple goals of flood control and improved water quality important for human wellbeing and biodiversity (European Commission 2013; Izadmehr and Rockne; 2018).

The federal and industry standard for reengineering floodplain and riverine urban areas and associated flood hazard analysis is the US Army Corps of Engineers (USACE) Hydrologic Engineering Center River Analysis Software (HEC-RAS) model (FEMA, 2019). The HEC-RAS model has limits with respect to ecological restoration. In the case of thermal restoration, while it simulates river temperature, it neglects the role of riparian shade, substrate, and groundwater-surface water exchange (e.g., hyporheic fluxes) when simulating river temperature, making it difficult to assess whether restoration achieved thermal pollution and flood hazard goals. To create a more holistic model package, we created a set of functions that incorporate HEC-RAS model outputs of river water surface profiles, designed for flood hazard mapping, into the i-Tree Cool River Model (Abdi and Endreny, 2019), designed for ecological restoration. This model package can then simulate how river basin naturalization affects thermal pollution and flood hazard goals (Armal et al., 2018).

The present study aims to create functions that incorporate HEC-RAS model outputs of river water surface profiles, used in flood hazard analysis, into the i-Tree Cool River Model (Abdi and Endreny, 2019). The i-Tree Cool River model updates maintain the HEC-RAS model water surface profiles and allow for inflows of cool groundwater inflows from green infrastructure, riverine shading from riparian trees, and hyporheic exchange in a permeable riverbed. Each model operates by simulating the water and energy balance in reach segments between river cross-sections. The study provides the

i-Tree Cool River model as freeware to plan and design thermal restoration, while optionally using river water surface profile data for flood hazard Methods

3.2 Methods

3.2.1 Study Areas

This study analyzed two watersheds. The first watershed was a 2 km reach of Sawmill (SM) Creek draining a 15 km2 watershed in Tannersville, New York (Fig. S1). The second watershed included 0.5 and 17.5 km reaches of the Los Angeles (LA) River draining a 1270 km2 watershed in LA, California (Fig. 1 and S2). The LA River is situated between Griffith Park and downtown LA and is notable for its channelized form, concrete beds, lack of riffle-pool bedform morphology, and largely devoid of riparian vegetation. The LA River reach is part of the multi-million dollar Los Angeles River Ecosystem Restoration Project managed by the US Army Corps of Engineers (USACE) in partnership with the City of LA (USACE, 2019).

3.2.2 Model Equations

The model used for these simulations is an updated version of i-Tree Cool River model (Abdi and Endreny, 2019). This model was updated to include HEC-RAS model river water surface routines. The i-Tree Cool River model uses standard advection, dispersion, and reaction equations to simulate the water transport and a change in water temperature between two cross-sections. River temperature is estimated as:

$$T = T^{t-1} + \Delta t \left[V \frac{T_{up} - T}{\Delta x} - D_L \frac{T_{up} - 2T - T_{dn}}{(\Delta x)^2} \right] + R_h + R_i \tag{1}$$

where T (°C) is the temperature at a river cross-section, the superscript *t-1* indicates the

prior time, Δt (s) is the time step, the subscript *up* indicates the upstream cross-section,

the subscript *dn* indicates the downstream cross-section, V (m/s) is the cross-section

velocity, Δx (m) is the length of the reach segment bounded by the cross-section and

upstream cross-section, D_L (m²/s) is the reach longitudinal dispersion computed as a

function of cross-section velocity and depth, R_h (°C) is the loss or gain (i.e., reaction

term) of temperature due to heat flux, and R_i (°C) is the loss or gain of temperature due

to lateral inflows (Abdi and Endreny 2019, USACE 2016). The velocity is determined by

a separate set of hydraulic equations, which in steady-state mode involves

simultaneously estimating depth and velocity to satisfy the conservation of energy,

mass, and momentum, i.e., the 5-step algorithm used in HEC-RAS (USACE, 2016),

which is now an alternative to the Newton-Raphson algorithm used in i-Tree Cool River

(see supplementary materials section S1, Abdi and Endreny, 2019).

The heat flux reaction term is defined as:

$$R_h = \frac{\phi}{\rho \cdot C_p \cdot y} \tag{2}$$

where φ (W/m²) is heat flux at the cross-section and represents the heat flux within the

adjacent upstream reach segment, ρ (kg/m³) is water density, C_p (J/kg/°C) is specific heat

of water, and y (m) is water depth at the cross-section (Abdi and Endreny 2019, USACE

2016). For HEC-RAS, φ is the combined terms of shortwave energy flux from solar

radiation, longwave energy flux from atmospheric temperature radiation, longwave

energy flux from river temperature radiation, latent heat flux from wind entraining river

evaporation, and sensible heat flux from wind entraining river temperature. For i-Tree Cool River, φ includes the above HEC-RAS terms, as well as: a) additional parameters in the shortwave radiation and atmospheric longwave radiation calculations to represent the effects of trees, hills and buildings on receiving and emitting radiation via shade and view to sky factors, and b) additional flux terms for vegetation longwave radiation and riverbed substrate radiation (Abdi and Endreny, 2019).

The lateral inflow reaction term is defined as:

$$R_i = \frac{Q_{up}T_{up} + Q_aT_a + Q_bT_b + Q_cT_c}{Q_{up} + Q_a + Q_b + Q_c} - T_{up} \tag{3}$$

where Q (m^3/s) is the discharge, T (°C) is the temperature, and subscripts a, b, and c represent separate inflows to that segment; there is no maximum number of inflows, but the minimum number of inflows is 0 ($R_i = 0$). For HEC-RAS, only lateral inflows of tributaries are simulated, while i-Tree Cool River simulates lateral inflows of tributaries, groundwater, and hyporheic exchange. The groundwater inflow is assigned to each cross-section based on hydrological analysis or differencing the upstream and downstream flow rates, while hyporheic exchange flux is auto-computed by the model as a function of the local substrate conductivity and hydraulic gradient between cross-sections (see Eq S1 in Abdi and Endreny, 2019).

To combine the i-Tree Cool River model simulation of green infrastructure impacts on temperature with the HEC-RAS model simulation of water surface profiles, Eq 1 was modified,

$$T = \frac{\left[T_{up}^{t-1} + \Delta t_r R_{h2}\right] Q}{Q} + \frac{R_{i2}}{Q} \tag{4}$$

where T_{up}^{t-1} is the temperature of the upstream cross-section at the prior time step, Δt_r (s) is the retention time step defined as $\Delta t_r = \Delta x / V$ and V (m/s) is the HEC-RAS velocity at the cross-section, Q (m³/s) is the HEC-RAS discharge at the cross-section, and R_{h2} is the heat flux reaction term, and R_{i2} is lateral inflows reaction term. An updated heat flux reaction term is needed for Eq 4,

$$R_{h2} = \left[\frac{\phi}{\rho \cdot C_p \cdot y} - D_L \frac{\left(\frac{\phi}{\rho \cdot C_p \cdot y \cdot V} - \frac{\phi_{up}}{\rho \cdot C_p \cdot y_{up} \cdot V_{up}} \right)}{\Delta x} \right] \tag{5}$$

where φ is defined to include the i-Tree Cool River model tree-based terms (for more detail, see equation 4 of Abdi and Endreny, 2019). An updated lateral inflows reaction term is needed for Eq 4,

$$R_{i2} = \frac{Q_a T_a + Q_b T_b + Q_c T_c}{Q_a + Q_b + Q_c} \tag{6}$$

where subscripts *a*, *b*, and *c* are defined as the i-Tree Cool River form with Eq 3 above.

3.2.3 Model Inputs and Scenarios

The updated i-Tree Cool River model was run in steady state, defined as $dQ/dt = 0$, and non-uniform conditions, $dQ/dx \neq 0$, where Q is discharge, *t* is time (s), and *x* is river distance (m). This approach keeps the water surface profile constant

86

through time at all locations and allows it to vary with location due to groundwater and other inflows, which is a standard process for flood hazard analysis (USACE, 2016).

3.2.3.1 Sawmill Creek

The simulation of SM Creek on July 2 and 3, 2007 received 0.1 m^3/s baseflow discharge at the upstream boundary cross-section (river station 0 m), then received urban drainage via storm sewers at cross-sections 620 m and 790 m, and lastly received retention basin discharge at cross section 1450 m. The alternative scenarios for the SM Creek are: a) simulating the system without the cooling effect of the subsurface inflow, b) deactivating the warming effect of the lateral inflows from the urban drainage and retention basin, and c) simulating the river temperature with estimated upstream river temperature boundary conditions in place of the observed upstream river temperature boundary condition. In the simulations, the cross-section data needed by the HEC-RAS model were obtained for the SM Creek from field surveys (Crispell, 2008). In the base case scenario for SM Creek, the upstream boundary condition and lateral inflow temperature time series were obtained from observed hourly data (Crispell, 2008). Inputs of hourly weather data including the direct normal irradiance (DNI) and diffuse horizontal irradiance (DHI) shortwave radiation as well as air temperature and relative humidity for SM Creek were obtained from the National Solar Radiation Data Base (NSRDB), at station ID #1227776. The groundwater temperature was set as a function of the annual average air temperature, at 13°C for SM Creek base case and alternative scenarios.

3.2.3.2 LA River

The simulation of the LA River was for June 17 and 18, 2016 for reach lengths of 0.5 and 17.5 km, each with no riparian forest, no riffle-pool bedform and warm surface inflows entering at cross-section 250 m. These base cases were estimated by U.S. Geological Survey StreamStats (U.S. Geological Survey, 2016) to receive 4.34 m^3/s baseflow discharge at the upstream boundary cross-section (0 m). The alternative scenarios for the LA River simulated: a) infiltrating tertiary treated wastewater flows of 0.8 m^3/s (Mongolo et al., 2017) into green infrastructure so it entered the reach as cool groundwater inflow rather than warm surface inflow at cross-section 250 m; b) replacing the featureless channel bottom with riffle-pool bedform morphology to increase hyporheic exchange; c) replacing the bare concrete channel banks with riparian forest to increase shade and reduce substrate and water temperature; and d) expanding the floodplain forest in the LA residential area from 12.1% cover to the potential of 36% cover to cool the air and upstream water temperature, and shade upstream reservoirs. The floodplain forest is defined as any forest extending from the riparian area into the greater watershed, and for this scenario it extended upstream of the study reach. The potential forest cover was inventoried by Endreny et al., (2017).

The analysis was conducted by first running the HEC-RAS model to generate water surface profile data, then running the i-Tree Cool River model with Eqs 4 to 6 in place of Eqs 1 to 3. The cross-section data needed by the HEC-RAS model were obtained for the LA River from document analysis and photo interpretation (Mongolo et al., 2017; USACE, 2015). The HEC-RAS model provided the water surface profile

88

outputs needed by the i-Tree Cool River model for each cross-section: x (m); discharge, Q (m^3/s); minimum channel elevation (m) and water surface elevation (m) used to compute flow depth, y (m); velocity in channel, V (m/s); top width, w (m), flow area (m^2); and wetted perimeter (m). The i-Tree Cool River model resamples HEC-RAS outputs with linear interpolation to refine the spacing of cross-sections to 5 m or finer and resolve spatial variation channel and riparian features and reduce inconsistencies between temperature and hydraulic transport in Eq 1.

The i-Tree Cool River model uses the resampled HEC-RAS outputs along with the boundary condition temperatures, radiation fluxes, shading, substrate, and other features affecting river temperature estimates. For the LA River hourly temperature data did not exist, and base case data were generated using a two-step process: 1) applying a non-linear regression (Mohseni et al., 1998) transforming hourly air temperature into river temperature, with air temperature from nearby Burbank Airport station, and regression coefficients of α=32.48, β=15.18, and γ=0.17 (Eq 7); and 2) applying a linear regression transforming the 1st estimate to match observed June river temperature statistics at the upstream boundary, with slope 1.206 and intercept 1.665 determined from the linear regression between the minimum and maximum river temperatures from observed June 2016 data (Mongolo et al., 2017) and the 1st estimate of river temperature. This linear regression was used to match inflow temperatures not predicted by the non-linear regression with air temperature is presumed to account for the urban heat island impact, including warm surface inflows from tertiary treated wastewater in upstream lakes (e.g., the Japanese Garden Lake and Balboa Recreation

Lake) noted by Mongolo et al., (2017). Inputs of hourly weather data including the DNI and the DHI shortwave radiation for the LA River were obtained from the NSRDB, at station ID #81603.

$$T_w = \mu + \frac{\alpha - \mu}{1 + e^{\gamma(\beta - T_{air})}} \tag{7}$$

The groundwater temperature was set as a function of the annual average air temperature, at 20°C for the LA River base case and restoration scenarios. The LA River scenario with floodplain forest expansion was estimated to cool the June 17-18, 2016 air temperatures due to evapotranspiration, simulated by i-Tree Cool Air (Yang et al., 2013). These scenario air temperatures, with an average of 21.5℃ (2.2°C cooler than the base case), were used in the non-linear regression of Mohseni et al., (1998) to estimate new river temperatures, with an average of 25.1℃, which represented mitigation of the urban heat island (see Table 1). The LA River riparian forest scenario was estimated to increase the shade factor from 0, no shade, to 1, full shade, and cool June 17-18, 2016 average river substrate temperature from 32℃ to 27℃, based on analysis of daily average June to August river corridor temperatures provided by Weng and Fu (2014). Details on other i-Tree Cool River model inputs used to simulate temperature are provided in the supplementary materials section S1, and a manual and sample inputs can be downloaded at http://www.itreetools.org/research_suite/coolriver/.

3.3 Results

3.3.1 The SM Creek

The simulated and observed average river temperature for SM Creek was 13.8°C, and spatial and temporal variation in that temperature was used for validation of the i-Tree Cool River model; the model was not calibrated to the observed data. The temporal pattern in simulated and observed reach-averaged river temperature captured the sinusoidal heating and cooling due to diurnal variation in radiation, with additional temporal variation due to cloud cover, and wind (Fig. S3). The model simulation underestimated the observed variation in river temperature by 0.85°C, split between overestimating the nighttime minimum and underestimating the daytime maximum temperature. The spatial performance of the i-Tree Cool River model in SM Creek was assessed against observed data at 12 cross-sections, with water entering the reach at 12.5°C and warming by 3.6°C due to lateral inflows, primarily from a surface reservoir. At the upstream boundary, the model used observed values and hence had a perfect coefficient of determination R^2 of 1 (Fig. S4), and at the other 11 locations the smallest R^2 was 0.8, the largest R^2 was 0.95, and the average R^2 was 0.88. To validate the model, a Nash-Sutcliffe Efficiency (NSE) metric was used to assess the goodness of fit between observed and simulated reach-average time series, achieving an NSE of 0.93, close to the perfect NSE of 1. The simulated vs observed time series had a coefficient of determination R^2 of 0.95, and a root mean square error (RMSE) of 0.1°C. A statistical t-test of the observed and simulated temperature time series having no meaningful difference, with an α=0.05, had a p-value of 0.90, showing there was no meaningful

difference between the simulated and observed temperatures. To understand the role of different drivers of urban river temperature to guide the LA River restoration scenarios, a sensitivity analysis was conducted to confirm the importance of cool groundwater inflow and hyporheic exchange, warm surface water inflows, and a cool upstream boundary condition (Fig. 5S).

3.3.2 The LA River

The simulated river temperature in the LA River for the base case 0.5 km reach length had an average river temperature of 28.7°C, with a diurnal pattern of warming and cooling (Fig. 3), and the average temperature rose by 0.05°C per km to 29.5°C at the 17.5 km reach length (see Table 2). The average river temperature associated with each restoration scenario was then subtracted from the base case river temperature at the equivalent reach length to generate the cooling, noted as ΔT in Table 2. The paired-samples t-test with $\alpha = 0.05$ showed significant differences ($p < 0.05$) between simulated average river temperatures for each scenario and those of its 0.5 or 17.5 km reach length base case. The scenario of using green infrastructure inflows of infiltrated treated wastewater entering the river at groundwater temperature generated a ΔT of 0.3°C from the 17.5 km reach base case (Table 2). The scenario of using riffle-pool bedform morphology to increase hyporheic exchange generated a ΔT of 0.7°C from the 17.5 km reach base case. Combining the restoration treatments of green infrastructure and riffle-pool bedforms generated a ΔT of 0.9°C from the 17.5 km reach base case, with the simulated average water temperature still increasing by 0.01°C per km of reach due to the absence of riparian forest and full solar exposure on the river. Combining the

restoration treatment of riparian shade with the restoration of green infrastructure and riffle-pool bedforms generated a ΔT of 4.4°C from the 17.5 km reach base case, with the simulated average water temperature now decreasing by 0.17°C per km of reach.

The single scenario of riparian shade generated a ΔT of 3.6°C from the 17.5 km reach base case, with average water temperature decreasing by 0.14°C per km of reach when cooling was not provided by the riffle-pool hyporheic exchange and green infrastructure induced groundwater inflows. Combining the four restoration treatments of floodplain forests with riparian shade, green infrastructure, and riffle-pool bedforms generated the largest ΔT of 7.2°C from the 17.5 km reach base case, 64% cooler than the ΔT of 4.4°C when riparian shade, green infrastructure, and riffle-pool bedforms were combined. The combination of 4 restoration treatments caused average water temperature to decrease by 0.15°C per km of reach. The impact of the floodplain forest scenario cools the upstream boundary river temperature, and when combined with the riparian forest this cooler water propagates down river. This is evident in the 0.5 km reach when comparing the ΔT of 3.5°C for the scenario with only riparian shade and floodplain forest and ΔT of 0.7°C for the scenario combining treatments of riparian shade, green infrastructure, and riffle-pool bedforms.

The simulated cooling of the LA River temperature by the restoration scenarios led to the potential for higher saturated DO levels (Fig. 4). The percent difference between the average DO associated with each base case and restoration scenario, relative to the base case at the equivalent reach length of 0.5 or 17.5 km, was used to compute the ΔDO (%). The lowest DO saturation was 7.6 mg/L for the 17.5 km reach

base case, and the highest DO saturation was 8.7 mg/L for the 17.5 km reach with all

four treatments. The restoration scenarios without riparian shade on the 17.5 km reach

had an average ΔDO_{sat} of 2% (Fig. 4). The scenario of riparian shade as the only

restoration treatment increased the ΔDO_{sat} to 6%, and the combination of riparian

shade, green infrastructure, and riffle-pool bedforms increased the ΔDO_{sat} to 8%. The

scenario of floodplain forests increased the ΔDO_{sat} to 12.5%, while the combination of all

4 restoration treatments increased the ΔDO_{sat} to 14.5%. The error bars about the ΔDO_{sat}

values represent uncertainty in model view-to-sky factors, generating ±0.2°C variation in

river temperatures, which led to 0.08 to 0.12 mg/L variation in DO_{sat} and a ±0.5% to

±1.6% error bar, with smaller values for the lower percentages.

3.4   Discussion

This study updated i-Tree Cool River model to utilize water surface profile data

from the HEC-RAS model and thereby coordinate evaluations of thermal and flood

hazard impacts. By coupling the hydraulic transport model of HEC-RAS with the

temperature transport model of i-Tree Cool River, Eq 4 can lead to differences in the

volume of water predicted by the two transport models. This is due to the first right hand

side term in Eq 4 representing temperature transport as plug flow, with upstream

temperature from the prior time step replacing downstream temperature in the current

time step, even when upstream and downstream volumes may not be equal for each

reach segment. To avoid this continuity error, the i-Tree Cool River model maintains the

HEC-RAS model volume for each reach segment, and uses cross-section spacing of 5

m or less to constrain the error in the temperature estimate.

94

This HEC-RAS model has a similar continuity error problem when combining its

hydraulic and temperature transport models. The HEC-RAS manual (USACE, 2016)

explains Eq 1 can also lead to cross-section volume predictions that are slightly different

than the volume predicted by the HEC-RAS hydraulic model used to determine water

surface profiles. To handle this continuity error, the HEC-RAS model corrects the

temperature model volume and allow erroneous estimates in temperature, or it

maintains the temperature model volume and allows erroneous estimates in water

depth and velocity (USACE, 2016). Users can alternatively perform these simulations

without the HEC-RAS model outputs, using Eq 4 to 6 with the i-Tree Cool model version

of the HEC-RAS model 5-step hydraulic routine, or with Eq 1 to 3, by selecting these

options in the configuration file. An advantage of using the HEC-RAS model to generate

the water surface profile is its ability to simulate a vast array of aquatic grey

infrastructure, e.g., bridges, gates, weirs, culverts, channel constrictions, and levees.

The reduction in warm water inflows at the upstream boundary and along the

reach was a major contribution to the cooling of the LA River in simulations by the i-Tree

Cool River model, an outcome supported by field observation and prior model

development. The thermal impact of warm surface inflows was observed in the cool

mountain area of SM Creek in NY when a lateral reservoir inflow caused a 2.4°C

warming of river temperature, the greatest warming along the reach (see Fig. S3 and

S5). In the South Fork Yuba River of California, selective withdrawal from deeper,

cooler layers within reservoirs is the recommended strategy to decrease summer river

temperatures (Rheinheimer et al., 2015). The amount of cooling is a function of the relative volume and temperatures of the inflow compared with the river flow. Null et al. (2017) needed to increase the inflow of 21°C reservoir water to 40% of the river flow during the 2015 summer in order to reduce >28°C water temperatures on the East Walker River of Nevada by 5°C and bring DO levels above 5 mg/L to reduce fish stress. Nichols et al. (2014) documented how cool groundwater inflows could mimic reservoir releases to lower the temperature of a Shasta River tributary in northern California, but how the unshaded tributary allowed this cool water to warm as it flowed downstream. This LA River simulations captured a similar phenomenon, generating 20°C groundwater inflows by infiltrating warm surface waters in green infrastructure, which entered the river at 18% of its flowrate in the first 0.5 km section, decreasing the average river temperature by 0.3℃ yet not reversing the downstream warming trend in river temperature.

Periodic instances of hyporheic exchange along the reach length had a larger cooling effect in the LA River simulations than the instance of groundwater inflow via green infrastructure within the first 0.5 km. Loheide and Gorelick (2006) observed the importance of periodic instances of hyporheic exchange in a restored section of Cottonwood Creek in northern California caused summer river temperatures to cool in the downstream direction, and then simulated how its absence led to river temperatures to warm in the downstream direction. This concept was used with the riffle-pool bedform simulations along the LA River, which induced regular replacement of 10% of the warm river water with 20°C groundwater and led to a 0.7°C cooling of average river

temperatures. Loheide and Gorelick (2006) also showed how periodic inflows of groundwater also cooled the river in the downstream direction, and Risely et al. (2010) warn of the loss of such subsurface inflows, documenting how the pumping of wellfields reduced inflows by 18% and caused summer river temperatures to warm by 0.5°C.

The urban heat island phenomena warms the surface and air of Los Angeles (Weng and Fu, 2014), and this can be mitigated with forest plantings (Endreny, 2018; Yang et. al., 2013). In the LA River scenarios, the ambient air temperature was simulated to decrease by 2.2°C as a result of establishing riparian and floodplain forest a restoration treatment, leading to a decrease in average river temperature of 6.4°C for the 17.5 km reach. The restoration scenario of riparian shading as the only restoration treatment led to a decrease in average river temperature of 3.6°C for the 17.5 km reach, which is a response supported by other studies. Ketabchy et al. (2019) used a watershed heat budget model to demonstrate urban forest expansion cooled July and August 2015 water temperature in Stoubles Creek, Virginia by 1.4°C to help meet targets for native fish habitat. Roth et al. (2010) simulated how the loss of urban riparian forest along the Boiron de Morges River in Switzerland warmed August 2007 average maximum air temperature by 1.6°C and river temperature by 0.7°C. Sun et al. (2015) showed how observed and modeled peak river temperatures in Mercer Creek of Washington has decreased by 4°C in reaches that had more riparian and floodplain forest.

Decreasing the river temperature in the LA River would improve the saturation DO level, and thereby lead to better habitat for desired fish and other aquatic

97

organisms. Our LA River scenario of all 4 restoration treatments lowered river temperature by 7.2℃, resulting in a 14.5% increase in DO_{sat} level, improving conditions for desired fishes. As of 2011, 83% of California's native inland fish were extinct or declining (Moyle et al., 2011), and Carter (2005) reports in southern California, cold-water fishes such as trout (Oncorhynchus mykiss) avoid areas with DO less than 5 mg/L; for trout eggs, DO levels below 11 mg/L will delay their hatching, and DO below 8 mg/L will impair young trout growth and lower their survival rates. Due to climate change, the warm season river temperatures in the Sierra Nevada of California are predicted to increase by up to 5.5℃ by 2100, resulting in a 10% decrease in DO levels (Ficklin et al., 2013). Lower DO levels are a major reason for the hypoxic system in the LA River estuary (Diaz and Rosenberg, 2008), likely caused by excess loading of nutrients from human activity (Booth, 2015). The model developed in this study can assist planners such as those involved in the LA River restoration, where restoration might include floodplain and riparian forests for wildlife habitat and riffle-pool bedform morphology to encourage native fish habitat (USACE, 2015).

3.5   Conclusions

In this study, an updated version of i-Tree Cool River model was created to assess thermal restoration using water surface profile data from the HEC-RAS model. The updated i-Tree Cool River model can help planners assess the thermal benefit of floodplain and riverine restoration that naturalizes the hydrologic cycle, using HEC-RAS model water surface profiles approved for flood hazard mapping. Various restoration

scenarios were simulated on a 17.5 km reach of the LA River targeted for ecological restoration. Findings are summarized as:

- Groundwater inflows coming from surface inflows that had been infiltrated to green infrastructure decreased the average river temperature by 0.3℃.

- Hyporheic exchange coming from riffle-pool bedforms decreased the average river temperature by 0.9℃.

- Diminished shortwave radiation from riparian forests decreased average river temperatures by 3.6℃.

- Lower air temperatures and upstream reservoir temperatures decreased the temperature of the river at its upstream boundary, and when combined with the 3 above restoration treatments decreased average river temperature by 7.2°C.

3.6   References

Abdi, R., Endreny, T.A., (2019). Urban river temperature modeling of unsteady stormwater inflows and riparian shading. Water. 11(5), 1060

Abdi, R., Yasi, M., 2015. Evaluation of environmental flow requirements using eco-hydrologic-hydraulic methods in perennial rivers. Water Science and Technology. 72(3), 354–363.

Anderson, D.M., Hoagland, P., Kaoru, Y., White, A.W., (2000). Estimated annual economic impacts from harmful algal blooms (HABs) in the United States. Woods Hole (MA): Department of Biology, Woods Hole Oceanographic Institution. WHOI-2000-11.

Armal, S., Devineni, N., Khanbilvardi, R.M. (2018). Trends in extreme rainfall frequency in the contiguous united states: Attribution to climate change and climate variability modes. 31(1), 369-385.

Bernhardt, P. M. A., A. J. D. Alexander, G. K. Barnas, S. Brooks, J. Carr, S. Clayton, C. Dahm, J. Follstad-Shah, D. Galat, S. Gloss, P. Goodwin, D. Hart, B. Hassett, R. Jenkinson, S. Katz, G. M. Kondolf and P. S. Lake (2005). "Synthesizing River Restoration Efforts." Science, 308, 636-637.

Bodnaruk, E.W., Kroll, C.N., Yang, Y., Hirabayashi, S., Nowak, D.J., Endreny, T.A. (2017). Where to plant urban trees? A spatially explicit methodology to explore ecosystem service tradeoffs. Landscape and Urban Planning. 157, 1872-6062.

Booth, A. (2015). State of the Bay Report. Looking Ahead: Nutrients and Hypoxia. Urban Coast, 5(1), 190-193.

Carter, K., (2005). The effects of dissolved oxygen on steelhead trout, Coho Salmon, and Chinook Salmon biology and function by life stage. California Regional Water Quality Control Board, North Coast Region.

Chen, W.Y. (2017). Environmental externalities of urban river pollution and restoration: A hedonic analysis in Guangzhou (China). Landscape and Urban Planning, 157, 170–179.

Crispell, J.K., (2008). Hyporheic exchange flow around stream restoration structures and the effect of hyporheic exchange flow on stream temperature. Master of

science degree thesis. State University of New York, College of Environmental Science and Forestry. 63 pp

Diaz, R., & Rosenberg, R. (2008). Spreading dead zones and consequences for the marine ecosystem. Science, 5891, 926-929

Dodds, W.K., Bouska, W.W., Eitzmann, J.L., Pilger, T. J., Pitts, L., Riley, A. J., … Thornbrugh, D. J. (2009). Eutrophication of U. S. freshwaters: Analysis of potential economic damages. Environmental Science and Technology, 43(1), 12–19.

Endreny, T.A. (2018). "Strategically growing the urban forest will improve our world." Nature Communications, 9(1): 1160.

Endreny, T.A., Santagata, R., Perna, A., De Stefano, C., Rallo., R.F., Ulgiati, S. (2017). Implementing and managing urban forests: a much needed conservation strategy to increase ecosystem services and urban wellbeing. Ecological modelling, 360, 328-335.

European Commission. (2013). Individual natural water retention measures (NWRM): Stream Bed Re-Naturalization. European Commission. 11 pp.

FEMA (2019). Hydraulic Numerical Models Meeting the Minimum Requirement of National Flood Insurance Program, https://www.fema.gov/hydraulic-numerical-models-meeting-minimum-requirement-national-flood-insurance-program.

Ficklin, D.L., Stewart, I.T., & Maurer, E.P., (2013). Effects of climate change on stream temperature, dissolved oxygen, and sediment concentration in the Sierra Nevada in California. Water Resources Research, 49, 2765–2782.

Gitay, H., Suárez, A., Watson, R., Dokken, D.K. (2002). Climate change and biodiversity. Intergovernmental Panel on Climate Change (IPCC), 24, 77 pp.

Hester, E. T. and M. N. Gooseff (2010). "Moving Beyond the Banks: Hyporheic Restoration Is Fundamental to Restoring Ecological Services and Functions of Streams." Environmental Science & Technology, 44(5): 1521-1525.

Izadmehr, M., Rockne, K. (2018). "Pocket Wetlands" for Nutrient Removal in Tile-Drained Agriculture. Talk session presentation at World Environmental and Water Resources Congress. Minneapolis, MN.

Ketabchy, M., D. J. Sample, T. Wynn-Thompson and M. N. Yazdi (2019). "Simulation of watershed-scale practices for mitigating stream thermal pollution due to urbanization." Science of The Total Environment 671: 215-231.

Loheide, S.P., and Gorelick, S.M. (2006). Quantifying Stream-Aquifer Interactions through the Analysis of Remotely Sensed Thermographic Profiles and In Situ Temperature Histories. Environmental Science & Technology, 40(10), 3336–3341.

Mazrooei, A., Sinha, T., Sankarasubramanian, A., Kumar, S., Peters-Lidard, C.D., (2017). Decomposition of sources of errors in seasonal streamflow forecasting over the U.S. Sunbelt. Journal of Geophysical Research. 120(23), 11809-11825.

Mohseni, O., Stefan, H.G., & Erickson, T.R. (1998). A nonlinear regression model for weekly stream temperatures. Water Resources Research, 34(10), 2685.

Mongolo, J., Trusso, N., Dagit, R., Aguilar, A.A., Drill, S.L. (2017). A longitudinal temperature profile of the Los Angeles River from June through October 2016: Establishing a baseline. Southern California Academy of Sciences. 26 pp.

Mosleh, L., Zamani-Miandashti, N. (2013). An investigation of objectives and problems of Shiraz green belt. International Journal of Advanced Biological and Biomedical Research. 1(10), 1246-1252.

Moyle, P.B., Katz, J.V.E., Quinones, R.M. (2011). Rapid decline of California's native inland fishes: a status assessment. Biol. Conserv. 144, 2414e2423.

Nichols, A.L., Willis, A.D., Jeffres, C.A., & Deas, M.L. (2014). Water temperature patterns below large groundwater springs: Management implication for Coho Salmon in the Shasta River, California. River Research and Applications, 30, 442–455.

Null, S.E., Mouzon, N.R., & Elmore, L.R., (2017). Dissolved oxygen, stream temperature, and fish habitat response to environmental water purchases. Journal of Environmental Management, 197, 559–570

Ohio EPA (2019). Nonpoint Source Program - Permitting Guidance for Stream

 Restoration Projects, accessed at:

 https://www.epa.state.oh.us/portals/35/nps/319DOCS/FINAL%20Stream%20Res

 toration%20Permitting%20GUIDANCE%2001-07.pdf.

Pretty, J.N., Mason, C.F., Nedwell, D.B., Hine, R.E., Leaf, S., & Dils, R. (2003).

 Environmental costs of freshwater eutrophication in England and Wales.

 Environmental Science and Technology, 37(2), 201–208.

Rheinheimer, D. E., S. E. Null and J. R. Lund (2015). Optimizing Selective Withdrawal

 from Reservoirs to Manage Downstream Temperatures with Climate Warming.

 Journal of Water Resources Planning and Management 141(4): 04014063.

Risley, J.C., Constantz, J., Essaid, H., & Rounds, S. (2010). Effects of upstream dams

 versus groundwater pumping on stream temperature under varying climate

 conditions. Water Resources Research, 46(6).

Roth, T.R., Westhoff, M.C., Huwald, H., Huff, J.A., Rubin, J.F., Barrenetxea, G.,

 Parlange, M.B. (2010). Stream temperature response to three riparian vegetation

 scenarios by use of a distributed temperature validated model. Environmental

 Science and Technology, 44(6), 2072–2078.

Shafiei Shiva, J., Chandler, D.J., Kunkel, K.E. (2019). Localized Changes in Heatwave

 Properties across the USA. Earth's Future. 7. 10.1029/2018EF001085

Seedang, S., Fernald, A.G., Adams, R.M., & Landers, D.H. (2008). Economic analysis of water temperature reduction practices in a large river floodplain: an exploratory study of the Willamette River, Oregon. River Research and Applications, 24, 941–959.

Somers, K. A., E. S. Bernhardt, J. B. Grace, B. A. Hassett, E. B. Sudduth, S. Wang and D. L. Urban (2013). "Streams in the urban heat island: spatial and temporal variability in temperature." Freshwater Science, 32(1): 309-326.

Stefan, H.G., & Sinokrot, B.A. (1993). Projected global climate change on water temperatures in five north-central U.S. streams. Climatic Change 24: 353–381.

Sun, N., Yearsley, J., Voisin, N., & Lettenmaier, D.P. (2015). A spatially distributed model for the assessment of land use impacts on stream temperature in small urban watersheds. Hydrological Processes, 29(10), 2331–2345.

US Army Corps of Engineers. (2016). HEC-RAS River Analysis System Hydraulic Reference Manual Version 5.0, CPD-68. US Army Corp of Engineers, Hydrologic engineering center, 960 pp.

US Army Corps of Engineers. (2015). Los Angeles River Ecosystem Restoration Feasibility Study. U.S. Army Corps of Engineers, Los Angeles District, 623 pp

US Army Corps of Engineers. (2019). Los Angeles River Ecosystem Restoration Project, https://www.spl.usace.army.mil/Missions/Civil-Works/Projects-Studies/Los-Angeles-River-Ecosystem-Restoration/

USDA-NRCS (2007). National Engineering Handbook - Part 654 Stream Restoration

Design Washington, DC, United States Department of Agriculture, Natural

Resources Conservation Service: 6: 6-36.

US EPA. (2013). EPA Periodic Retrospective Review of Existing Regulations; Reducing

Reporting Burden under Clean Water Act Sections 303 (d) and 305 (b). U.S.

Environmental Protection Agency, 303, 68 pp.

US EPA (2016). Community solutions for stormwater management, A Guide for

Voluntary Long-Term Planning. U.S. Environmental Protection Agency Office of

Water, 16 pp. www.epa.gov/npdes/stormwater-planning

Walsh, C. J., A. H. Roy, J. W. Feminella, P. E. Cottingham and P. M. Groffman (2005).

"The urban stream syndrome: Current knowledge and the search for a cure." J.

N. Am. Benthol. Soc. 24.

Weng, Q. and P. Fu (2014). "Modeling annual parameters of clear-sky land surface

temperature variations and evaluating the impact of cloud cover using time series

of Landsat TIR data." Remote Sensing of Environment 140: 267-278.

Yang, Y., Endreny, T.A., & Nowak, D.J. (2013), A physically based analytical spatial air

temperature and humidity model, Journal of Geophysical Research

Atmospheres, 118, 1–15.

https://lakestewardsofmaine.org/wp-content/uploads/2014/01/Maximum-Dissolved-

Oxygen-Concentration-Saturation-Table.pdf

3.7   Supplementary Materials

The performance of i-Tree Cool River Model in SM Creek was assessed at each of the 12 cross-sections along the simulated reach (Fig. S4). Due to thermal loading in the river from the urban storm sewers and reservoir, there is a trend of increasing water temperature with distance downstream as the river leaves the forest headwater. There average temperature is 12.5°C at the headwater cross-section (XS 01), which increases to 16.2°C in the last cross-section (XS 12). The average R^2 for the 12 cross-sections was 0.88. In the default mode used for this study, in the first timestep the model sets simulated river water temperature equal at all cross-sections, using the value of the upstream boundary condition at timestep 1. Due to this initial condition, the model will likely underestimate observed temperature for the first timestep at downstream cross-sections. The average value of this underestimation for XS 02 to XS 10 was 0.4°C and became as large as 3.4°C for the XS 11 and XS 12 which are located downstream of the reservoir inflow from Gooseberry Creek.

The i-Tree Cool River Model simulated inflows of warm water to SM Creek at cross-section 960 m due to storm sewers entering upstream, and at 2 km due to a reservoir entering via a tributary (Fig. S5a). The lateral inflows were the primary reason for water temperatures to increase by 3.6°C along the length of the reach, from 12.5°C at the headwater to 16.2°C at the outlet. While this warming had average slope of 0.18°C per 100 m, the observed data showed steeper increases in river temperature between cross-sections 600 m and 960 m at a rate of 0.2°C per 100 m, and between cross-sections 1440 m and 2 km at a rate of 0.5°C per 100 m. In areas without inflows,

the heat flux terms of Eq. 3 drove the warming, with water temperature between cross-sections 0 m and 600 m increasing by 0.1 °C per 100 m, and water temperature between cross-sections 960 m and 1440 m the increasing by 0.02°C per 100 m.

The validated i-Tree Cool River Model was next used to examine the individual impacts of groundwater discharge, hyporheic exchange flow, lateral inflows, and shading on the SM Creek temperature. By removing groundwater discharge and hyporheic exchange, the simulated average river temperature increased to 14.6°C from 13.8°C, at a rate of 0.2°C per 100 m, and was 0.8°C warmer than the average observed river temperature (Fig. S5b). The removal of these subsurface inflows caused the model RMSE to worsen from 0.1°C to 0.8°C. When the lateral inflows from storm sewers and the reservoir were removed from the simulation, but subsurface inflows remained, the simulated average river temperature decreased from 13.8°C to 13.3°C with a growth rate of 0.1°C per 100 m, and caused the model to underestimate observed temperatures by 0.5°C for all cross-sections (Fig. S5c). The removal of the lateral inflows caused the model RMSE to increase from 0.1°C to 1.0°C, and the R^2 worsened from 0.95 to 0.86. The removal of the upstream forest caused a warming of the upstream air temperature, which increased the water temperature at the upstream boundary, and caused the simulated average river temperature to increase by 17.2 ℃ from 15.2 ℃. This warmer boundary condition, together with removing riparian shading from the simulation caused the average river temperature to increase from 13.8°C to 15.2°C. The influence of the shading alone caused a warming growth rate of 0.1°C per 100 m (Fig. S5d).

3.8 Tables

Table 8 (Table 1): The i-Tree Cool River inputs of average temperature for air, groundwater, upstream boundary condition, substrate, and surface runoff for the base case and restoration scenarios.

Temperature (°C)	Scenarios		
	Full Sun (No riparian or floodplain forest expansion)	Riparian Forest (No floodplain forest expansion)	Riparian Shade and Floodplain Forest Expansion
Air	23.7	23.7	21.5
Groundwater	20.0	20.0	20.0
Boundary conditions	28.6	28.6	25.1
Substrate	32.0	32.0	27.0
Surface runoff	30.0	30.0	30.0

Table 9 (Table 2): The i-Tree Cool River model simulated average river temperature (°C) in the 0.5 and 17.5 km reach lengths of the LA River for base case and all scenarios, and the temperature differences (°C) between each scenario and the base case for the same reach length row.

Reach length (km)	Var. (°C)	Full Sun (No riparian or floodplain forest expansion)				Riparian Shade (No floodplain forest expansion)				Riparian Shade and Floodplain Forest Expansion			
		No Riffle-Pools		With Riffle-Pools		No Riffle-Pools		With Riffle-Pools		No Riffle-Pools		With Riffle-Pools	
		No GI	GI	No GI	GI	No GI	GI	No GI	GI	No GI	GI	No GI	GI
0.5	T	28.7	28.6	28.5	28.4	28.3	28.2	28.1	28.0	25.2	25.1	25.0	24.9
	ΔT	0.0	0.1	0.2	0.3	0.4	0.5	0.6	0.7	3.5	3.6	3.7	3.8
17.5	T	29.5	29.2	28.8	28.6	25.9	25.7	25.4	25.1	23.1	22.9	22.5	22.3
	ΔT	0.0	0.3	0.7	0.9	3.6	3.8	4.1	4.4	6.4	6.6	7.0	7.2

3.9 Figures
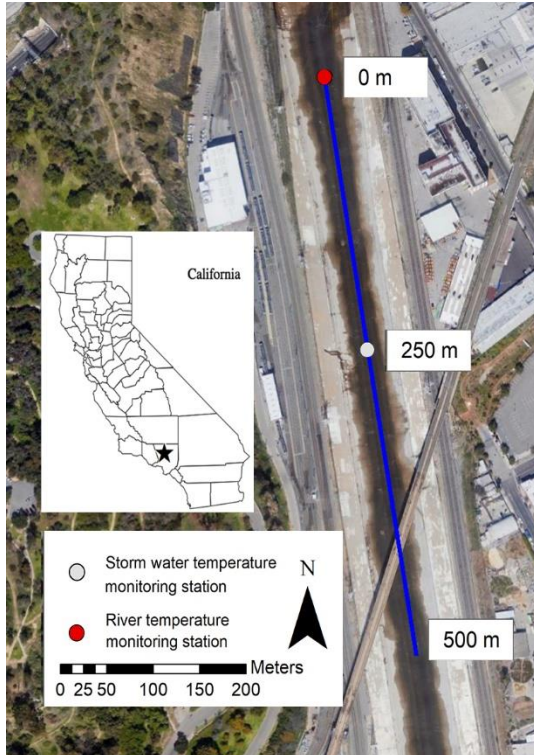
Figure 14 (Figure 1): The monitoring station of the LA River upstream boundary cross-section and a surface water inflow location. The inset with star shows the site locaiton within the state of California.
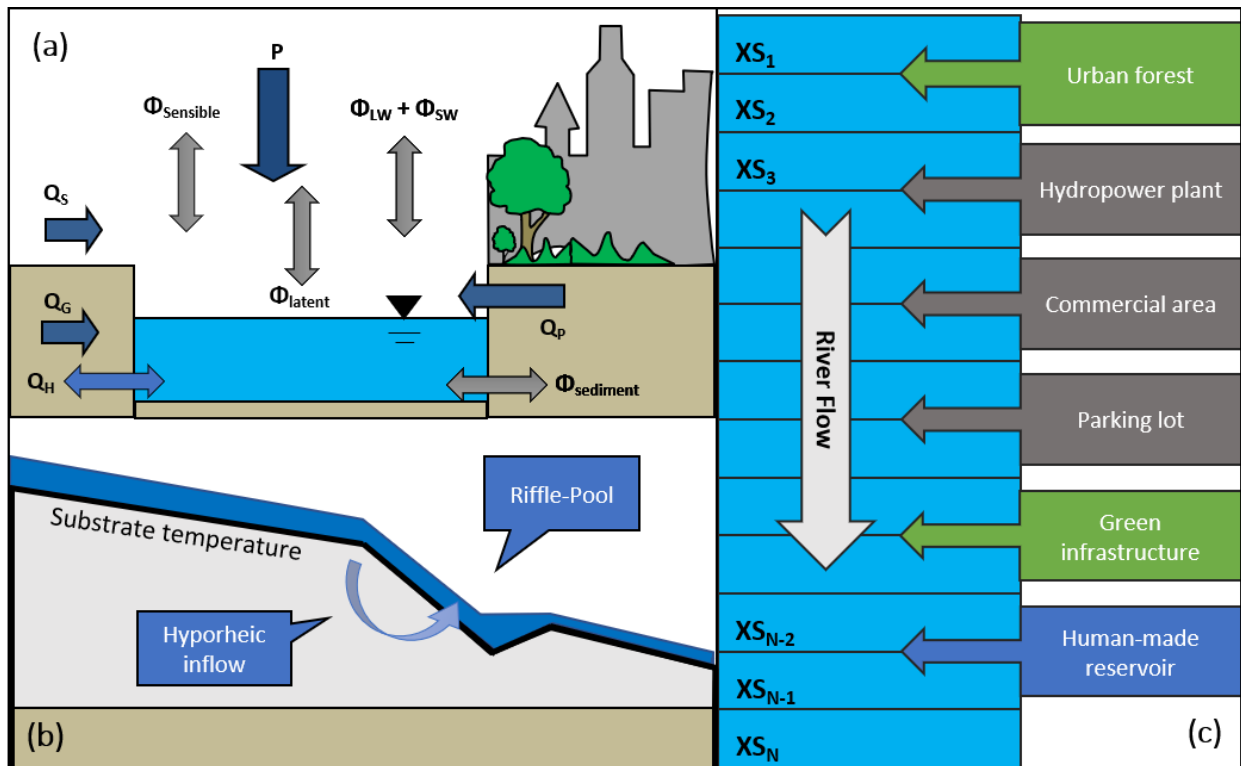
Figure 15 (Figure 2): Schematics of the i-Tree Cool River model: (a) River cross-section view, demonstrating the energy and water balances. In this figure, *P* represents precipitation, and Q_S, Q_G, and Q_P represent the surface flow, groundwater flow, and pipe flow, respectively. Φ is the heat flux, and subscripts LW is longwave radiation flux, SW is shortwave radiation flux, latent is latent heat flux, sensible is sensible heat flux, and sediment is bed sediment heat flux; (b) River longitudinal section for a riffle-pool bedform. The hyporheic inflow pathways around the riffle-pool and substrate temperature are shown in the panel; and (c) River plan view demonstrating the lateral inflows that can be added to the river flow in either dry or wet weather. *XS* represents the cross-section of the river reach.
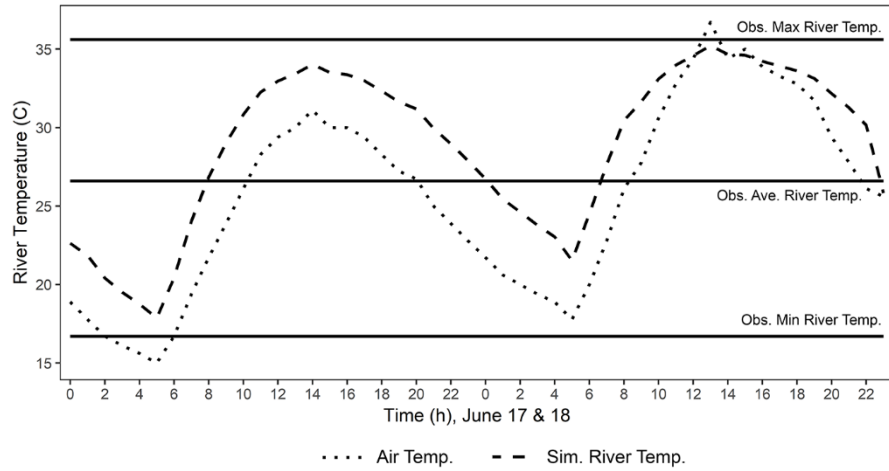
Figure 16 (Figure 3): The hourly observed air temperature and simulated river temperature in the LA River for June 17 to 18, 2016 with the observed average, minimum, and maximum river temperatures for the month of June.
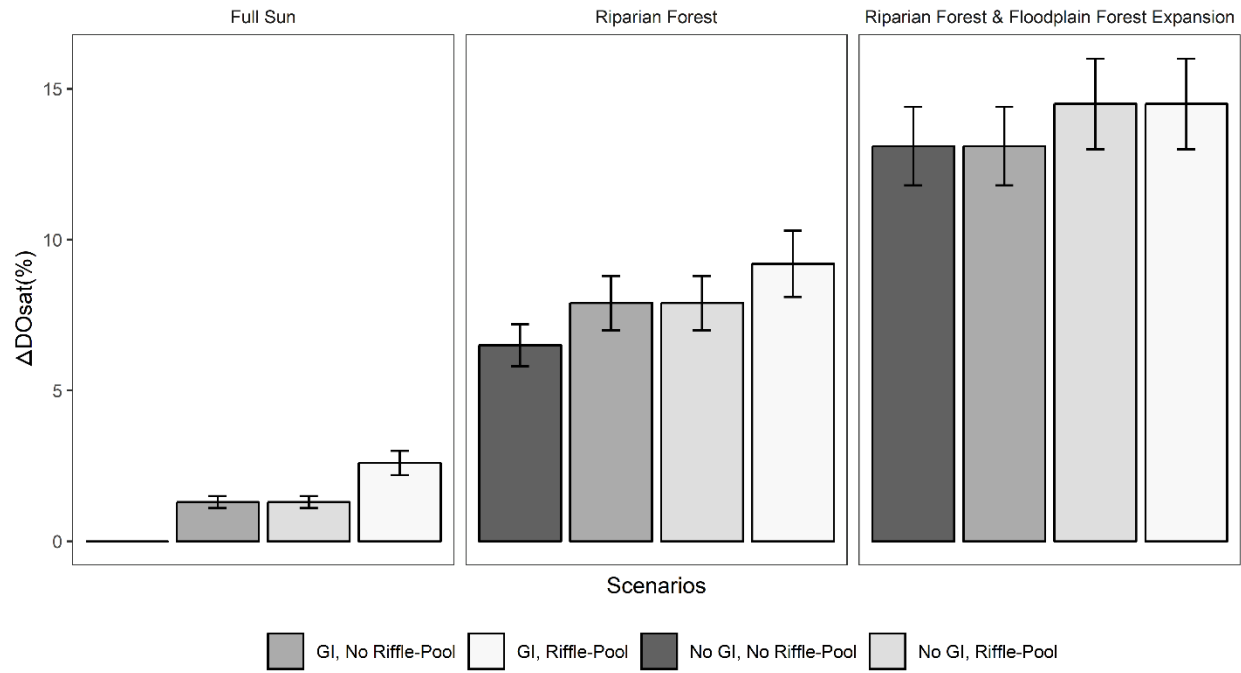
Figure 17 (Figure 4): The simulated average change (%) in saturated DO between the base case and all restoration scenarios for the 17.5 km reach of the LA River, June 17 to 18, 2016. The error bars show the uncertainty levels in the percentage of the ΔDO_{sat} associated with the view-to-sky factor.
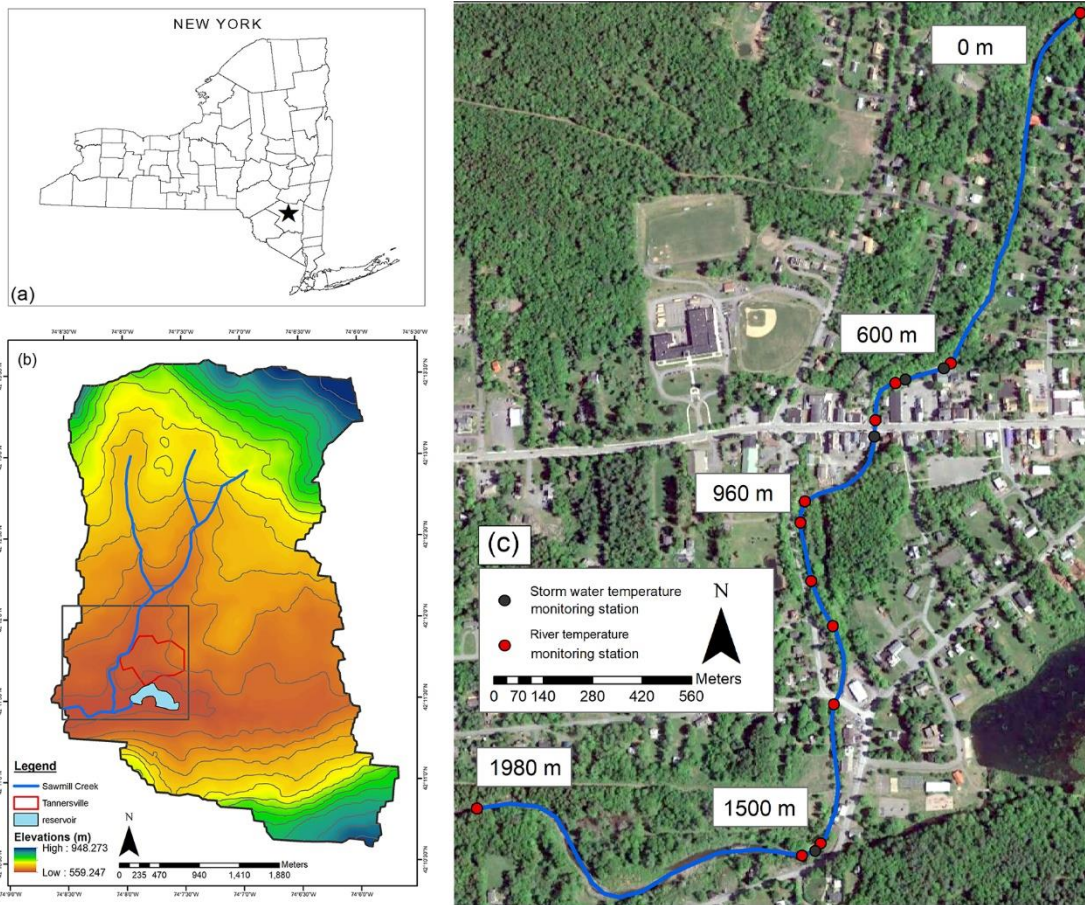
Figure 18 (Figure S1): (a) New York State (NYS) with the study area (b) Location of the SM Creek watershed within the study sites outlined by a black box. (c) Monitoring stations of the study site in the SM Creek, NY.
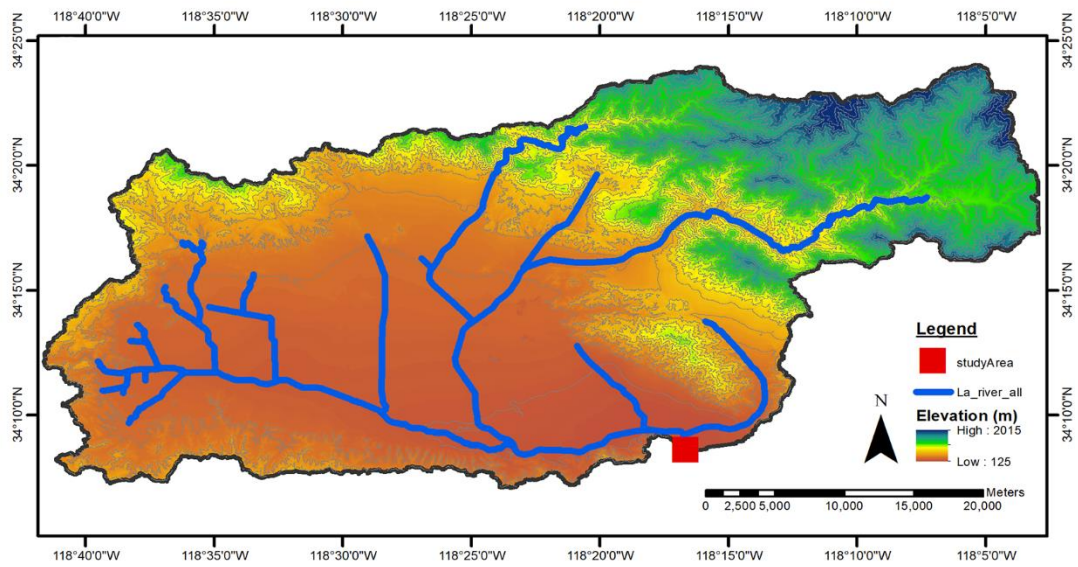
Figure 19 (Figure S2): Location of he LA River watershed within the study sites shown by a redpoint.
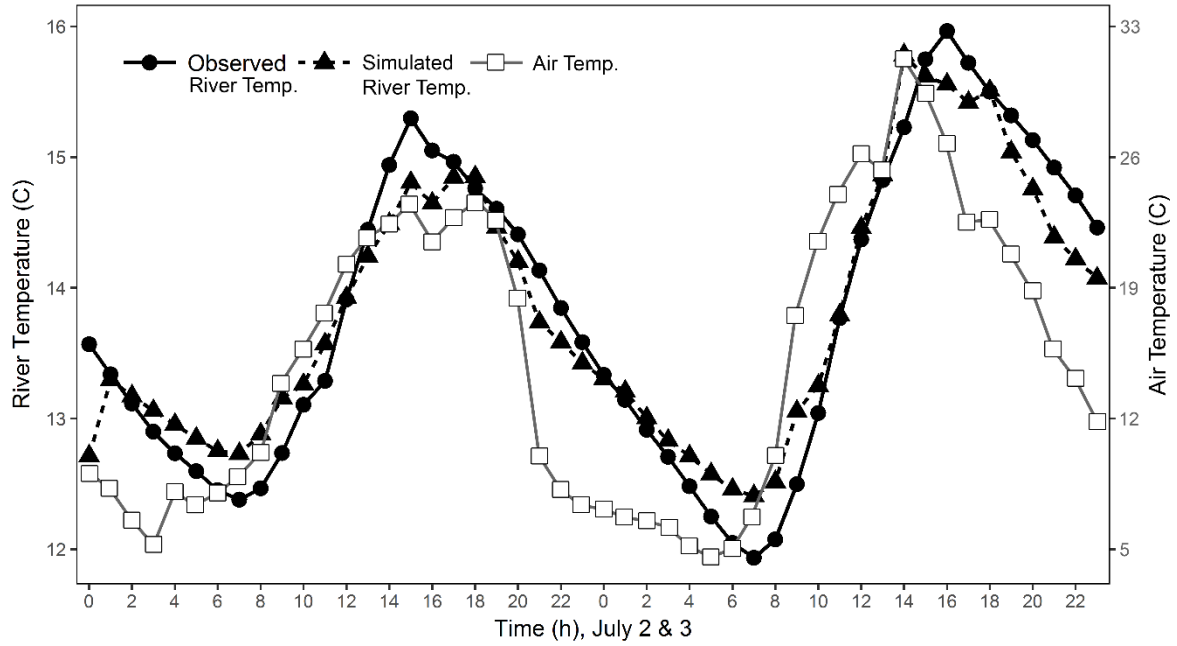
Figure 20 (Figure S3): Hourly air temperature and average observed and simulated river temperatures in SM Creek, NY

117
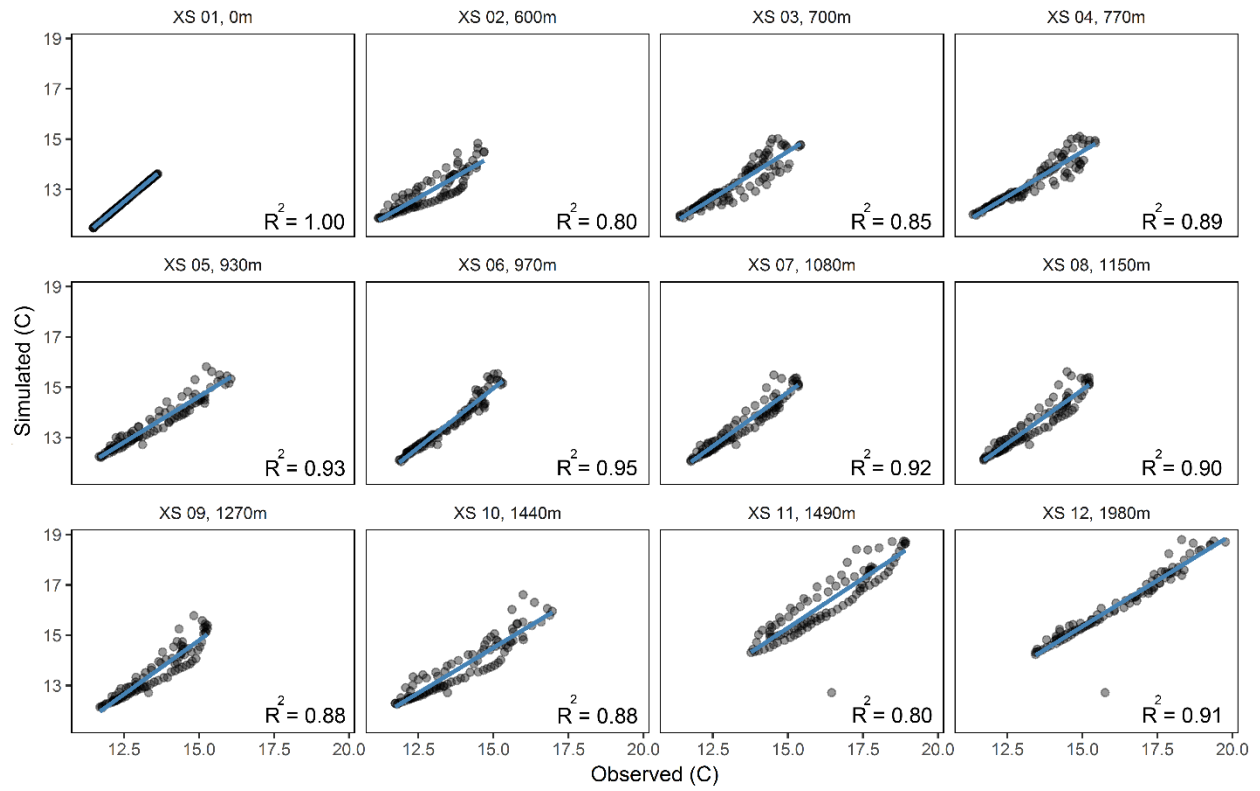
Figure 21 (Figure S4): Scatterplots of observed and simulated river temperatures for the 12 cross-sections (XS) of SM Creek, indicating their river stations from 0 to 2 km.
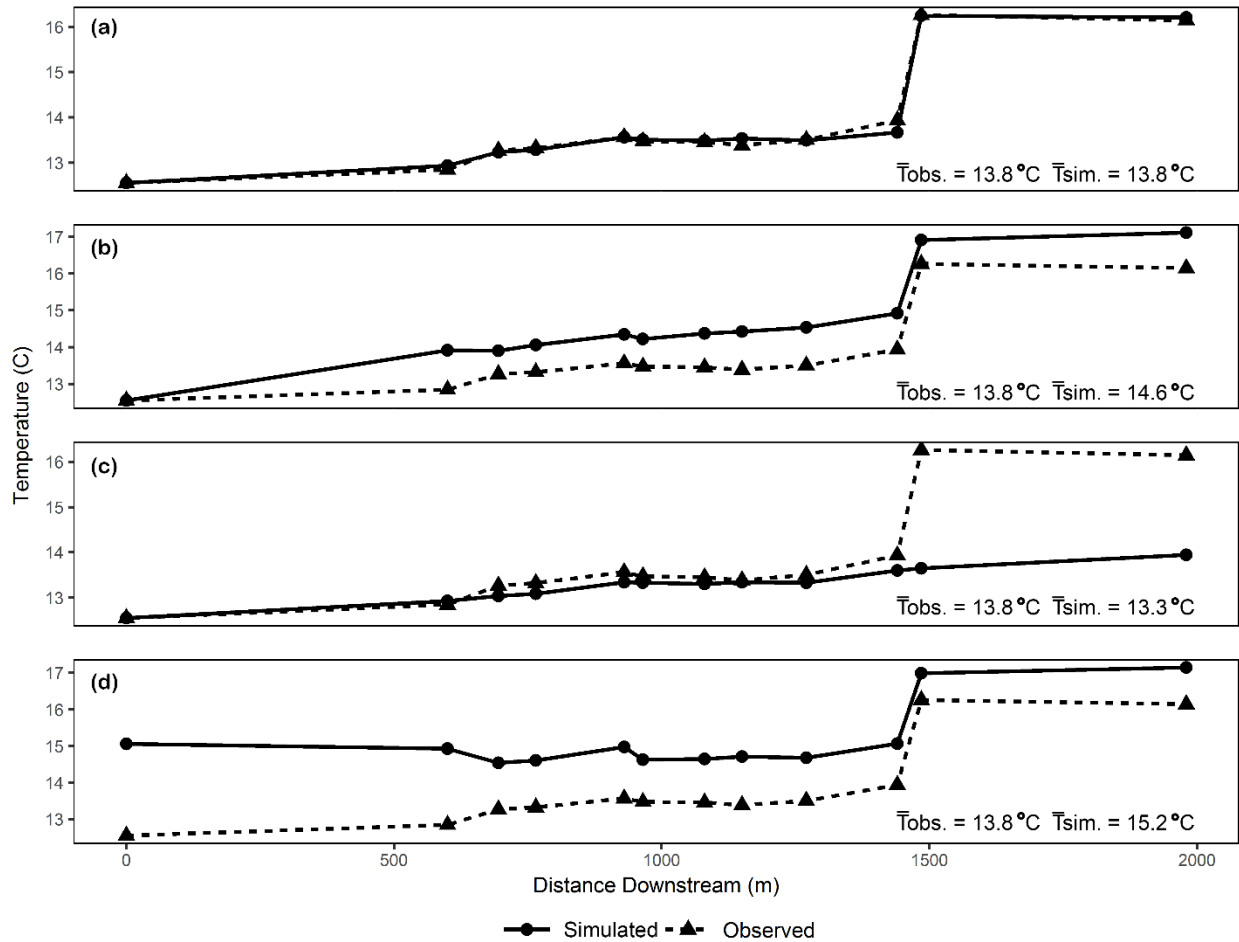
Figure 22 (Figure S5): Observed and simulated river temperatures in SM Creek. The plots represent the average river temperature along the reach for the (a) original condition, (b) no cooling effect of subsurface inflows, (c) no warming effect of lateral inflows in Tannersville area and the Gooseberry Creek, and (d) no observed boundary condition.

4   Comparison of Urban Stormwater Runoff Modeling Performance By i-Tree Hydro and EPA SWMM

Abstract: Impervious landcover in urban watersheds have long been implicated in the decline of watershed integrity, due to its effects on stormwater runoff quantity and quality. To facilitate urban watershed management, hydrologic models are used to assess how stormwater runoff will respond to different management and land cover scenarios. This study aims to compare the runoff quantity estimates of two hydrologic models, the i-Tree Hydro model and the Environmental Protection Agency's Stormwater Management Model (EPA SWMM), each using similar methods to represent impervious depression storage and infiltration, but different methods to represent pervious depression storage, canopy interception, evaporation, subsurface flow, and hydrograph routing. The models simulated a 2-hr design storm event at a 5-min time step for six distinct sub-basins totaling 11.7 ha in size, each with distinct land cover characteristics affecting runoff. To reduce differences in model predictions of runoff, inputs for both models set potential canopy interception and pervious depression to 0. The i-Tree Hydro model estimated a total effective runoff of 15.4 mm, 3% higher than SWMM. The i-Tree Hydro model simulated a peak effective runoff of 3.6 mm, 5% higher than SWMM. Both models estimated the same time to peak runoff, with SWMM using a kinematic wave algorithm and the i-Tree Hydro model using 2 calibrated parameters in a diffusive wave algorithm. The i-Tree Hydro model estimated a total infiltration of 8.5 mm, 1% higher than SWMM and total evaporation of 0.8 mm, 40% less than the

SWMM. Based on this study, the two models are equivalent in estimating total runoff, and can be adjusted to represent the same peak runoff characteristics.

Key Terms: Surface Runoff Simulation, i-Tree Hydro, SWMM, Urban Forest Management, Urban Watershed

4.1 Introduction

Urbanization is a disruptive form of land cover change that alters how water flows during and following storm events, degrading physical, chemical, and biological indicators of water quality in receiving waters (NRC, 2009). The vulnerability and value of urban waters will remain high as the world's population transitions from 55% urban residents in 2018 to 68% urban residents by 2050, adding 2.5 billion people to large and small urban areas across the globe (United Nations, 2018). The United Nations has identified urbanization as one of the critical sustainability challenges for our planet, specifying the need for infrastructure to deliver key services, and resource management to reduce environmental impact (United Nations, 2016). In recognition of human dependence on the services provided by water and the risk of water scarcity in urban areas, the United Nations has emphasized nature-based solutions to managing stormwater (Houngbo, 2018). Endreny et al., (2017) estimated the economic rationale for such nature-based solutions in megacities, finding existing tree cover provided a median annual value of $11.3 million in avoided stormwater treatment. Computer models can help communities design and assess nature-based solutions to managing stormwater (Abdi and Endreny, 2019; Abdi et al., 2019), and in selecting or designing

the appropriate stormwater model it is useful to consider the NRC (2009) review of stormwater modeling goals, current approaches, and recommended improvements.

The limits in scientific theory and measurement prohibit any model from reproducing all of the interactions of the actual stormwater runoff process. The NRC (2009) explains stormwater models vary in how they address the tradeoffs between model accuracy and complexity, as well as user priorities and constraints. In general hydrologic model accuracy and ease of use can vary with the different fundamental approaches for representing the system, including the simulated area (spatially lumped vs distributed land cover and soils), the weather (single storm event vs continuous record for a year), the model equations (empirically derived vs mechanistic processes of cause and effect), and the uncertainty in equation parameters (deterministic vs stochastic). Specific to stormwater modeling, these tradeoffs extend to whether and how models represent runoff production (Curve Number vs infiltration routine), the pollutant sources (build-up and wash-off vs event mean concentrations), the runoff transport (e.g., storm sewer routing vs overland flow), stormwater control measures or green infrastructure (e.g., street sweeping or rain gardens), the pollutant fate (conservative vs physical, chemical and biological transformation); and receiving water response (NRC, 2009).

The NRC (2009) reviewed what it considered the most widely used stormwater models, which included: the Rational Method (Kuichling, 1889); the Simple Method (Schueler, 1987); TR-20 (SCS, 1983) and TR-55 (USDA, 1986); the Generalized Watershed Loading Function (GWLF; Haith et al., 1992); the Program for Predicting

Pollutant Particle Passage through Pits, Puddles, and Ponds (P8; Walker, 1990); the

Model for Urban Stormwater Improvement Conceptualization (MUSIC; Wong et al. 2002

and 2006); the Storm Water Management Model (SWMM; Rossman, 2010); the Source

Loading and Management Model (SLAMM; Pitt and Voorhees 2002); the Soil and Water

Assessment Tool (SWAT; Neitsch et al., 2002); the Hydrologic Simulation Program

Fortran (HSPF; Jia and Culver, 2008); the Western Washington Hydrologic Model

(WWHM3; Clear Creek Solutions, 2006); and the Chesapeake Bay Watershed Model

(CMWM; US EPA, 1998). The NRC (2009) recognized the value of the above models in

providing options along the accuracy vs complexity spectrum, and then encouraged the

development and use of a new generation of models that can mechanistically link

surface and subsurface systems in order to incorporate green infrastructure within the

actual surface and subsurface flow networks, and represent catchment-scale impacts of

urbanization.

The new generation of models representing the linkage between surface and

subsurface systems used mechanistic infiltration and evaporation routines dependent

on more detailed soil and vegetation data and used spatially- or statistically-distributed

topography data to mechanistically represent the local to catchment scale flow

networks. The NRC (2009) identified this more advanced set of models to include: the

Distributed Hydrology Soil Vegetation Model (DHSVM; Wigmosta et al., 1994); the

Regional Hydro-Ecologic Simulation System (RHESSys; Tague and Band, 2009); the

ParFlow-Common Land Model (CLM; Maxwell and Miller, 2005); the Penn State

Integrated Hydrologic Model (PIHM; Qu and Duffy, 2007); the Soil Moisture Distribution

and Routing (SMDR; Soil and Water Laboratory, 2003) model; and i-Tree Hydro, which is the new name of the Wang, et al., (2008) model referenced in the report and formally known as the UFORE-Hydro model.

The importance of this mechanistically representing surface-subsurface interaction is illustrated with the simulation of a bioretention basin and similar green infrastructure designed to capture and infiltrate runoff from a larger drainage area, making stormwater available for transpiration by vegetation and recharge to groundwater and then receiving waters. Endreny and Collins (2009) used a mechanistically coupled surface-subsurface model to design the spacing between bioretention basins to maximize infiltration while avoiding groundwater mounding and its potential damage to infrastructures such as roads and buildings. In another example, the NRC (2009) noted how Wang et al., (2008), using the UFORE-Hydro model pre-cursor to the i-Tree Hydro model, linked canopy interception, evaporation, infiltration, and subsurface water table redistribution to evaluate the effectiveness of tree cover on increasing stormwater storage across the catchment.

This study aims to update the i-Tree Hydro model to operate at a sub-hourly time step and represent the fast and slow components of a rainfall partitioning and runoff generation, a first step in updating the model to simulate stormwater control measures such as green infrastructure. To date, the i-Tree Hydro model has not explicitly represented green infrastructure devices such as bioretention basins and has limited simulation to a 1-hour time step (Wang et al., 2008; Yang et al., 2013), however the need for nature-based stormwater management together, with the small size and short

124

time of concentration of urban sub-catchments using green infrastructure devices requires sub-hourly simulation (US Climate Resilience Toolkit, 2019). By contrast, the SWMM code, maintained by the US Environmental Protection Agency (Rossman, 2015) offers sub-hourly simulation and represents green infrastructure devices, but does not simulate some critical nature-based processes, such as tree canopy interception and topography driven subsurface water balance, features within i-Tree Hydro.

4.2 Methods

The i-Tree Hydro model version 6 (USDA Forest Service, 2018) was created for this study to enable easy application of a sub-hourly simulation time step and manage inputs, parameters, and outputs using a configuration.xml file. The i-Tree Hydro model is a freeware stand-alone desktop application tool written in the C++ language and designed to simulate the effects of changes in urban tree cover and other land cover on the hydrological cycle, including streamflow and water quality, in watershed and non-watershed areas (Wang et al., 2008; Yang et al., 2011). The new model version enabled the generation of extended model outputs which provide time series of all simulated water stores (e.g., depression storage) and fluxes (e.g., runoff rate, soil infiltration rate), which are used to compare model outputs with those of SWMM version 5.1 (Rossman, 2015), a tool with a proven record of accurate simulations (US Climate Resilience Network, 2019).

The i-Tree Hydro model consists of five main routines for simulating the rainfall-runoff process including canopy interception, depression storage, evaporation and evapotranspiration, infiltration and soil moisture, and semi-spatial distribution of runoff

125

generation (Fig. 1). The canopy interception routine simulates the precipitation (rain and snow) interception by the vegetation canopy with a seasonally varying leaf area index. The depression storage routine represents pervious and impervious depression storages, such as road potholes, as user-defined average storage depths for the area of interest. The potential evaporation and evapotranspiration rates computed using a modified Penman-Monteith equation, with actual rates set as a function of available water in each storage unit (Wang et al., 2008).

The i-Tree Hydro model infiltration is simulated using a modified Green-Ampt routine with hydraulic conductivity decaying with depth as an exponential function (Beven, 1984) or power function (Wang et al., 2006). Soil moisture and water-table depth is simulated using a TOPMODEL routine (Beven and Kirby, 1979) representing the influence of topography on available soil moisture storage across the catchment, distributed between 30 different topographic index bins derived from a digital elevation map of the catchment. The topographic index bins provide a statistical distribution of runoff generation per unit watershed area for flow components of pervious surface runoff from infiltration and saturation excess, directly connected impervious area surface runoff, and saturated zone subsurface flow. Runoff hydrographs for pervious and impervious sub-areas are generated with a two-parameter (α, β) surface diffusion algorithm (Yang and Endreny, 2013).

The study area and model parameters used to compare the i-Tree Hydro model with the SWMM code were directly adopted from example 4 in a set of SWMM case studies developed by Gironás et al., (2009) to illustrate how to use SWMM. The model

domain is an 11.7-hectare area in Fort Collins, Colorado divided into 6 sub-catchments, numbered S1 to S6 (Fig 2), each with different areas and impervious land cover fractions (Table 1). The site is drained by surface runoff pathways and has no storm sewers. The simulation did not include the low impact development controls (e.g., bioretention basin, swale) and set the pervious depression storage to zero for both the SWMM and the i-Tree Hydro model due to the inability of the models to treat these systems equivalently.

The rain event for the test case was a 2-hour duration rainfall event with a frequency of 2-year return period, simulated with a 5-minute temporal resolution with a depth of 24.89 mm. The potential evaporation rate for the study area in SWMM was a constant daily value equal to 5.08 mm/day and we used the same rate with the i-Tree Hydro model to keep the consistency. Soil infiltration was calculated by the Green–Ampt equation for both models use identical values for parameters of suction head (88.9 mm), hydraulic conductivity (5.08 mm/hr), and soil moisture initial deficit (0.2 fraction). The models sent all pervious and impervious runoff as hydrographs to the outlet O1. The SWMM simulation computed runoff rate with the Manning equation for a uniform depth across the sub-catchment with a given roughness and slope, updating depth at each time step with a nonlinear reservoir routine (Rossman and Huber, 2016). The i-Tree Hydro model set its α and β parameters used in hydrograph routing by calibrating to the SWMM hydrograph peak and time to peak, to keep consistency. The canopy cover in the case study simulation was set to 0 for both models due to the SWMM code not

representing canopy interception and evaporation. Additional details about the parameters used for the SWMM and i-Tree Hydro model are in Table 2.

To assess the updated i-Tree Hydro model performance relative to SWMM predictions, outputs including the simulated total runoff, infiltration, and evaporation from both models were analyzed using coefficient of determination (R^2) values and paired t-test statistical analysis. The SWMM output was analyzed at the default output time step of 1 min, and the i-Tree Hydro model output was analyzed at the 5-min time step.

4.3 Results

Comparing the i-Tree Hydro model and SWMM simulated runoff time series for the 11.7-hectare Fort Collins study site showed the two models have good agreement. The average runoff depth for the 2 hours rainfall event was simulated by SWMM as 14.9 mm (59.9% of precipitation) and was simulated by the i-Tree Hydro model as 15.4 mm (61.9% of precipitation) (Figure 3). For both simulated runoff time series, the time to peak runoff was 30 minutes and the duration of the runoff event was 160 minutes. The peak flow for the SWMM simulated runoff was 3.4 mm, 6% less than the i-Tree Hydro simulated runoff, which was 3.6 mm. Statistical analysis showed that the i-Tree Hydro model simulation of the 5-minute runoff time series was not significantly different than that of the SWMM simulations, based on the p-values calculated using a paired-samples t-test and the α = 0.05. When compared with the SWMM outputs tor the three hours of the simulation containing the storm event and the subsequent runoff, the i-Tree Hydro model outputs had a root-mean-square error (RMSE) of 0.17 mm and a

coefficient of determination (R^2) of 0.97, and no significant difference based on a p-value of 0.62.

The relative goodness of fit between the i-Tree Hydro model and SWMM predictions for 3-hours of runoff was visualized using scatterplots for the Fort Collins six sub-catchments (Figure 4). The total runoff simulated by the i-Tree Hydro model differed from that of SWMM for the sub-catchments S1 to S6 with a range of 0% for S2, S4, and S5 to 1.6% for S3, with an average of 0.4%. For sub-basin S6 with no impervious landcover, the percentage of difference for total runoff between the i-Tree Hydro model and SWMM was 0.0%. The runoff duration difference for the six sub-catchments and the total area ranged from 0% for S1, S5, S6, and the total area to 1.5% for S3, with an average of 0.5% (Table 3). For the six sub-catchments and 11.7-hectare total area, the absolute differences between the simulated peak runoff for the SWMM and i-Tree Hydro model predictions ranged between 0% in S2 and S4 to 8.3% in S6, with an average of approximately 3.8% (Table 3).

For the total infiltration values of the i-Tree Hydro model compared with SWMM for the Fort Collins 11.7-hectare total area, the simulated total infiltration of i-Tree Hydro had a <5% smaller value for the first 25 min, then at <5% higher total infiltration for the next 55 min, and then they increased at the same rate (Figure 5). For the 11.7-hectare total area, the duration of infiltration for the i-Tree Hydro model was 120 minutes which was 3 minutes more than the duration of infiltration for the SWMM simulation, showing a 2.5% difference between the infiltration duration for the two models (Table 3). The magnitude of the total infiltration simulated by the i-Tree Hydro model was 8.5 mm

129

(34.2% of precipitation), nearly identical to the total infiltration simulated by SWMM of

8.4 mm (33.8% of precipitation). For the 120 minutes of the infiltration period, the i-Tree

Hydro model and SWMM had an R^2 of 0.98. In the period between 25 minute and 65

minutes, the total infiltration simulated using the i-Tree Hydro model was larger and at a

steeper slope compared with the SWMM results. The largest difference between the

model results was in minute 50 when the total infiltration for the i-Tree Hydro simulation

was 5.7 mm which was 0.8 mm larger than the total infiltration for the SWWM

simulation.

The scatterplots of the 3-hour simulated infiltration rate for the six sub-

catchments in the Fort Collins study area provide insights on the relative goodness of fit

for each sub-basin and the associated drivers of the i-Tree Hydro model accuracy

compared with SWMM in calculating the infiltration rate (Figure 6). Comparison of the

total infiltration depths for the six sub-catchments from the i-Tree Hydro model and

SWMM showed that the differences were between 0% for S1, S2, S3 to 4.2% for S5,

with an average of 1.2%. The distribution of the infiltration rates for six sub-catchments

showed that the R^2 for the sub-catchments were approximately 0.74 (Table 3),

demonstrating that even though the error range between total values for the simulated

infiltration was approximately 1%, their distribution doesn't have as high goodness of fit

as the simulated runoff values. The maximum calculated infiltration rate for the six sub-

catchments using the i-Tree Hydro model was approximately 0.6 mm larger than the

maximum infiltration rate simulated by the SWWM. The differences between the

maximum simulated infiltration rates from the i-Tree Hydro model and SWMM showed

130

that the maximum simulated infiltration rate using i-Tree Hydro was approximately 1.7 times larger than the maximum infiltration rate calculated by SWMM.

The box plots for the simulated evaporation rates from the i-Tree Hydro model and SWMM demonstrated that the evaporation rate for the SWMM simulation was the constant value from the input files, whereas the evaporation rate from the i-Tree Hydro model had variation for most of the sub-catchments which was because of the function the model uses for calculating the evaporation rate in pervious and impervious land covers (Figure 7). The average of the evaporation depths for the SWMM simulations in five sub-catchments S1 to S6 was 0.9 mm. The average of the evaporation depths for the i-Tree Hydro model results for the five sub-catchments S1 to S6 was 0.7 mm. The total evaporation depth differences between SWMM and i-Tree Hydro model for the sub-catchments S1 to S6 ranged from 12.5% to 28% with an average difference of 19% (Table 3). For the 11.7-hectare total area, the total evaporation depth for the i-Tree Hydro model simulation was 0.8 mm (3.2% of precipitation), which was 40% less than the SWMM simulation of 1.4 mm (5.6% of precipitation) (Table 3).

4.4   Discussion

The SWMM simulations provided a useful benchmark for the i-Tree Hydro model, with this use of SWMM as a standard likely due to its decades of testing and improvement in predicting total and peak runoff for 1000s of municipalities (Huber and Roesner, 2012). Both the i-Tree Hydro model and SWMM estimated nearly 60% of the 24.89 mm in precipitation was partitioned to total runoff (59.9% for SWMM, 61.9% for i-Tree Hydro). This close agreement in total runoff estimates between the models is

131

attributed to each model using an identical land surface and nearly equivalent Green-Ampt infiltration routines. The total infiltration estimated by the i-Tree Hydro model and SWMM simulations were nearly 34% of the 24.89 mm of precipitation (33.8% for SWMM, 34.2% for i-Tree Hydro). Reasons for the 0.5 mm model disagreement in the total runoff, 2% of the precipitation, include the different approaches used to parameterize essentially similar model concepts for infiltration and soil moisture algorithms.

The i-Tree Hydro model and SWMM simulations of the Fort Collins, CO catchment used the same impervious area, impervious depression storage, and soil properties of hydraulic conductivity and suction head, and deliberately set pervious depression storage and vegetation canopy to values of zero to reduce differences. Differences between the models include the i-Tree Hydro model using exponential decay in hydraulic conductivity while SWMM uses a uniform value, and the i-Tree Hydro model simulating a 3 layer sub-surface with a ~15 cm depth for soil evaporation while SWMM uses a uniform soil and infinite depth for soil evaporation.

The magnitude of differences in runoff depth between the i-Tree Hydro model and SWMM estimates is smaller than that reported by other studies comparing stormwater models to SWMM. Bhaduri et al. (2001) developed the L-THIA model for decadal simulations of changes in the runoff with changes in impervious cover, designing their model to use only 3 inputs, far less data and preparation time than SWMM, and forgo the burden of simulating the details of runoff peak or totals for individual storms. Based on a comparison of model results for two areas in Chicago,

132

Illinois, with SWMM estimating 3% more total runoff for each 10% increase in impervious, Bhaduri et al. (2001) considered their model suitable for planning work and initial assessments of land use change prior to undertaking design-based SWMM simulations. Granata et al., (2016) and Wang and Altunkaynak (2012) each developed support vector machine and fuzzy logic algorithms, respectively, to predict runoff using observed data from cities in northern Italy, and generated some estimates within 2% of SWMM, but others off by >5%. These machine learning type algorithms may not work so well for predicting future scenarios, without observed data for model training, while the i-Tree Hydro model and SWMM approaches use mechanistic simulations that allow for a detailed description of the past, present, or future stormwater system.

Despite the i-Tree Hydro model and SWMM codes using different mechanistic algorithms to generate the runoff hydrograph and determine runoff peak magnitude and timing, these values for all sub-catchments were essentially identical due to calibration. In order to achieve predictive agreement when possible, the i-Tree Hydro model adjusted the α and β parameters of the runoff hydrograph to fit the SWMM estimate. Calibration of these celerity- and diffusivity-related time parameters is typically done against observed data using the PEST auto-calibration function (Doherty, 2010) within the i-Tree Hydro code. Yang and Endreny (2013) developed the two-parameter surface flow diffusion algorithm for the i-Tree Hydro model to generate hydrographs with the fewest possible parameters yet represent observed hydrograph inflection points and their double-peaks composed of fast and slow flow (Yang et al, 2015). The SWMM code does not offer the same algorithm, and the case study used the kinematic wave routing

133

algorithm, which controls the hydrograph shape with sub-catchment parameters for channel roughness, width, and slope (Rossman, 2015).

Selecting SWMM hydrograph algorithm parameters is likely easier for users, given the kinematic wave theory is more familiar and in most introductory physical hydrology textbooks, while the surface flow diffusion theory is newer and is not covered by such texts (Chin, 2013; Maidment, 1993). Selecting α and β parameters for the stormwater system with no observed data or knowledge of the target hydrograph shape can be difficult for new users, and some odd combination of values can generate more runoff than is available. To avoid the erroneous generation of runoff, there are several options. One option is to focus on the storm's total runoff load, or the runoff depth at each time step, rather than the within-storm hydrograph, given there is little difference between these values when simulating small catchments at sub-hourly time steps. Other options are to re-adjust the *α* and *β* parameters if the hydrograph depth differs from the total runoff or have the i-Tree Hydro model offer the kinematic wave routing algorithm as an alternative. The kinematic wave algorithm is a mechanistic representation of runoff routing, using parameters familiar to SWMM users, and could provide useful flexibility for the i-Tree Hydro modeling community.

Evaporation was a relatively small portion of the storm total 24.89 mm, which is expected for a simulation period of 12 hours duration. Precipitation allocated to total runoff and infiltration totaled 93.6% for SWMM and 96.0% for the i-Tree Hydro model. The 0.6 mm difference in the estimated total evaporation depth for the two models is a relatively small part of the storm total precipitation but represents a 40% difference

between the two evaporation depths. Similar to efforts made to minimize the model

differences in surface depression storage and infiltration, we removed trees and

herbaceous grass in the simulations to turn off i-Tree Hydro simulation of transpiration

and canopy evaporation, which are not simulated by SWMM. Further, the i-Tree Hydro

model parameters were set to avoid any wetland areas with an exposed water table,

which is also not simulated by SWMM or part of the case study. One likely driver for

model differences in evaporation is the soil depth used for evaporation in the two

models, with the i-Tree Hydro model limiting this to the top 15 cm, and SWMM

extending this to the entire soil. Another driver is the diurnal cycle of time-varying

potential evaporation used by the i-Tree Hydro model, while the SWMM simulation

maintained a constant value and was able to evaporate more water for the period.

The NRC (2009) encouraged use and development of stormwater models using

enhanced inputs, such as land cover and elevation data, and representing the whole-

catchment linkages between the surface, subsurface, atmospheric and vegetation

zones, in order to improve the simulation of nature-based stormwater management.

Both the i-Tree Hydro model and the SWMM codes provide advanced features

important for simulation of nature-based stormwater management, and with respect to

advanced options for simulation of runoff into green infrastructure, transport through

storm sewers, and water quality loading, SWMM is the superior model. With respect to

vegetation, however, the SWMM code does not explicitly represent the canopy

interception, canopy evaporation, and transpiration, all links between the soil and

atmosphere water budget. The SWMM code also does not provide a method to use

elevation data to represent the sub-surface water budget, and use a uniform depth to water table for each sub-catchment, as contrasted with the i-Tree Hydro model using the topographic index to auto-divide the catchment into 30 distinct wetness zones. Establishing the good fit between the i-Tree Hydro model and SWMM estimates of common stormwater metrics, such as total runoff depth, is the first step in our effort to design green infrastructure features for the i-Tree Hydro model.

4.5 Conclusion

This study updated the i-Tree Hydro model to simulate the stormwater water balance of runoff, infiltration, and evaporation at a sub-hourly time step in order for it to represent the dynamics of design storms used in sizing green infrastructure devices. To judge the adequacy of the updated model, it was compared against the proven SWMM code in a well-documented case study with a 2-yr return interval storm simulated at a 5-min time step. The i-Tree Hydro model and SWMM codes use the same algorithms for imperious depression storage and infiltration, and have differences in simulating pervious depression storage, soil moisture, evaporation and evapotranspiration, and hydrograph routing. By removing pervious depression storage and canopy cover from the case study, the i-Tree Hydro model predicted an evaporation depth 0.6 mm smaller than the 1.4 mm predicted by SWMM, which led to i-Tree Hydro allocating 0.5 mm more water into runoff (3% more than SWMM) and 0.1 mm more water into infiltration (1% more than SWMM). The simulation results showed that the two models are almost equivalent in estimating the 12 hours of stormwater dynamics for a 2-hour design storm with a 5 min time step.

The model inter-comparison found that the i-Tree Hydro model and SWMM codes can adopt some algorithms from each other, such as the kinematic wave routing from SWMM, and links between vegetation, soils and atmosphere from i-Tree Hydro, to provide more flexibility and capabilities for managers of urban development. The results of this study showed that the i-Tree Hydro model has the accuracy and required features to proceed with inclusion of green infrastructure simulation.

4.6   References

Abdi, R., Endreny, T. (2019). A river temperature model to assist managers in identifying thermal pollution causes and solutions. Water, 11(5), 1060.

Abdi, R., Endreny, T., Nowak, D. (2019) A model to integrate analysis of urban river thermal cooling and flood risk in river restoration. Urban Forestry and Urban Greening (under review)

Beven, K. (1984). Infiltration Into a Class of Vertically Non-Uniform Soils. Hydrological Sciences Journal. 29, 425

Beven, K., and Kirkby, J. (1979). A Physically Based, Variable Contributing Area Model of Basin Hydrology. Hydrological Sciences Bulletin, 24(1): 43

Bhaduri, B., Minner, M., Tatalovich, S., Harbor, J. (2001). Long-term hydrologic impact of urbanization: a tale of two models. Journal of Water Resources Planning and Management. 127(1):13-19.

Chin, D.A. (2013). Water Resources Engineering, Third Edition. Upper Saddle River, NJ, Pearson.

Clear Creek Solutions. (2006). Western Washington hydrology model version 3.0 (WWHM3). Washington State Department of Ecology, WA.

Doherty, J. (2010). PEST, model-independent parameter estimation—user manual. 5th edition, with slight additions. Brisbane, Australia, Watermark Numerical Computing.

Endreny, T., and Collins, V. (2009). Implications of bioretention basin spatial arrangements on stormwater recharge and groundwater mounding. Ecological Engineering, 35, 670–677.

Endreny, T., Santagata, R., Perna, A., Stefano, C. De, Rallo, R. F., Ulgiati, S. (2017). Implementing and managing urban forests : A much needed conservation strategy to increase ecosystem services and urban wellbeing. Ecological Modelling, 360, 328–335.

Gironas, J.L., Roesner, A., Rossman, L.A., Davis, J. (2010). A new applications manual for the Storm Water Management Model (SWMM). Environmental Modelling & Software, 25(6): 813-814.

Granata, F., Gargano, R., Marinis, G.D. (2016). Support vector regression for rainfall-runoff modeling in urban drainage : A comparison with the EPA's storm water management model. Water, 8, 69.

Haith, D.A., Mandel, R., Wu, R.S. (1992). Generalized watershed loading function, User's manual. Department of agriculture and biological engineering, Cornell University, Ithaca, NY.

138

Huber, W.C., Roesner, L.A. (2013). The history and evolution of the EPA SWMM fifty years of watershed modeling - past, present and future. A.S. Donigian, R. Field and M.J. Baker, ECI Symposium.

Jia, Y., Culver, T.B. (2008). Uncertainty analysis for watershed modeling using generalized likelihood uncertainty estimation with multiple calibration measures. Journal of Water Resources Planning and Management. 134(2): 97–106.

Kuichling, E. (1889). The relation between the rainfall and the discharge of sewers in populous districts. Transactions, American Society of Civil Engineers 20, 1–56.

Maidment, D.R. (1993). Handbook of Hydrology. New York, McGraw-Hill.

Maxwell, R.M., Miller, N.L. (2005). Development of a Coupled Land Surface and Groundwater Model. Journal of Hydrometeorology, 6, 233–247.

National Research Council (NRC), (2009). Urban Stormwater Management in the United States. Washington, DC, The National Academies Press.

Neitsch, S.L., Arnold, J.G., Kiniry, J.R., Srinivasan, R., Williams, J.R. (2002). Soil and Water Assessment Tool user's manual, TWRI Report TR-192, Texas Water Resources Institute, College Station, TX.

Pitt, R., Voorhees, J. (2002). SLAMM, the source loading and management model. Wet-weather flow in the urban watershed: technology and management, 103–139.

Qu, Y., Duffy, C.J. (2007). A semidiscrete finite volume formulation for multiprocess watershed simulation, Water Resources Research, 43, W08419

Rossman, L.A. (2010). Storm Water Management Model User's Manual Version 5.0. US EPA National Risk Management Research Laboratory.

Rossman, L.A. (2015). Storm water management model user's manual, version 5.1 (EPA- 600/R-14/413b). National Risk Management Research Laboratory, Office of Research and Development, US Environmental Protection Agency, Cincinnati, OH, U.S.

Rossman, L.A., Huber, W.C. (2016). Storm water management model reference manual volume I – Hydrology. U.S. Environmental Protection Agency EPA/600/R-15/162

Schueler, T. (1987). Controlling urban runoff: a practical manual for planning and designing urban BMPs. Metropolitan Washington Council of Governments. Washington, DC

Soil and Water Laboratory, (2003). The soil moisture distribution and routing (SMDR) model. Biological and Environmental Engineering Dept. Cornell University, Ithaca, NY.

Soil Conservation Service. (1983). Computer program for project formulation-hydrology. SCS Technical Release 20. Washington, DC.

Tague, C., Band, L. (2004). RHESSys: Regional Hydro-ecologic simulation system: An object-oriented approach to spatially distributed modeling of carbon, water and nutrient cycling, Earth Interactions, 8(19), 1-42.

United States Department of Agriculture (USDA). (1986). Urban hydrology for small watersheds (PDF). Technical Release 55 (TR-55). Natural Resources Conservation Service, Conservation Engineering Division.

United States Environmental Protection Agency (USEPA). (1998). Chesapeake Bay Watershed Model Application and Calculation of Nutrient and Sediment Loadings. U.S. Environmental Protection Agency for the Chesapeake Bay Program, Annapolis, MD.

United States Department of Agriculture Forest Service (USDA FS), (2018). i-Tree Hydro V6 User Manual. Syracuse, NY.

Walker, W. (1990). P8 urban catchment model program documentation, v1.1. Prepared for IEP, Inc., Northborough, MA and Narragansett Bay Project, Providence, RI

Wang, K., Altunkaynak, A. (2012). Comparative case study of rainfall-runoff modeling between SWMM and Fuzzy Logic Approach. Journal of Hydrologic Engineering, 17(2), 283–292.

Wang, J., Endreny, T. A., Hassett, J. M. (2006). Power function decay of hydraulic conductivity for a TOPMODEL-based infiltration routine. Hydrological Processes, 20, 3825–3834.

Wang, J., Endreny, T. A., Nowak, D. J. (2008). Mechanistic simulation of tree effects in an urban water balance model. Journal of American Water Resources Association,. 1. 44(1), 75–85.

Wigmosta, M.S., Vail, L.W., Lettenmaier, D.P. (1994). A distributed hydrology-vegetation model for complex terrain. Water Resources Research, 30(6): 1665–1679.

Wong, T.H., Fletcher, T.D., Duncan, H.P., Coleman, J.R., Jenkins, G.A. (2002). A model for urban stormwater improvement conceptualisation. Global Solutions for Urban Drainage, 8–13.

Wong, T.H., Fletcher, T.D., Duncan, H.P., Jenkins, G.A. (2006). Modelling urban stormwater treatment—a unified approach. Ecological Engineering, 27, 58–70

Yang, Y., Endreny, T.A. (2013). Watershed hydrograph model based on surface flow diffusion. Water Resources Research. 49, 507–516.

Yang, Y., Endreny, T.A., Nowak, D.J. (2011). iTree-Hydro: Snow Hydrology Update for the Urban Forest Hydrology Model. Journal of American Water Resources Association. 47(6), 1211–1218.

Yang, Y., Endreny, T.A., Nowak, D.J. (2013). A physically based analytical spatial air temperature and humidity model. Journal of Geophysical Research Atmospheres, 118(18), 10449–10463.

Yang, Y., Endreny, T.A., Nowak, D.J. (2015). Simulating double-peak hydrographs from single storms over mixed-use watersheds. Journal of Hydrologic Engineering. 20(11): 06015003.

United Nations, 2018. https://www.un.org/development/desa/publications/2018-revision-of-world-urbanization-prospects.html

US Climate Resilience Toolkit, 2019 https://toolkit.climate.gov/tool/storm-water-management-model

4.7 Tables

Table 10 (Table 1): The fundamental data required for simulating the six sub-basins and 29-ac total area test case

Basin	Area (ac)	Area (m²)	Imper. Cover (fraction)	Veg. cover (fraction)	Imper. Dep. (mm)	Per. Dep. (mm)	α Per. (unitless)	β Per. (unitless)	α Imper. (unitless)	β Imper. (unitless)
S1	4.55	18413	0.57	0.43	1.14	0	0.18	35.5	0.18	35.5
S2	4.74	19182	0.63	0.37	1.14	0	0.18	35.5	0.18	35.5
S3	3.7	14973	0.40	0.60	1.14	0	0.18	37.5	0.18	37.5
S4	6.82	27599	0.50	0.50	1.14	0	0.18	35.5	0.18	35.5
S5	6.6	26709	0.88	0.12	1.14	0	0.18	35.5	0.18	35.5
S6	2.58	10440	0.0	1.0	1.14	0	10.2	7.8	10.2	7.8

Imper.: Impervious, Per.: Pervious, Veg.: Vegetation, Dep.: Depression

Table 11 (Table 2): The details of the parameters have been used for the simulation in i-Tree Hydro model for all the watersheds

Parameter	Value
Soil Transmissivity (m^2/h)	0.33
Soil macropore (%)	0
Scale parameter of soil transmissivity (m)	0.2
DCIA	1
Soil Filed capacity (fraction)	0.2
effective Porosity (fraction)	0.4
Maximum Root Zone Deficit (m)	0.05
Surface hydraulic conductivity (m/h)	1.00E-07
Wetting front suction (m)	0.089
Unsaturated zone time delay (h)	10
Initial stream discharge (m/h)	8.33e-07
Initial upper soil zone saturation (%)	0
Infiltration excess governed area (fraction)	1

Table 12 (Table 3): The i-Tree Hydro and SWMM simulation results for six sub-basins and 11.7-hectars total area in Fort Collins, CO. In the Table, ET is accumulated evapotranspiration, F is the accumulated infiltration, Q is the accumulated runoff, Q_p is the accumulated peak flow, t_p is the time to reach the peak runoff, t_d is the runoff duration, and F_d is the infiltration duration.

Basin	Model	Q (mm)	Q_p (mm)	F (mm)	ET (mm)	t_p (min)	t_d (min)	F_d (min)
S1	Hydro	15.6	3.7	8.3	0.8	30	140	120
	SWMM	15.5	3.6	8.3	1	30	140	117
	Difference (%)	-0.6	-2.7	0.0	20.0	0.0	0.0	-2.5
S2	Hydro	16.7	3.9	7.1	0.9	30	145	120
	SWMM	16.7	3.9	7.1	1.1	30	144	117
	Difference (%)	0.0	0.0	0.0	18.2	0.0	-0.7	-2.5
S3	Hydro	12.3	3.1	11.7	0.5	30	135	120
	SWMM	12.5	2.9	11.7	0.7	30	133	117
	Difference (%)	1.6	-6.5	0.0	28.0	0.0	-1.5	-2.5
S4	Hydro	14.3	3.6	9.7	0.7	30	140	120
	SWMM	14.3	3.6	9.6	0.8	30	139	117
	Difference (%)	0.0	0.0	-1.0	12.5	0.0	-0.7	-2.5
S5	Hydro	21.1	4.5	2.4	1.2	30	160	120
	SWMM	21.1	4.7	2.3	1.5	30	160	117
	Difference (%)	0.0	4.4	-4.2	20.0	0.0	0.0	-2.5
S6	Hydro	4.6	1.2	20.2	0.22	35	65	120
	SWMM	4.6	1.1	19.8	0.25	35	65	117
	Difference (%)	0.0	-8.3	-2.0	15.0	0.0	0.0	-2.5
S total	Hydro	15.4	3.6	8.5	0.8	30	160	120
	SWMM	14.9	3.4	8.4	1.4	30	160	117
	Difference (%)	-3.2	-5.1	-1.2	40.0	0.0	0.0	-2.5

4.8   Figures
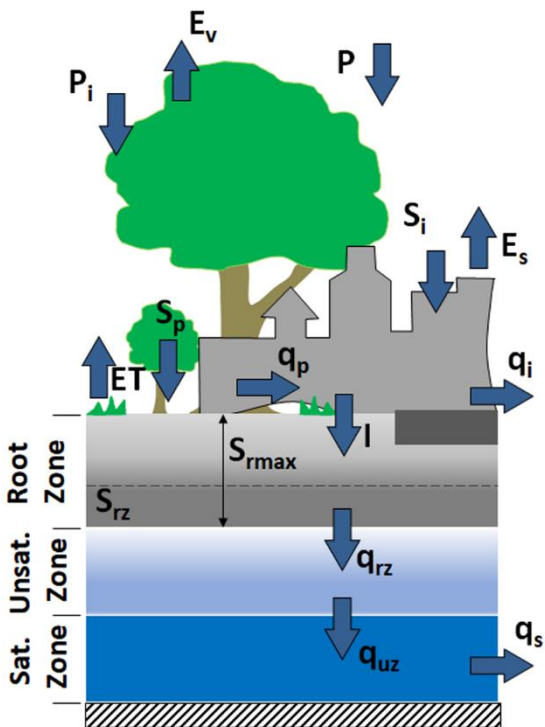
Figure 23 (Figure 1): The i-Tree Hydro model algorithm system. In the figure, P is the precipitation, P_i is the canopy interception, S_p is the pervious depression storage, S_i is the impervious depression storage E_v is the vegetation evaporation, E_s is the surface Evaporation, ET is the evapo-transpiration, q_p is the pervious runoff, q_i is the impervious runoff, q_s is the subsurface runoff, I is the infiltration, S_{rmax} is the maximum root zone depth, S_{rz} is the root zone storage, q_{rz} is the root zone to unsaturated zone percolation, and q_{uz} is the unsaturated zone to saturated zone percolation.
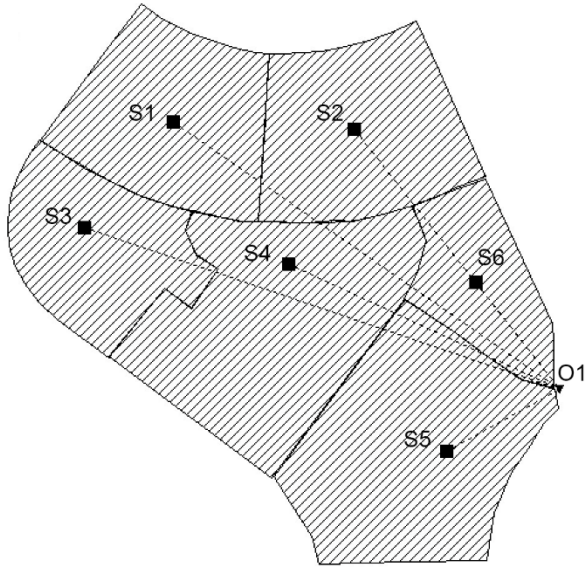
Figure 24 (Figure 2): The schematic of the SWMM practical example, the 29-ac test case, and six sub-basins in Fort Collins, CO.
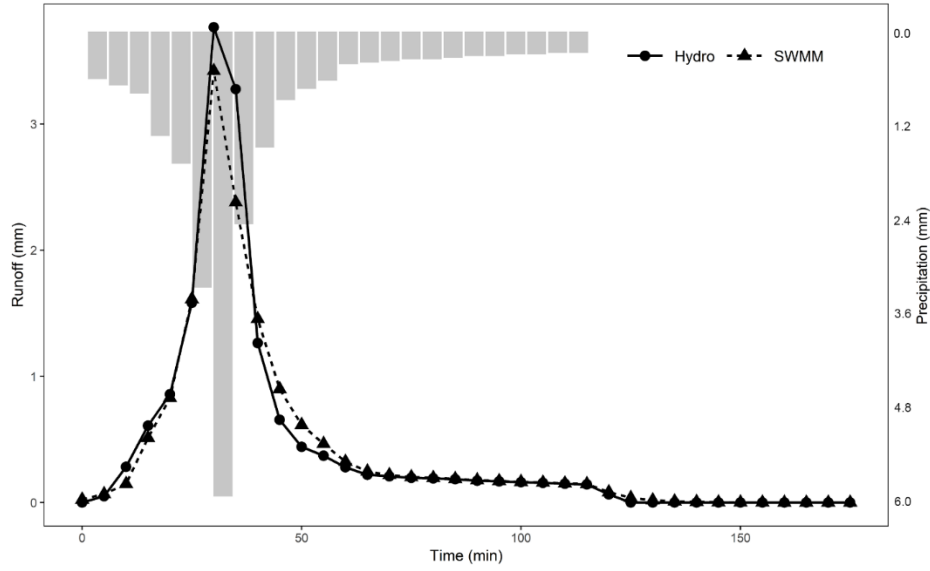
Figure 25 (Figure 3): The simulated stormwater runoff for the 29-ac test case in Fort Collins, CO using the SWMM and i-Tree Hydro. The 2-year rainfall event is also shown in the figure.
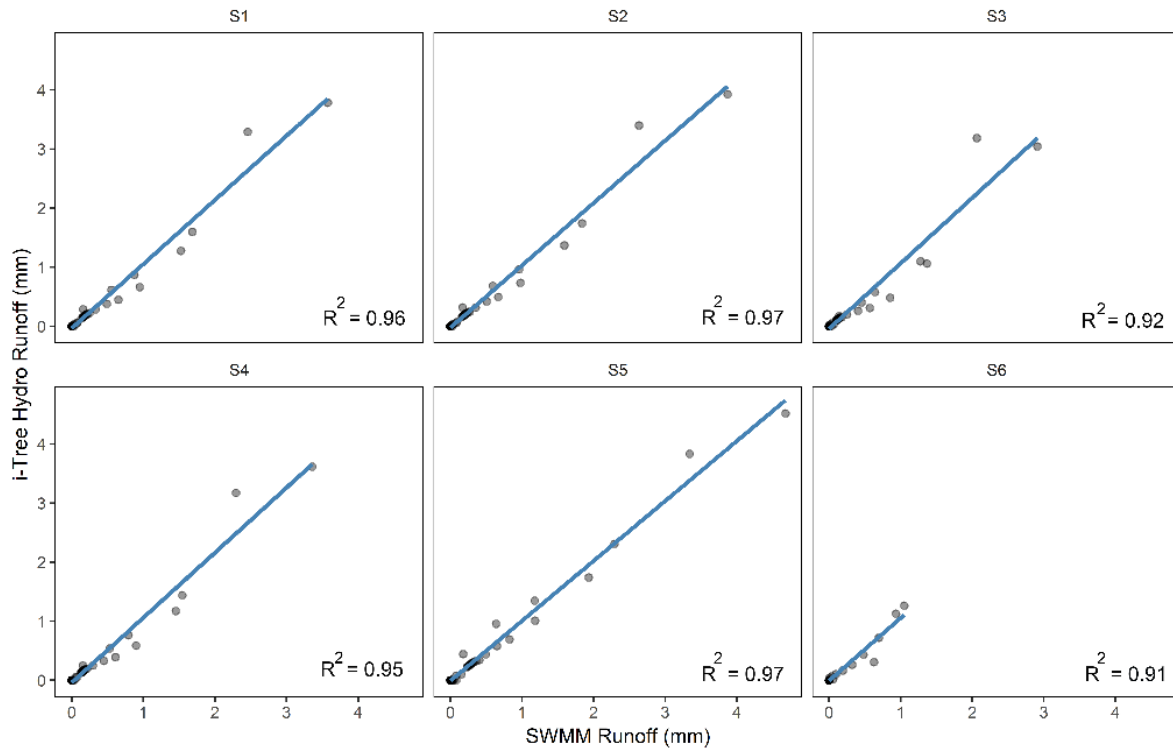
Figure 26 (Figure 4): Performance of i-Tree Hydro compared with SWMM in simulating stormwater runoff for the six sub-basins in Fort Collins.
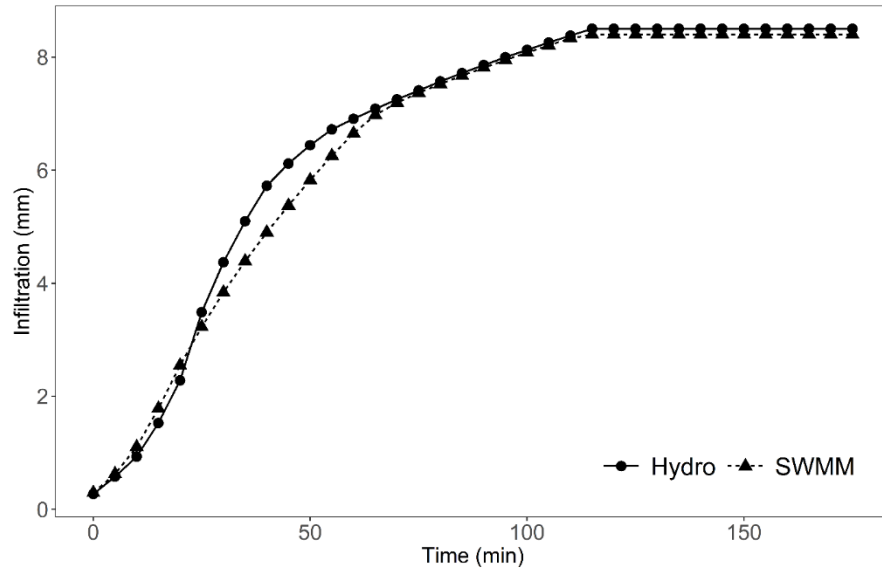
Figure 27 (Figure 5): The accumulated values of the infiltration rate for the 11.7-hectare total area in Fort Collins using the SWMM and i-Tree Hydro models.
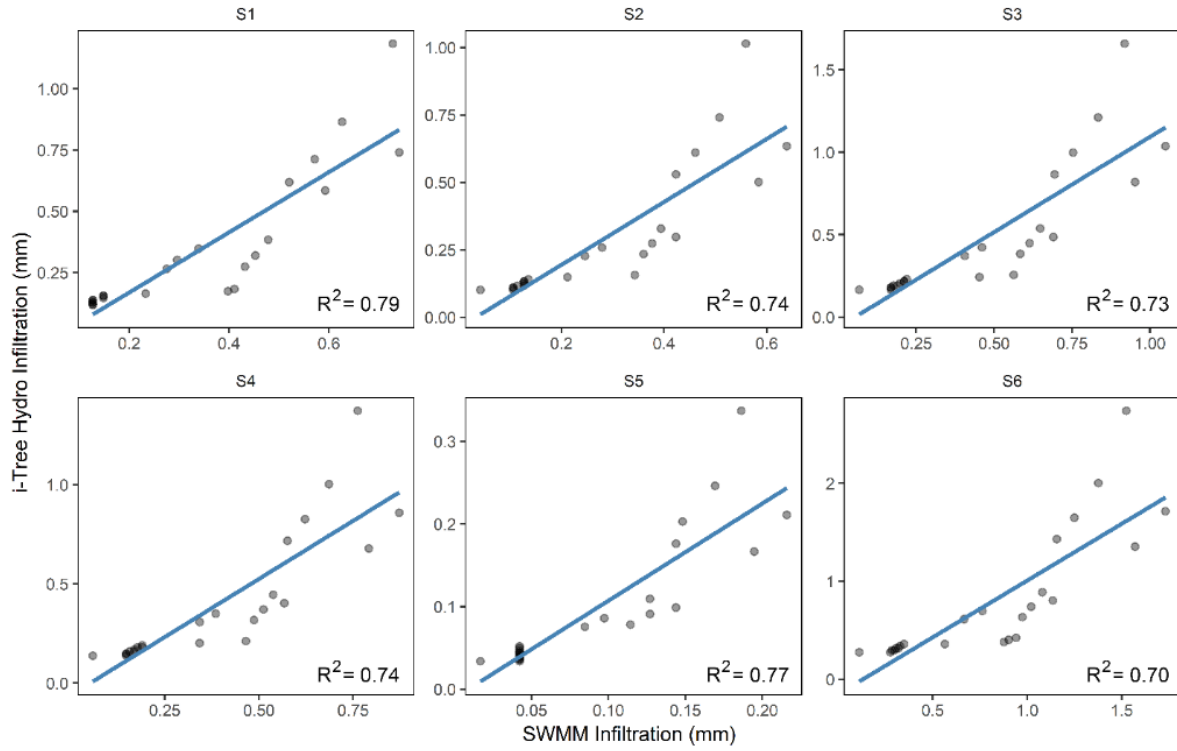
Figure 28 (Figure 6): The scatter plots for the simulated infiltration in the i-Tree Hydro model and SWMM for the six sub-basins in Fort Collins, CO.
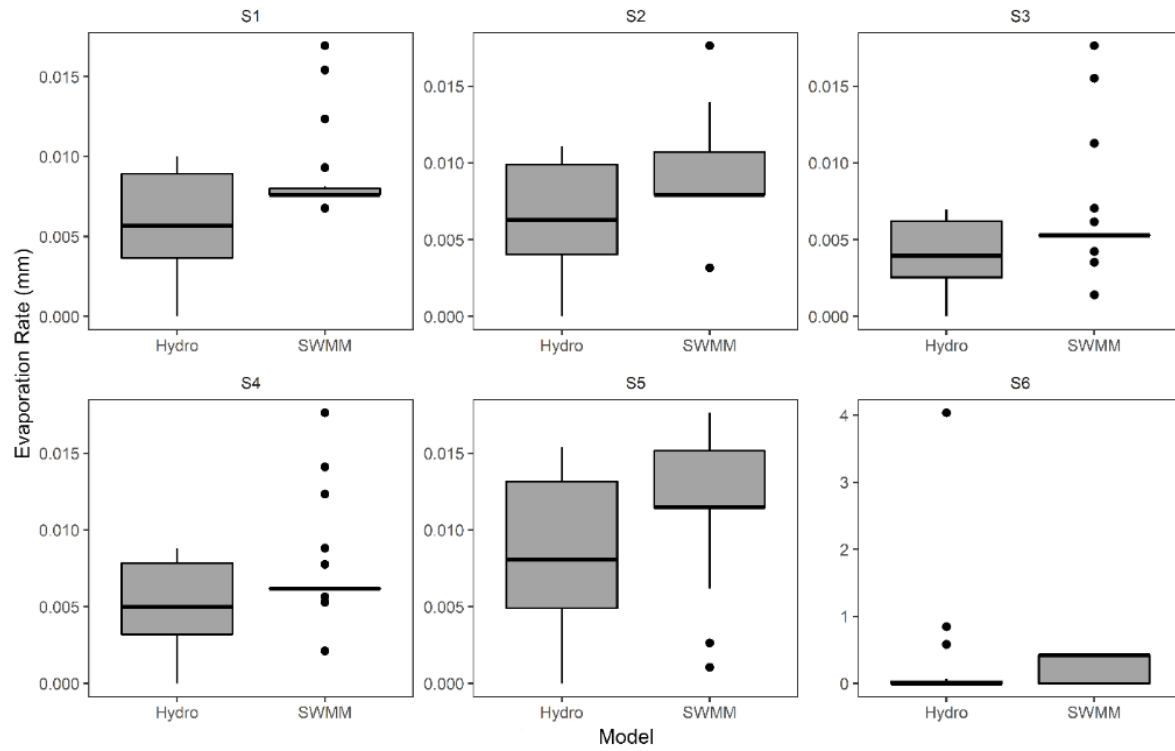
Figure 29 (Figure 7): The box plots for the simulated evaporation rate using the i-Tree Hydro model and SWMM for the six sub-basins in Fort Collins, CO.

5   Development of Permeable Green Infrastructure Algorithms with Water-table and Vegetation Linkages in the i-Tree Hydro Model.

Abstract: The United Nations advocates the use of green infrastructure devices in stormwater management to address the needs of urban sustainability, noting the devices can utilize stormwater for natural irrigation of urban greening projects, reduce pollution of receiving waters, and address water scarcity. Computer models that simulate green infrastructure within the catchment water balance are called for by the National Academy of Sciences. In this study, we update the urban runoff model, i-Tree Hydro, to represent the permeable green infrastructure water balance of ponding, infiltration, percolation, evaporation, and surface and subsurface drainage, and then link that balance with the catchment redistribution of subsurface water and water interception and evapotranspiration by vegetation. The green infrastructure devices modeled were bioretention basin, rain garden, infiltration trench, swale, and permeable pavement, with their design taken from the US Environmental Protection Agency's Storm Water Management Model (SWMM). Each green infrastructure device was simulated within the i-Tree Hydro model, comparing its water balance against that of SWMM, for a 2-yr return interval, 2-hr duration design storm, on a 2.7 ha urban area, simulated for 12-hr at a 5-min time step. The updated model was then used to estimate how a bioretention device changes the catchment water balance for a 1-yr simulation. Results showed that for the five green infrastructure devices, the two models estimated infiltration within 10%, percolation within 5%, evaporation within 2%, surface outflow within 15%, subsurface outflow within 13%, and exfiltration to native soils within 4%. On

average total runoff volume reduction estimated by the i-Tree Hydro model was 28%, 1.6% less than SWMM. The differences in the water balance of the two models are attributed to different soil moisture algorithms, with slightly different code structure for infiltration and percolation. The new i-Tree Hydro model helps advance nature-based design by connecting the permeable green infrastructure devices with the catchment redistribution of subsurface water and the vegetation processes of interception and evapotranspiration.

Key Terms: Urban watershed, Green Infrastructures, Runoff Reduction, i-Tree Hydro, SWMM

5.1 Introduction

Stormwater is a valuable resource that when mismanaged, can lead to more harm than good. The United Nations has identified stormwater as an under-utilized and important means of addressing water scarcity affecting hundreds of millions of global citizens (WWAP, 2019). Managing water resources to provide drinking water, sanitation and hygiene allows communities to take the next steps in sustainable development of reducing poverty, increasing peace and prosperity, and improving biodiversity (WWAP, 2019). The United Nations has identified nature-based solutions as a stormwater management approach that recognizes the value to humans of water resources and their ecosystem services (WWAP, 2018).

Green infrastructure is one nature-based solution for stormwater management, and it typically involves a device capturing runoff and using the water in some part of the natural hydrological cycle such as ponded storage, evapotranspiration, and infiltration,

resulting in improved water quality in more manageable quantities (WWAP, 2018). These green infrastructure systems are powered by renewable energy, with gravity for example powering infiltration, and solar energy powering evapotranspiration; this reduces operational costs. For most urban areas, stormwater is predominantly managed by grey infrastructure such as roadside gutters and storm sewers, which discharge the runoff and its pollutants to receiving waters, which can suffer from flooding, erosion, and water quality conditions unsuitable for biodiversity (WWAP, 2018). The flooding from urban areas adversely impacts urban riverine ecosystems essential for the livelihood and food security (WMO, 2006).

Green infrastructure in stormwater management is a means to addressing major environmental and social challenges in urban systems, reducing the ecological footprint, improving human health and wellbeing, adapting to climate change, as well as water resources management (WWAP, 2018; Zölch et al., 2017). The task for communities trying to improve sustainability is to design opportunities for green infrastructure to replace or complement grey infrastructure, and thereby improve human wellbeing and biodiversity benefits (WWAP, 2018). Impervious land cover in urban catchments has long been implicated in the decline of natural resource integrity (Klein, 1979; Brattebo and Booth, 2003). Impermeable surfaces such as parking lots and buildings disrupt the natural hydrological cycle and water balance by decreasing the infiltration rates and increasing runoff rates (Nie et al., 2011; Kamali et al., 2017). With climate change, the flood risk due to increased frequency of short-duration and high intensity rains has become a major concern in most urban areas (United Nations, 2014).

In the past few decades, the management of urban drainage systems has undergone major changes, shifting from limited-focus plans (typically for flood control) to approaches with multiple objectives to deliver improved environmental, economic, social, and cultural outcomes (Wong, 2007; Fratini et al., 2012; Fletcher et al., 2014). Besides flood control, increasing attention to nonpoint source urban discharge pollution control led to the definition of an infrastructure generation based on best management practices (BMPs) or sustainable drainage systems (SUDS) as well as low-impact developments (LIDs; Walker et al. 2011; Ellis, 2013). Recently, low impact development and green infrastructure systems, which are considered synonymous systems in this study, have become increasingly popular methods to mitigate the adverse hydrologic and water quality issues caused by the urbanization (Elliott and Trowsdale, 2007). Bioretention cells, swales, rain gardens, infiltration trenches, and porous pavements features have become common permeable green infrastructure devices which manage for stormwater quantity and quality (CIRIA, 2000; Ellis et al. 2004; Damodaram et al., 2010).

Despite the well-understood importance of green infrastructure approaches as potential solutions for stormwater management and urban sustainability, their adaptation in stormwater management remains a priority (WWAP, 2018). One reason for the limited adoption of green infrastructure in stormwater management is the need for design plans that address local site concerns and operate effectively at the needed range of scales in urban greening (Beck et al., 2017). Such designs are typically not obtained with monitoring data due to the need to forecast changes in a specific

157

stormwater system different in many ways than that monitored (Rode and Suhr, 2007; Dotto et al., 2014). An alternative approach to generating designs for green infrastructure devices is use of computer modeling software.

Models used to design green infrastructure should to account for the different structural ways the devices partition water between their layers. Typically, the top surface layer is designed for specific storage depth, setting the top elevation of a section of its berm, or a flow control within the berm, such as a weir or pipe. The types of permeable layers below the surface typically vary with device type. For the top layer, the bioretention basin and rain garden use well-drained soils suitable for vegetation, the swale uses native soils, the infiltration trench uses gravel, and the permeable pavement can range from pervious concrete and asphalt to polymer-bound rock or shredded tires able to withstand mechanical loading. Other differences include drainage, with the bioretention basin, infiltration trench, and permeable pavement typically using drainage pipe laid in gravel to remove some percolated water. By contrast, the swale is designed as a grassed channel with a longitudinal slope and trapezoidal cross-section to convey water at the surface from inlet to a more distant outlet, allowing infiltration along the way.

The Storm Water Management Model (SWMM) version 5.1 (Rossman and Huber, 2016) is a computer model for the design of permeable green infrastructure devices such as the bioretention basin, rain garden, infiltration trench, permeable pavement, and swale. These devices have common features of receiving stormwater runoff from an upslope contributing area into a bermed storage area, either flat or

158

sloped, and then providing a chance for the water to infiltrate into native soils (NYS DEC, 2015). The SWMM was a leader in simulating green infrastructure and serves as a benchmark for new model development given its endorsement for resilient stormwater management (US Climate Resilience Network, 2019). The US National Research Council (2009) has called for a new generation of stormwater models to represent the linkage between surface and subsurface systems, with mechanistic infiltration and evaporation routines using detailed soil and vegetation data, and representation of the green infrastructure within local to catchment scale flow networks. The SWMM code meets some but not all of these goals for the next generation of stormwater models.

This study aims to integrate permeable green infrastructure devices developed for the SWMM code into the i-Tree Hydro model, which offers a catchment representation of atmospheric, topographic, and vegetation drivers on the vertical and lateral movement of water. The i-Tree Hydro model will improve the SWMM simulation of green infrastructure by: a) linking the devices with the vegetation canopy processes of interception, evaporation, and transpiration; b) linking the devices with subsurface groundwater aquifer which is distributed across the catchment based on topography; and c) representing the influence of a shallow water-table on device performance, which could include an increase of storage drain outflow, saturation of soil layers, and a decrease of surface infiltration. This model development will place permeable green infrastructure within the catchment water balance and allow for simulation of nature-based designs in stormwater management. The new model will allow users to simulate

a single green infrastructure device within a small sub-catchment, or multiple units of a variety of green infrastructure devices within a large catchment.

5.2 Methods

5.2.1 Model theory and equations

The i-Tree Hydro model version 6.1 (USDA Forest Service, 2018) was created for this study to simulate permeable green infrastructure devices within the catchment water balance and manage related inputs, parameters, and outputs using a configuration.xml file. The updated i-Tree Hydro model is a freeware stand-alone desktop application tool written in the C++ language. The permeable green infrastructure devices developed for the i-Tree Hydro model are the bioretention basin, rain garden, infiltration trench, swale, and permeable pavement (Fig. 1), derived from those simulated in the SWMM version 5.1 (see equations #6-1 to #6-43 in Rossman and Huber, 2016). In this study we refer to these devices as green infrastructure, and in the SWMM these devices are referred to as low impact development controls.

The lateral and vertical water balance within each green infrastructure device (e.g., inflow and outflow, infiltration and evaporation) was modified from SWMM code to fit within the i-Tree Hydro lateral and vertical water balance (Fig. 2). The 3-layer soil represented by the i-Tree Hydro model are the root zone, unsaturated zone, and saturated zone, and their overlap with the green infrastructure layers is described below. The i-Tree Hydro model maintains a water balance for the entire catchment using two types of structures, the bulk area, and the green infrastructure, and each type is sub-divided into 30 topographic index bins which represent the lateral variation in

160

depth to water-table. The bulk area contains contributing areas that send their surface runoff to the green infrastructure. For each structure type, the vertical water balance represents the effects atmosphere, vegetation, land cover, and soil, including canopy interception, depression storage, evaporation and evapotranspiration, infiltration and soil moisture. At the end of each time step, the soil moisture storage available in each topographic index bin is updated using an algorithm that represents lateral redistribution of a mounded water-table having received relatively large recharge, such as in green infrastructure devices.

To reduce the complexity of the green infrastructure water balance simulation, the i-Tree Hydro model adopts the following simplifying assumptions used by the SWMM code (Rossman and Huber, 2016): the inflow is represented by a one-dimensional uniform flow within a prismatic cross-sectional area; the infiltration into soils is represented as a uniform wetting front into the soil layer; and the deeper storage layer is represented with matric forces of zero and it freely exchanges water with its upper and lower layers. In green infrastructure layers where water is modeled as a depth within the layer, such as the surface and storage layers, the depth, d (m), is updated each time step following SWMM equations (Rossman and Huber, 2016) as:

$$d_{j,t} = d_{j,t-1} + \frac{\Delta d_j}{\Delta t} \qquad\qquad\qquad \text{Eq 1}$$

where j represents the layer number (1 for surface, 3 for storage, 4 for pavement), t is the time step, and Δt represents the interval between time steps (5 min was used in this study). In the soil layer water is modeled as a fraction, θ_2 (m/m), Eq 1 is modified so

that d_x is replaced with θ_2. The incremental change in water varies with green

infrastructure layer and is a function of several processes, some of which are not active

at each time step.

The water balance for the incremental change in water depth in the green

infrastructure surface layer is similar to SWMM code (Rossman and Huber, 2016) and

given as:

$$\phi_1 \frac{\Delta d_1}{\Delta t} = i_e + q_0 - e_1 - f_1 - q_1 + u_1 \qquad \text{Eq 2}$$

where ϕ_1 (m/m) is the void fraction remaining after accounting for vegetation and other

objects (1 is completely open, 0 is completely filled), i_e (m/Δt) is the effective

precipitation within the green infrastructure device after accounting for canopy

interception and depression storage using the i-Tree Hydro model approach described

by Wang et al., (2008), q_0 (m/Δt) is the surface inflow to the green infrastructure device

from the contributing area and defined below, e_1 (m/Δt) is the evaporation from the

surface water defined using a Penman Monteith equation (Wang et al., 2008), f_1 (m/Δt)

is the infiltration of surface water into the lower layer defined using the Green-Ampt

equation with exponential or power function decay of hydraulic conductivity (Wang et

al., 2006), q_1 (m/Δt) is the surface outflow from the green infrastructure through an outlet

in the berm and defined below, and u_1 (m/Δt) is the upwelling of water from the water-

table.

The upwelling of water into the surface layer is defined as:

$$u_1 = \max\left[-Z_i / \Delta t, 0\right]$$

Eq 3

where Z_i (m) is local water-table depth, positive when below the soil surface, and subscript i denotes the topographic index bin, of which there are 30. The water-table depth is related to the local soil moisture deficit, S_i (m):

$$Z_i = \frac{S_i}{\theta_e}$$

Eq 4

where θ_e (m/m) is the soil effective porosity. The local soil moisture deficit is related to the bulk area catchment average soil moisture deficit, $\bar{S}$ (m), defined as:

$$S_i = \bar{S} + m\left(\lambda - J_i\right)$$

Eq 5

where m is a scaling parameter, λ is the catchment average topographic index, and J_i is the local topographic index (typically a real number between 3 and 30), following the theory presented by Bevin and Kirby (1979). The $\bar{S}$ term is computed at the start of simulation as:

$$\bar{S} = -m \cdot \ln\left[\frac{q_0}{T \cdot e^{-\lambda}}\right]$$

Eq 6

where q_0 (m/Δt) is catchment subsurface drainage at the start of the simulation, and T (m²/Δt) is saturated transmissivity, and then is updated at each time step as:

$$\bar{S} = \bar{S} - q_{uz} + q_b$$

Eq 7

where q_{uz} (m/Δt) is the unsaturated zone drainage and q_b (m/Δt) is catchment subsurface drainage at the time step, defined using Eq 6. This set of computations

163

within the i-Tree Hydro model links the subsurface water-table dynamics with all layers of the green infrastructure water budget.

The surface inflow to the green infrastructure device surface layer is defined as,

$$q_0 = q_{ca,imp} + q_{ca,pi} + q_{ca,ps} + q_{gi,imp}$$

Eq 8

where $q_{ca,imp}$ (m/Δt) is the contributing area impervious runoff, $q_{ca,pi}$ (m/Δt) is the contributing area pervious runoff from infiltration excess, $q_{ca,ps}$ (m/Δt) is the contributing area pervious runoff from saturation excess, and $q_{gi,imp}$ (m/Δt) is the green infrastructure area impervious runoff. Each of these terms are generated by water balance algorithms within the i-Tree Hydro model. The surface outflow from the green infrastructure device is computed following SWMM code (Rossman and Huber, 2016) for non-swale devices such as the bioretention basin, rain garden, infiltration trench, and permeable pavement, and for swales, as:

$$q_1 = \begin{cases} \dfrac{w_1}{n \cdot A_{GI}} \left(d_1 - h_{bc} \right)^{5/3} \cdot s_0^{1/2} \cdot \Delta t & \text{if device} \neq \text{swale} \\[4mm] \dfrac{A_{xs}}{n \cdot A_{GI}} R_1^{2/3} \cdot s_0^{1/2} \cdot \Delta t & \text{if device} = \text{swale} \end{cases}$$

Eq 9

where w_1 (m) is the width of the berm crest allowing for an outlet, n is the Manning roughness, A_{GI} (m^2) is the green infrastructure area, h_{bc} (m) is the height of the berm crest, s_0 (m/m) is the longitudinal slope of the green infrastructure, A_{xs} (m^2) is the cross-sectional area of the flow in the swale, R (m) is the hydraulic radius of the flow in the swale, with A_{xs} and R computed by the i-Tree Hydro model at each time step based on d_1 and the swale geometry of maximum top width and trapezoidal channel side slopes.

164

The water balance defining the incremental change in water fraction in the green infrastructure soil layer is similar to SWMM code (Rossman and Huber, 2016) and given as:

$$D_2 \frac{\Delta\theta_2}{\Delta t} = f_1 - e_2 - f_2 + u_2$$

Eq 10

where D_2 (m) is the soil layer thickness, e_2 (m/Δt) is the evapotranspiration from the soil water defined using a Penman Monteith equation (Wang et al., 2008), f_2 (m/Δt) is the percolation of soil water into the lower layer, and u_2 (m/Δt) is the upwelling of water from the water-table. The soil thickness term D_2 is defined as:

$$D_2 = \frac{L_r}{\theta_e}$$

Eq 11

where L_r (m) is the maximum root zone storage deficit, a term used in the i-Tree Hydro model (Fig. 2), that can be set to a unique value for each green infrastructure type and the bulk area. The percolation term f_2 is defined as:

$$f_2 = q_{rz}$$

Eq 12

where q_{rz} (m/Δt) is the root zone drainage term computed in the i-Tree Hydro model as a function of L_r and the local root zone storage deficit. The upwelling term u_2 is defined as:

$$u_2 = \max\left[(D_2 - Z_i)\cdot\theta_e, 0\right]$$

Eq 13

where it is only adding water to the soil layer when the water-table depth is shallower than the soil layer thickness.

The water balance defining the incremental change in water depth in the green infrastructure storage layer is similar to SWMM code (Rossman and Huber, 2016) and given as:

$$\phi_3 \frac{\Delta d_3}{\Delta t} = f_2 - e_3 - f_3 - q_3 + u_3$$

Eq 14

where ϕ_3 (m/m) is the void fraction of the storage layer substrate, e_3 (m/Δt) is evapotranspiration from the storage layer, f_3 (m/Δt) is the exfiltration of storage water into the lower layer of native soils, q_3 (m/Δt) is the storage layer outflow through a drainage pipe, and u_3 (m/Δt) is the upwelling of water from the water-table. The exfiltration term f_3 is defined for two conditions as:

$$f_3 = \begin{cases} q_{uz} & \text{if } Z_i \leq D_2 + D_3 \\ q_{uz} / \left(\dfrac{Z_i}{D_2 + D_3} \right) & \text{if } Z_i > D_2 + D_3 \end{cases}$$

Eq 15

where q_{uz} (m/Δt) is the unsaturated zone drainage, and in cases when the water-table is below the storage zone, the f_3 is computed as a fraction of q_{uz}. The drainage term q$_3$ is based on the SWMM code (Rossman and Huber, 2016) and defined as:

$$q_3 = \begin{cases} 0.3048 \cdot a_3 \left(d_3 - h_p \right)^{b_3}, & \text{if } d_3 \geq h_p \\ 0, & \text{if } d_3 < h_p \end{cases}$$

Eq 16

where 0.3048 converts ft to m, a_3 is a flow coefficient, h_p (m) is height of the drainage pipe crest relative to the bottom of the storage layer, and b_3 is a flow exponent. In time steps when q_3 is generated due to water-table upwelling above the drainage pipe crest,

that water is treated as q_3 and tracked as q_{3_wt} for use in a catchment water budget described below. The upwelling term u_3 is defined for two conditions as:

$$u_3 = \begin{cases} \max[(D_2 + D_3 - Z_i) \cdot \phi_3, 0] & \text{if } D_2 < Z_i \\ D_3 \cdot \phi_3 & \text{if } Z_i \leq D_2 \end{cases} \qquad \text{Eq 17}$$

where the water-table is either partially or fully occupying the storage layer.

The water balance defining the incremental change in water depth in the green infrastructure permeable pavement layer is similar to SWMM code (Rossman and Huber, 2016) and given as:

$$\phi_4 \frac{\Delta d_4}{\Delta t} = f_1 - e_4 - f_4 + u_4 \qquad \text{Eq 18}$$

where e_4 (m/Δt) is evapotranspiration from the permeable pavement layer, f_4 (m/Δt) is the exfiltration of permeable pavement water into the lower layer, and u_4 (m/Δt) is the upwelling of water from the water-table, defined similarly to those terms in the soil layer.

The water balance for the green infrastructure device is checked against layer water holding capacity at each time step, following the algorithm in the SWMM code, and water leaving the device is routed to the catchment outlet. The depth of water in layers 1, 3, and 4 is reset to a maximum or minimum if the depth is beyond the thickness of the layer, as:

$$d_{j,t} = \begin{cases} 0 & \text{if } d_{j,t} \leq 0 \\ d_{j,t} & \text{if } 0 < d_{j,t} < D_j \\ D_j & \text{if } d_{j,t} \geq D_j \end{cases} \qquad \text{Eq 19}$$

where j represents surface layer 1, storage layer 3, or permeable pavement layer 4. For the soil water fraction, the fraction of water is similarly reset as:

$$\theta_{2,t} = \begin{cases} \theta_{wp} & \text{if } \theta_{2,t} \leq \theta_{wp} \\ \theta_{2,t} & \text{if } \theta_{wp} > \theta_{2,t} < \theta_e \\ \theta_e & \text{if } \theta_{2,t} \geq \theta_e \end{cases} \qquad \text{Eq 20}$$

where θ_{wp} (m/m) is the wilting point moisture and θ_{fc} (m/m) is the field capacity moisture. When the layer water is reset to a maximum, the excess water goes to the next upper layer, which is to the soil layer for the storage excess, to the surface layer for the soil and permeable pavement excess, and to an emergency spillway. The surface flow from the green infrastructure, $q_{s,GI}$ (m/Δt), is defined as:

$$q_{s,gi} = q_1 + q_3 + q_e \qquad \text{Eq 21}$$

where q_e (m/Δt) is emergency spillway water. The total surface flow from the catchment at each time step is defined as the sum of $q_{s,gi}$ and surface flow from the bulk area, q_{ba} (m/Δt), which contains the same contributing area terms in the q_0 of Eq 8, but from the bulk area.

The i-Tree Hydro model, at each time step, first computes the bulk area water balance and then the green infrastructure water balance. At the end of the bulk area water balance, Eq 5 and 7 are computed to update bulk area soil moisture deficits. At the end of the time step, once green infrastructure vertical fluxes are completed, the green infrastructure the local soil moisture deficit, $S_{GI,i}$ is updated based on subtraction of catchment groundwater, $q_{3\_wt,i}$, and the addition of stormwater exfiltration, $f_{3,i,}$ similar to Eq 5, as:

168

$$S_{GI,i} = S_{GI,i} + q_{3\_wt,i} - f_{3,i}$$
<div align="right">Eq 22</div>

The Eq 22 is applied for each topographic index bin *i* with green infrastructure. These local $S_{GI,i}$ values are then used to compute the green infrastructure average soil moisture deficit, as:

$$\bar{S}_{GI} = \sum \left(S_{GI,i} . x_i \right)$$
<div align="right">Eq 23</div>

where x_i is the fractional area of each topographic index bin in the green infrastructure part of the catchment. The catchment average soil moisture deficit is then updated as:

$$\bar{S} = \left[(1 - x_{GI}) \cdot \bar{S} \right] + \left[x_{GI} \cdot \bar{S}_{GI} \right]$$
<div align="right">Eq 24</div>

where the right-hand side term $\bar{S}$ represents the bulk area, computed using Eq 7, and the x_{GI} is the fraction of the catchment in green infrastructure. The Eq 24 left hand side term $\bar{S}$ is then used in the next time step on the right hand side of Eq 7, thereby linking the green infrastructure exfiltration with the bulk area subsurface water budget.

5.2.2 Study area, inputs, and parameters

The above model was tested with the 2-yr return interval and 2-hr duration design rainfall event on the 2.75 ha sub-catchment #4 of the Fort Collins, Colorado case study developed by Gironás et al., (2009) to illustrate how to use SWMM (Fig. 3). The model time step was 5-min, and the potential evaporation rate for both models was set to the constant value for each time step, totaling 5.08 mm for the day. The sub-catchment was simulated without and with each of the permeable green infrastructure devices, by the SWMM and i-Tree Hydro model. When green infrastructure was simulated, the contributing area was defined as 80% of sub-catchment #4, leaving 20%

to drain directly to the outlet. Each green infrastructure device was simulated separately from the other devices, using a distinct device area and number of devices (see Table 1). The soil physical parameters controlling infiltration were set to equivalent values in both models. This analysis did not simulate the permeable depression storage or the presence of vegetation in order to minimize unnecessary simulation differences in this test of the i-Tree Hydro model given the SWMM code uses a different approach to represent these features, as described by Abdi et al. (2019).

The model outputs included time series of all simulated green infrastructure water stores (e.g., surface, soil, storage) and fluxes (e.g., runoff, infiltration, percolation, drainage). These outputs were converted to a common unit of depth, multiplying the flux by the time step, to facilitate comparison between terms in the green infrastructure water balance generated by the i-Tree Hydro model and SWMM simulations. In addition to this model inter-comparison of the 2-hr duration design storm, the i-Tree Hydro model was used to simulate the entire 2018 calendar year of continuous weather at a 1-hr time step, for the same sub-catchment #4 in Fort Collins, without and with green infrastructure device. This additional simulation was used to demonstrate the use of longer time step simulations analysis of green infrastructure devices on the annual water balance.

5.3 Results

Both the i-Tree Hydro model and SWMM simulation of the 2-hr duration design storm without green infrastructure generated 394.7 m^3 of stormwater runoff from the case study sub-catchment (Table 2). This result demonstrates the SWMM and i-Tree

Hydro models can generate equivalent estimates of stormwater runoff for catchments without green infrastructure, and provides a base case against which to compare the reduction in runoff caused by green infrastructure.

For the bioretention basin, the i-Tree Hydro model simulated an inflow depth, q_0, of 286 mm, and 95% of this infiltrated as f_1 (Fig. S1), and 13 mm left as surface outflow q_1 through the berm outlet (Table 3, Fig. 4a). The SWMM simulated inflow of 260 mm (10% less than in i-Tree Hydro), with 95% of this infiltrating and 11 mm leaving through the berm outlet, 18% less q_1 than generated by the i-Tree Hydro model. The total simulated evaporation was 2.5 mm in both models, with each model simulating 10 hrs of additional time after the 2-hr storm ended. The total depth of simulated storage drain runoff, q_3, was nearly identical for the models, with 157 mm estimated by the i-Tree Hydro model, 1 mm more than that estimated by the SWMM (Table 3).

The i-Tree Hydro model simulated inflow q_0 to the bioretention basin at the start of the storm, hour 12:00, initiated a steady increase in the water surface depth d_1, until it reached the berm outlet and generated surface outflow q_1 at hour 13:00 (Fig. 4a). After the end of the rainfall, the water depth in the surface layer began decreasing, and went to zero about hour 19:00, and this triggered the infiltration to drop to zero from its capacity at 40 mm per time step (Fig. 4b). The end of infiltration caused a decrease in the percolation, soil moisture, and storage drain flow, and before the end of the simulation period, the storage drain flow and percolation reached zero (Fig 4a and 4b). At the end of the 12-hr simulation, the i-Tree Hydro model predicted the bioretention basin released 59% of the inflow q_0 as simulated runoff via q_1 and q_3, while the SWMM

predicted a surface runoff release of 64% of the inflow. At the end of the 1-yr simulation, the i-Tree Hydro model predicted the bioretention basin retained 32% of the inflow (Table 4).

For the rain garden, the i-Tree Hydro model simulated an inflow depth, q_0, of 286 mm, and 72% of this infiltrated as f_1 (Fig. S2), and 14 mm left as surface outflow q_1 through the berm outlet (Table 3, Fig. S2). The SWMM simulated inflow of 260 mm (10% less than in i-Tree Hydro), with 80% of this infiltrating and 9 mm leaving through the berm outlet. The total simulated evaporation was 2 mm in both models for the 12 hours of the simulation period. The inflow q_0 steadily increased water surface depth d_1, until it reached the berm outlet and generated surface outflow q_1 at hour 13:00 (Fig. 5a). When surface depth was infiltrated to zero, the infiltration stopped, and the soil moisture content and percolation depth started a decreasing trend (Fig. 5b). At the end of the 12-hr simulation, the i-Tree Hydro model and the SWMM predicted the rain garden released 5% and 4% of the inflow q_0 as simulated runoff, q_1 respectively.

For the infiltration trench, the i-Tree Hydro model simulated the inflow depth, q_0, of 286 mm, and 100% of the inflow infiltrated as f_1 (Fig. S3), with no surface outflow (Table 3, Fig. S3). The SWMM simulated inflow of 260 mm, and infiltrated 100% of this water, generating no surface outflow. Both the i-Tree Hydro model and SWMM simulated negligible evaporation (<1 mm) for the 12-hr simulation period. The total depth of simulated storage drain runoff, q_3, was 221 mm for the i-Tree Hydro model, which was 21 mm more than the simulated storage drain runoff for the SWMM, a 10% difference between the models (Table 3). The i-Tree Hydro model simulated the start of

172

storage drain flow 20 minutes after the beginning of the storm, and which reduced

storage and the exfiltration rate, f_3 (Fig. 6a and 6b). At the end of the 12-hr simulation,

the i-Tree Hydro model and SWMM predicted the infiltration trench released 77% of the

inflow q_0 as simulated runoff via q_1 and q_3.

For the swale, the i-Tree Hydro model simulated the inflow depth, q_0, of 286 mm,

and 12% of inflow infiltrated as f_1 (Fig. S4), and 263 mm left as surface outflow q_1

through the berm outlet (Table 3, Fig. S4). The SWMM simulated inflow of 260 mm, and

infiltrated 16% of this water, and 248 mm left through the berm outlet as q_1, 6% less q_1

than generated by the i-Tree Hydro model (Table 3, Fig. S4). The i-Tree Hydro model

simulated the start of q_1 surface runoff 20 min after the beginning of the rainfall, and this

continued 20 min after the end of the rainfall (Fig. 7a). The infiltration f_1 and surface

depth d_1 started increasing at the start of the storm and continued 20 min beyond the

storm duration (Fig. 7b). At the end of the 12-hr simulation, the i-Tree Hydro model

predicted the swale released 92% of the inflow q_0 as simulated runoff via q_1, while the

SWMM predicted a surface runoff release of 95% of the inflow.

For the permeable pavement, the i-Tree Hydro model simulated the inflow depth,

q_0, of 286 mm, and approximately 99% of the inflow infiltrated as f_1 (Fig. S5), with no

surface outflow q_1 (Table 3, Fig. S5a). The SWMM simulated inflow of 260 mm,

infiltrating 99% of this water and generating no surface outflow. The total simulated

evaporation was 3 mm in both models for the 12-hr period. The total depth of simulated

storage drain runoff, q_3, was 66 mm for the i-Tree Hydro model and 97 mm for SWMM,

a 30% larger depth (Table 3). The i-Tree Hydro model simulated the start of the f_4

percolation at the start of the storm, and this lasted nearly 5-hr as it processed ponded surface water (Fig. S5b). By the time the soil percolation reached zero, the storage depth dropped to zero, and the soil moisture depth leveled at a constant depth until the end of the simulation period (Fig. 8b). At the end of the 12-hr simulation, the i-Tree Hydro model predicted the permeable pavement had released 23% of the inflow q_0 as simulated storage drain flow via q_3, while the SWMM predicted a release of 37% of the inflow.

5.4 Discussion

The established SWMM green infrastructure algorithms (Rossman and Huber 2016), along with its case study (Gironás et al., 2009), provided an excellent benchmark to test the i-Tree Hydro model simulation of green infrastructure devices. The bioretention basin works as a great example to cross-compare the models, as it uses all vertical layers except pavement, and has surface and subsurface outflows. In simulating the bioretention basin, the i-Tree Hydro model and SWMM simulations were within 5% of each other for the estimated water balance and amount of water removed from stormwater runoff. There were predictive differences, and the biggest difference was the estimated depth of water received from the contributing area, which the i-Tree Hydro model estimated as 10% larger, or an extra 26 mm to process. This led to the i-Tree Hydro model infiltrating 26 mm more water and sending an additional 2 mm to surface outflow due to the extra inflow generating a deeper surface depth. The close agreement in model estimates of infiltration is attributed to their use of a nearly equivalent Green-Apmt infiltration algorithm and associated soil parameters.

The additional 26 mm of simulated inflow to the green infrastructure devices estimated by the i-Tree Hydro model, 10% larger than the inflow of the SWMM, is attributed to differences in the catchment hydrology routines of the two models. This difference in the inflow is not an indicator of the performance of the green infrastructure routines. The routine most likely for the difference in the inflow is soil moisture, and how it is parameterized and initialized. Where the SWMM code represents an undefined depth of soil in the non-green infrastructure catchment, the i-Tree Hydro model sets a root zone depth. Where the SWMM code gives an initial fraction of moisture in that soil, the i-Tree Hydro model simulates vertical and lateral variation, using an unsaturated and saturated zone under the root zone, and the topographic index to represent lateral variation in the soil moisture across catchment. This difference could lead to the i-Tree Hydro model having a fraction of the catchment with less available storage and generating additional runoff that was sent to the green infrastructure.

The water balance for the rain garden was notable for infiltrating all of the stormwater inflow, q_0, and not generating any surface outflow, q_1, while the bioretention basin released nearly 5% of inflow as q_1. This difference in device performance was due to the rain garden having a higher berm, which allowed for more surface ponding and more time to infiltrate the stormwater. The swale and infiltration trench water balances were notable for the release of a large fraction of stormwater inflow as surface outflow for the swale (q_1 was 92% of q_0), and subsurface drainage for the infiltration trench (q_3 was 77% of of q_0). The simulation captured the intent of the green infrastructure devices design. For the swale, it was to convey the stormwater to a surface outlet and allow for

175

relatively low rates of infiltration into native soils, and for the infiltration trench it was to rapidly infiltrate stormwater and subsequently remove much of that water with drain pipe. The i-Tree Hydro model allows for alternative stormwater designs with each of these permeable green infrastructure devices, such as reducing the berm outlet height in the swale or removing the drain pipe in the infiltration trench to increase exfiltration to native soils.

The i-Tree Hydro model approach to simulating the water balance, with mechanistic equations for canopy interception, evapotranspiration, depression storage, infiltration and the topographic index based lateral redistribution, differs from approaches used by other models, not just SWMM. In developing the RECARGA model to simulate the impacts of bioretention basin, rain garden, and infiltration trench green infrastructure on the reduction of total runoff, Wang et al., (2013) used the empirical curve number infiltration algorithm within the TR-55 model, which is designed for storms of 12 to 24-hr duration, and not recommended for sub-hourly simulation required for small urban sub-catchment time of concentration storms (Gaffield et al. 2008; Jayasooriya & Ng, 2014). The Program for Predicting Polluting Particle Passage Through Pits, Puddles, and Ponds Urban Catchment Model (P8-UCM; Walker, 1990) uses the curve number algorithm to quickly generate plans for green infrastructure devices at the catchment scale, and is not able to simulate the detailed water balance of individual green infrastructure devices, does not integrate the surface and subsurface water budgets, and does not represent vegetation effects on hydrology.

Stormwater tools popular outside the USA for assessing green infrastructure include MUSIC (Model for Urban Stormwater Improvement Conceptualisation, Chiew and McMahon, 1999), which is more a decision support system, and MOUSE (DHI, 2002), which features routines for analyzing storm sewers, and neither is freeware nor simulates the effects of vegetation on the water balance at the detail of the i-Tree Hydro model. Stormwater models such as RUNQUAL (Runoff Quality model, Haith, 1999), SLAMM (Source Loading and Management Model, Pitt, 1998), StormTac (Larm, 2000), and UVQ (Urban Volume and Quality, Mitchell et al., 2003) do not explicitly simulate green infrastructure and use a daily or longer time step. Considering this list of models, including the SWMM, each has its special purpose, and the i-Tree Hydro model is perhaps the best suited for representing the process-based interaction of green infrastructure within a catchment water balance with water-table and vegetation linkages.

The i-Tree Hydro model updates in this research link the green infrastructure water balance to catchment water-table fluctuations via device exfiltration to native soils (see Fig. S6). This linkage uses the topographic index theory, allowing the green infrastructure exfiltration, and the drainage of the local water-table, to update a soil moisture deficit budget that is separate from the budget of the catchment bulk area. Then, at the end of each time step, these two soil moisture deficits are combined, based on their fractional area of the catchment, and the water-table impacts of green infrastructure are distributed across the catchment. It was recognized by Beven and Kirkby (1979) that lateral redistributions at an hourly time step were likely too fast to

177

represent the time scales for catchment drainage, so the model can use a time delay function.

The parameterization of the terms associated with the average soil moisture deficit will affect the average and local depth to the water-table in the i-Tree Hydro model. In this study, the parameters set the initial average water-table depth to ~2 m, and the green infrastructure was placed in the local topographic index bin with a value J = 6, allowing us to match the SWMM case study of no water-table interaction. To use the i-Tree Hydro model for other case studies, the map of the topographic index values could be overlain on the study site map, and the simulation could investigate the potential design sites for water-table interaction with green infrastructure. This simulation could be run using 1-yr or more of weather data, and in most cases, the objective would be to find sites where the subsurface storage drain is above the high point of the local water-table. The SWMM code does not represent this water-table interaction, and the water-table upwelling terms were added to the green infrastructure water balance in this study.

This study represented the development of the permeable green infrastructure devices in the i-Tree Hydro model, integrating device water balance concepts from SWMM into the catchment redistribution of subsurface moisture. There are issues that should be addressed to improve the i-Tree Hydro model implementation of green infrastructure, and there remain many reasons to use the SWMM simulation for stormwater management. Although the i-Tree Hydro model gives the user the ability to simultaneously run multiple types of green infrastructure devices, the model does not

178

have an option to connect the green infrastructure devices in series, an option SWMM

offers. A series of devices allows analysis of networks of green infrastructure devices,

which is useful in distributing functions across multiple devices, such as efficient

conveyance of large volumes with a swale, followed by rapid infiltration with infiltration

trenches or ponding and water quality treatment via percolation with bioretention basins.

The green infrastructure algorithms in the i-Tree Hydro model are in the back-end

code, which uses a command line interface and configuration.xml to manage options for

inputs, parameters, outputs. There are also plans to introduce additional green

infrastructure devices, such as cisterns or rain barrels, green roofs, and roof

disconnects, into the i-Tree Hydro model, and to represent the impacts of green

infrastructure devices on water quality. There is also opportunity to improve the

algorithms used to model the water balance in the green infrastructure devices, as

researchers discover methods that work better to represent the partitioning of

stormwater into the device and catchment. The i-Tree Hydro model is built in a modular

structure to facilitate such updates.

5.5   Conclusion

There is a global effort coordinated by the United Nations to use nature-based

solutions such as green infrastructure in stormwater management, and thereby improve

urban sustainability. In this study, we coded permeable green infrastructure devices into

the i-Tree Hydro model, which is part of the i-Tree Tools used in urban greening,

provided by the of the USDA Forest Service and partners. The developed green

infrastructure devices in the i-Tree Hydro model are bioretention basins, rain gardens,

179

infiltration trenches, swales, and permeable pavement, each based on the code provided by the SWMM, a stormwater tool supported by the US Environmental Protection Agency. This i-Tree Hydro model provides a different approach than SWMM to integrating the green infrastructure within the catchment water balance and subsurface flow. This includes the i-Tree Hydro model representing linkages between the green infrastructure and topographically-driven water-table upwelling and with vegetation processes such as canopy interception and evapotranspiration. Based on the simulation of green infrastructure devices, the i-Tree Hydro model was able to represent the details provided by SWMM on how the stormwater was partitioned to surface and sub-surface runoff, evaporation, infiltration, percolation, and exfiltration water balance, and integrate the exfiltration into the regional water-table dynamics. The updated i-Tree Hydro model provides an opportunity for planners to design green infrastructure devices into urban greening plans and improve urban sustainability.

5.6   References

Abdi, R., Endreny, T.A., Coville, R., Nowak, D. (2019). Comparison of urban stormwater runoff modeling performance by i-Tree Hydro and EPA SWMM. Urban Forestry and Urban Greening. (Under preparation).

Beck, N.G., Conley, G., Kanner, L., Mathias, M. (2017). An urban runoff model designed to inform stormwater management decisions. Journal of Environmental Management, 193, 257–269.

Beven, K., and Kirkby, J. (1979). A Physically Based, Variable Contributing Area Model of Basin Hydrology. Hydrological Sciences Bulletin, 24(1): 43

Brattebo, B.O., Booth, D.B. (2003). Long-term stormwater quantity and quality performance of permeable pavement systems. Water Res. 37, 4369–4376.

Chiew, F., McMahon, T.A., (1999). Modelling runoff and diffuse pollution loads in urban areas. Water Science and Technology. 39, 241-248.

CIRIA, (2000). Sustainable urban drainage systems - design manual for Scotland and Northern Ireland. Dundee, Scotland: CIRIA Report No. C521.

DHI, (2002). MOUSE surface runoff models reference manual. DHI Software, Horsolm, Denmark.

Damodaram, C., Giacomoni, M.H., Khedun, C.P., Holmes, H., Ryan, A., Saour, W., Zechman, E.M. (2010). Simulation of combined best management practices and low impact development for sustainable stormwater management. J. Am.Water Resour. As. 46, 907e918.

Dotto, C.B.S., Kleidorfer, M., Deletic, A., Rauch, W., McCarthy, D.T. (2014). Impacts of measured data uncertainty on urban stormwater models. J. Hydrol. 508, 28-42.

Elliott, A. H., Trowsdale, S. A. (2007). A review of models for low impact urban stormwater drainage. Environmental Modelling and Software, 22(3), 394–405.

Ellis. J.B. (2013). Sustainable surface water management and green infrastructure in UK urban catchment planning. Journal of Environmental Planning and Management, 56(1), 24–41.

Ellis, J.B., Bryan, Chocat, B., Fujita, S., Marsalek, J., and Rauch, W. (2004). Urban drainage: a multilingual glossary. London: IWA Publishing.

Fletcher, T.D. et al., (2014). SUDS, LID, BMPs, WSUD and more – The evolution and application of terminology surrounding urban drainage.

Fratini, C., Geldof, G.D., Kluck, J., and Mikkelsen, P.S. (2012). Three Points Approach (3PA) for urban flood risk manage- ment: A tool to support climate change adaptation through transdisciplinarity and multifunctionality. Urban Water Journal, 9 (5), 317–331.

Gaffield, S., Montgomery, R., Severson, L., & Sigmarsson, S. (2008). Infiltration modelling to evaluate tradeoffs in planning for future development. Proceedings of the 11th International Conference on Urban Drainage.

Gironas, J.L., Roesner, A., Rossman, L.A., Davis, J. (2010). A new applications manual for the Storm Water Management Model (SWMM). Environmental Modelling & Software, 25(6): 813-814.

Haith, D.A. (1999). RUNQUAL runoff quality from development sites, User manual. Department of Agricultural & Biological Engineering. Cornell University. Ithaca NY.

Jayasooriya, V.M., Ng, A.W.M. (2014). Tools for modeling of stormwater management and economics of green infrastructure practices: A review. Water, Air, and Soil Pollution, 225(8).

Kamali, M., Delkash, M., Tajrishy, M. (2017). Evaluation of permeable pavement responses to urban surface runoff. Journal of Environmental Management, 187, 43–53.

Klein, R.D. (1979). Urbanization and stream quality impairment. Water Resources Bulletin 15, 948–963.

Larm, T. (2000). Watershed-based Design of Stormwater Treatment Facilities: Model Development and Applications [Dissertation]. KTH Royal Institute of Technology, Stockholm, Sweden, TRITA—AMI PHD 1038.

Mitchell, V.G., Diaper, C., Gray, S.R., Rahilly, M. (2003). UVQ: Modelling the movement of water and contaminants through the total urban water cycle. In: 28th International Hydrology and Water Resources Symposium, Wollongong, NSW. Institution of Engineers, Australia.

National Research Council (NRC), (2009). Urban Stormwater Management in the United States. Washington, DC, The National Academies Press.

Nie, W., Yuan, Y., Kepner, W., Nash, M.S., Jackson, M., Erickson, C. (2011). Assessing impacts of Landuse and Landcover changes on hydrology for the upper San Pedro watershed. J. Hydrol. 407 (1e4), 105e114

NYS DEC (New York State, Department of Environmental Conservation). (2015). Stormwater management Design manual. New York State, Department of Environmental Conservation. Albany, NY.

Pitt, R., Voorhees, J. (2002). SLAMM, the source loading and management model. Wet-weather flow in the urban watershed: technology and management, 103–139.

Rode, M., Suhr, U. (2007). Uncertainties in selected river water quality data. Hydrol. Earth Syst. Sci. Discuss. 11(2), 863-874.

Rossman, L.A., Huber, W.C. (2016). Storm water management model reference manual volume I – Hydrology. U.S. Environmental Protection Agency EPA/600/R-15/162

United Nations. (2014). Department of Economic and Social Affairs, Population Division: World Urbanization Prospects: The 2014 Revision, Highlight.

United States Department of Agriculture Forest Service (USDA FS), (2018). i-Tree Hydro V6 User Manual. Syracuse, NY.

Walker, W. (1990). P8 urban catchment model program documentation, v1.1. Prepared for IEP, Inc., Northborough, MA and Narragansett Bay Project, Providence, RI

Walker, L., et al. (2011). Are UK professionals predisposed to retrofit more sustainable surface water management measures? Proceedings of the 12th international conference on urban drainage (ICUD12), 11–16 September, Porto Alegre, Brazil. London: International Water Association (IWA).

Wang, J., Endreny, T. A., Hassett, J. M. (2006). Power function decay of hydraulic conductivity for a TOPMODEL-based infiltration routine. Hydrological Processes, 20, 3825–3834.

Wang, J., Endreny, T. A., Nowak, D. J. (2008). Mechanistic simulation of tree effects in an urban water balance model. Journal of American Water Resources Association,. 1. 44(1), 75–85.

Wang, Q., Li, S., Jia, P., Qu, C., Ding, F. (2013). A review of surface water quality models. Sci. World J.

Wong, T.H.F. (2007). Water sensitive urban design; the journey thus far. Australian Journal of Water Resources, 110 (3), 213–222.

WWAP (United Nations World Water Assessment Programme)/UN-Water. (2018). The United Nations World Water Development Report 2018: Nature-Based Solutions for Water. Paris, UNESCO.

WWAP (UNESCO World Water Assessment Programme). (2019). The United Nations World Water Development Report 2019: Leaving No One Behind. Paris, UNESCO.

WMO (World Meteorological Organization). (2006). Bulletin, the journal of the World Meteorological Organization. World Meteorological Organization. 55(3).

US Climate Resilience Toolkit, 2019 https://toolkit.climate.gov/tool/storm-water-management-model

United Nations, 2018. https://www.un.org/development/desa/publications/2018-revision-of-world-urbanization-prospects.html

US Climate Resilience Toolkit, 2019 https://toolkit.climate.gov/tool/storm-water-management-model

5.7 Tables

Table 13 (Table 1): The parameters used for the simulations in the i-Tree Hydro model and SWMM.

GI Type	Layer	Depth (m)	Void Ratio	Area (m^2)	GI unit number	Contributing Area (m^2)	Soil Conductivity (m/h)	Suction head (m)	Initial soil deficit (%)
BR	Surface	0.15	1.0	46.45	30	26206	0.0025	0.0613	0
	Soil	0.2	0.4						
	Storage	0.8	0.4						
RG	Surface	0.2	0.1	46.45	30	26206	0.0025	0.0613	0
	Soil	0.5	0.4						
IT	Surface	0.15	1.0	45.45	30	26206	n/a	n/a	n/a
	Storage	1.0	0.3						
PP	Surface	0.1	1.0	45.45	30	26206	0.0025	0.0613	0
	Pavement	0.2	0.3						
	Soil	0.2	0.4						
	Storage	0.8	0.4						
SW	Surface	0.7	1.0	464.5	3	26206	0.000423	0.0613	0
	Soil	0.2	0.4						

BR: Bioretention, RG: Rain Garden, IT: Infiltration Trench, PP: Permeable Pavement; SW: Swale

Table 14 (Table 2): Simulated surface runoff for the i-Tree Hydro model and EPA SWMM and their differences for the conditions with no green infrastructure control and with adding GI devices for the test case.

GI type	With GI/LID			Without GI/LID		
	i-Tree Hydro (m³)	EPA SWMM (m³)	Difference (%)	i-Tree Hydro (m³)	EPA SWMM (m³)	Difference (%)
Bioretention (BR)	315.9	315.4	0	394.7	394.7	0
Rain Garden (RG)	97.3	91.1	7	394.7	394.7	0
Infiltration Trench (IT)	384.5	357.5	7	394.7	394.7	0
Swale (SW)	445.4	427.6	4	394.7	394.7	0
Permeable Pavement (PP)	197.4	210.3	6	394.7	394.7	0

Table 15 (Table 3): Detailed results of the simulations for the test case using the i-Tree Hydro model and the EPA SWMM.

GI	Model	q0 (mm)	q1 (mm)	q3 (mm)	f1 (mm)	f2 (mm)	f3 (mm)	f4 (mm)
BR	i-Tree Hydro	286	13	157	271	231	58	n/a
	EPA SWMM	260	11	156	247	226	58	n/a
	Differences (%)	10	18	0	10	2	0	n/a
RG	i-Tree Hydro	286	14	n/a	206	55	n/a	n/a
	EPA SWMM	260	9	n/a	206	56	n/a	n/a
	Differences (%)	10	55	n/a	0	0	n/a	n/a
IT	i-Tree Hydro	286	0	221	286	n/a	65	n/a
	EPA SWMM	260	0	200	260	n/a	58	n/a
	Differences (%)	10	0	10	10	n/a	12	n/a
SW	i-Tree Hydro	286	263	n/a	35	n/a	n/a	n/a
	EPA SWMM	260	248	n/a	43	n/a	n/a	n/a
	Differences (%)	10	6	n/a	22	n/a	n/a	n/a
PP	i-Tree Hydro	286	0	66	283	199	133	281
	EPA SWMM	260	0	97	257	231	134	253
	Differences (%)	10	0	30	10	13	0	10

BR: Bioretention, RG: Rain Garden, IT: Infiltration Trench, PP: Permeable Pavement, SW: Swale, q0: Inflow, q1: Surface outflow, q3: Storage drain, f1: Infiltration, f2: Soil percolation, f3: Exfiltration, f4: Pave percolation

Table 16 (Table 4): Simulated annual surface runoff using the i-Tree Hydro model for the conditions with no green infrastructure and with adding bioretention for the test case.

Time period (Year)	No GI Total runoff (m^3)	With Bioretention GI device				Difference (%)
		Untreated (m^3)	Surface outflow (m^3)	Storage drain (m^3)	Total runoff (m^3)	
2018	2083.7	416.7	726.0	257.8	1400.5	32

Table 17 (Table S1): List of the parameters have been used for the simulations in i-Tree Hydro and SWMM models.

GI Type	Contributing area imp. fraction	Contributing area treated fraction	Directly Connected Impervious Area fraction	Imp. Depression storage (mm)	Per. Depression storage (mm)	Surface Berm Hight (m)	Surface emergency spillway height (m)	Surface Slope (%)	Surface Roughness	GI width at the outlet (m)	Soil Transmissivity (m²/h)
BR	0.5	0.8	1.0	1.14	0.0	0.15	0.8	1.5	0.1	4	0.33
RG	0.5	0.8	1.0	1.14	0.0	0.2	0.8	1.5	0.1	4	0.33
IT	0.5	0.8	1.0	1.14	0.0	0.15	0.8	0.4	0.24	4	0.33
PP	0.5	0.8	1.0	1.14	0.0	0.1	0.8	1.5	0.02	5	0.33
SW	0.5	0.8	1.0	1.14	0.0	0.7	0.7	1.5	0.1	5	0.33
GI Type	Maximum Root Zone Deficit (m)	Initial root zone deficit (%)	Soil macropore (%)	Soil Filed capacity (fraction)	effective Porosity (fraction)	Soil Conductivity slope	Soil wilting point (fraction)	Topographic Index (TI) bin number	Storage clogging factor	Storage Drain Offset (m)	Drain Orifice Coefficient
BR	0.08	0.0	0.0	0.2	0.4	10.0	0.1	24	0	0.05	0.3
RG	0.2	0.0	0.0	0.2	0.4	10.0	0.1	24	n/a	n/a	0.3
IT	0.0	0.0	0.0	n/a	n/a	n/a	n/a	24	0	0.05	0.3
PP	0.08	0.0	0.0	0.2	0.4	10.0	0.1	24	0	0.05	0.3
SW	0.08	0.0	0.0	0.2	0.4	10.0	0.1	24	n/a	n/a	0.3
GI Type	Drain Orifice Exponent	Storage seepage rate (m/h)	Pavement Thickness	Pavement Clogging Factor	Pavement Regen Days	Pavement Permeability (m/h)	Surface Side Slope				
BR	0.9	0.000423	n/a	n/a	n/a	n/a	n/a				
RG	n/a	n/a	n/a	n/a	n/a	n/a	n/a				
IT	0.9	0.00205	n/a	n/a	n/a	n/a	n/a				
PP	0.9	0.0010	0.2	0.0	0.0	2.12	n/a				
SW	n/a	n/a	n/a	n/a	n/a	n/a	3.0				

BR: Bioretention, RG: Rain Garden, IT: Infiltration Trench, PP: Permeable Pavement, SW: Swale, DCIA: Directly Connected Impervious Area, Imp.: Impervious, Per. Pervious

5.8 Figures
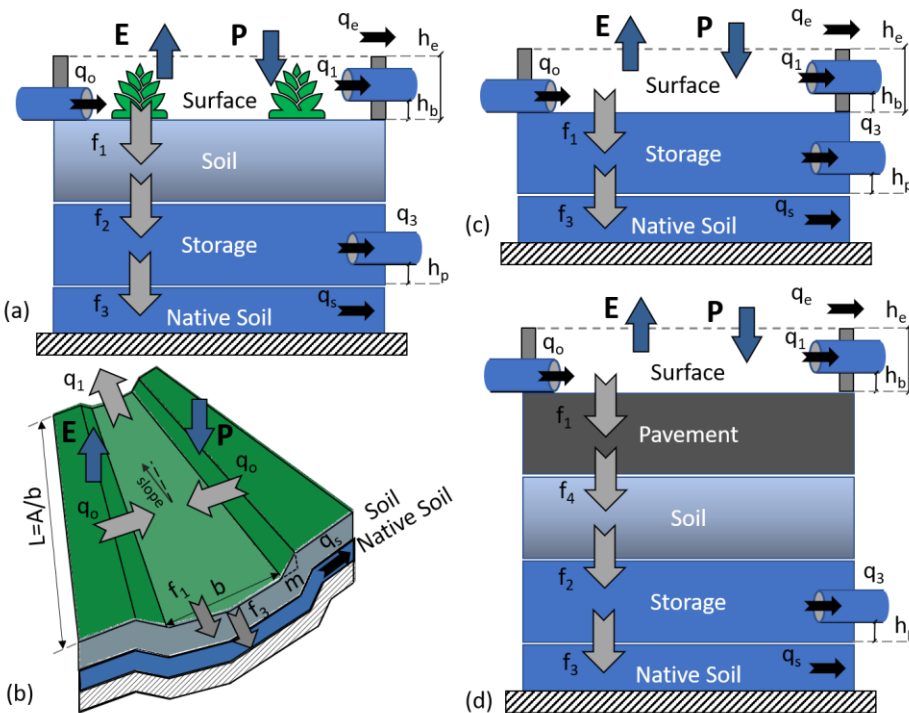
Figure 30 (Figure 1): The schematic design of the bioretention cell (a), vegetation swale (b), infiltration trench (c), and permeable pavement (d). In the figure, the term q represents the water flow to and from the GI design with the substrates of $_0$ for the inflow, $_1$ for the surface outflow, $_3$ for the underdrain, $_e$ for the emergency spillway outflow, and $_s$ for the base flow. The term f represents the movement of water in the vertical direction with the substrates of $_1$ for the infiltration, $_2$ for the percolation, $_3$ for exfiltration, and $_4$ for percolation through the pavement. The h_b is the outflow pipe height from the surface, h_e is the emergency spillway outflow height, and h_p is the drain offset height. In panel (b), L is the length of the swale, A is the swale area, b is the bottom width, P is the rainfall, E is the evaporation, and m is the side slope.
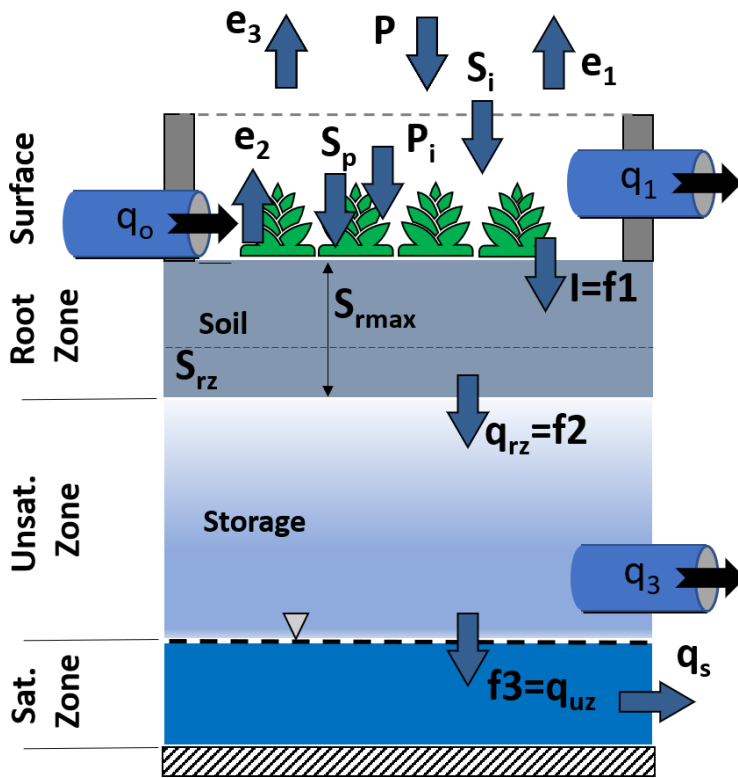
Figure 31 (Figure 2): The schematic of the flow variables in i-Tree Hydro and SWMM overlaid with the i-Tree Hydro model structure. In the figure P is the precipitation, P_i is the canopy interception, S_p is the pervious depression storage, S_i is the impervious depression storage e_3 is the vegetation evaporation, q_s is the base flow, I is the infiltration, S_{rmax} is the maximum root zone depth, S_{rz} is the root zone storage, q_{rz} is the root zone to unsaturated zone percolation, and q_{uz} is the unsaturated zone to saturated zone percolation. The terms f_1, f_2, and f_3 referred the infiltration, percolation, and exfiltration respectively in SWMM.
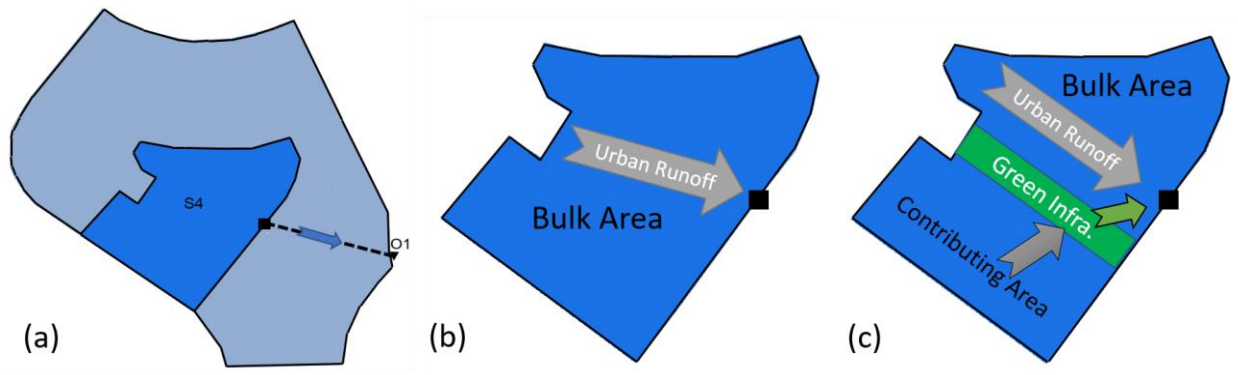
Figure 32 (Figure 3): The sub-catchment has been used in the simulations (a) without applying the green infrastructure devices (b) and after adding the GI devices (c).
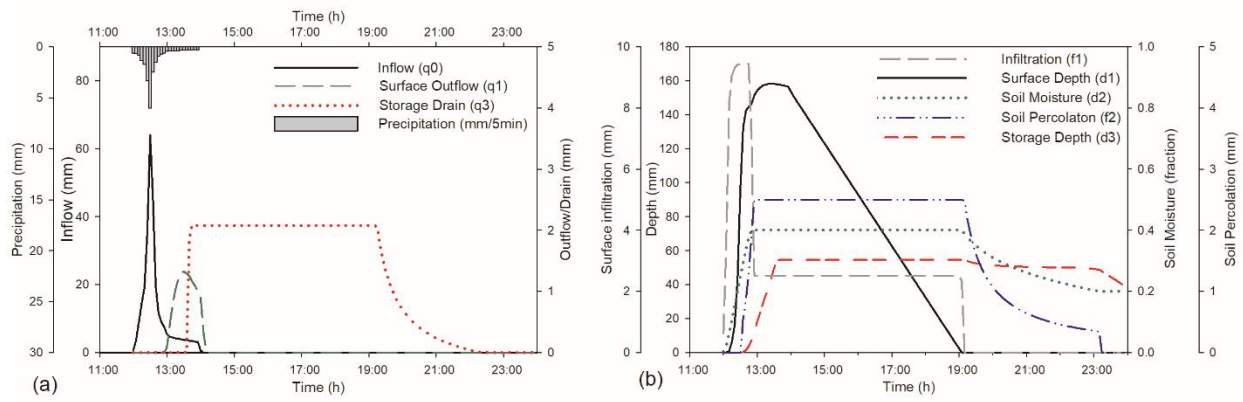
Figure 33 (Figure 4): The detailed results of simulating the bioretention GI using the i-Tree Hydro model for 12 hours. Panel (a) shows the precipitation, as well as the inflow and outflows. Panel (b) shows the active features of the GI device during and after the rainfall.
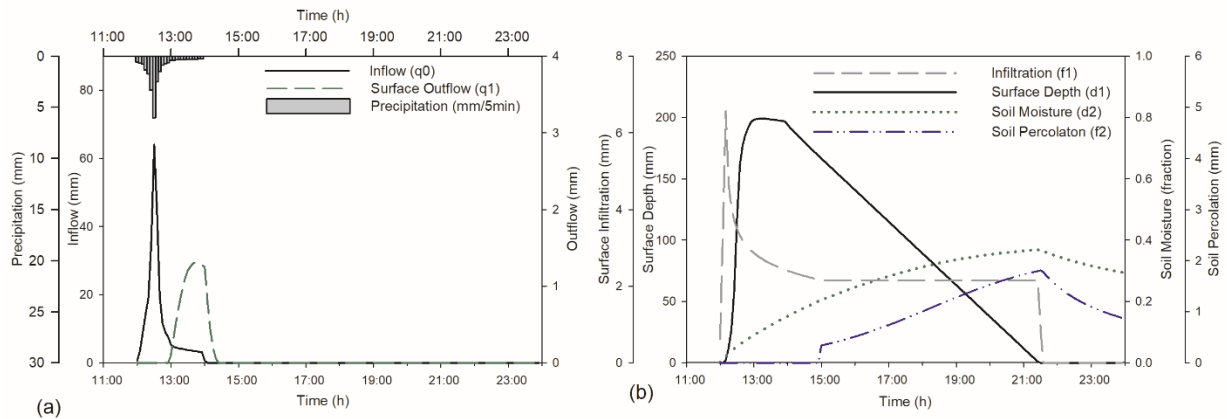
Figure 34 (Figure 5): The detailed results of the simulating the rain garden GI using the i-Tree Hydro model for 12 hours. Panel (a) shows the precipitation and the inflow, panel (b) shows the variation of the inflow only during the rainfall event, and panel (c) represents the active features of the rain garden during and after the rainfall.
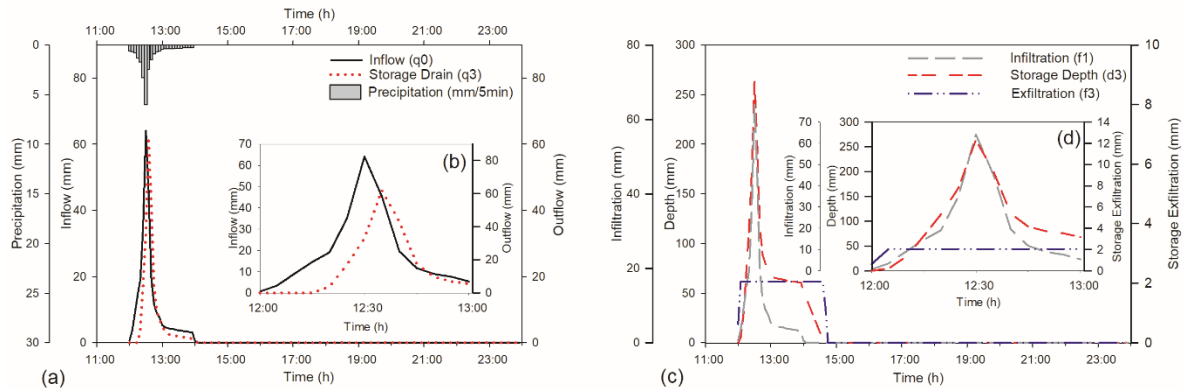
Figure 35 (Figure 6): The detailed results of the simulating the infiltration trench GI using the i-Tree Hydro model for 12 hours. Panel (a) shows the precipitation and the storage drain, panel (b) shows the inflow and storage drain in the first hour of the simulation, panel (c) shows the active features of the GI device during and after the rainfall, and panel (d) shows the infiltration rate, storage depth, and exfiltration rate in the first hour of the simulation.
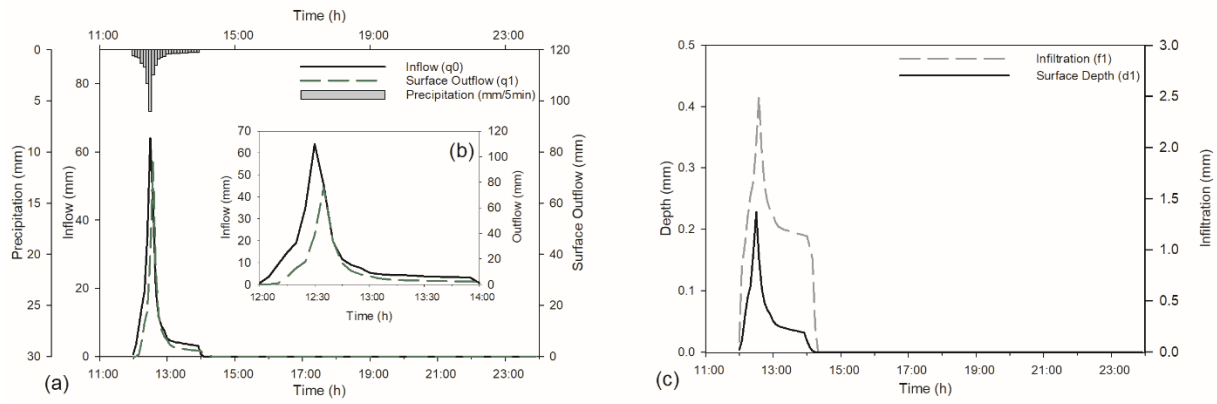
Figure 36 (Figure 7): The detailed results of the simulating the swale GI using the i-Tree Hydro model for 12 hours. Panel (a) shows the precipitation, as well as the inflow and the surface outflow, panel (b) shows the simulated inflow and surface outflow variation during the rainfall, and panel (c) shows the active features of the GI device during and after the rainfall.
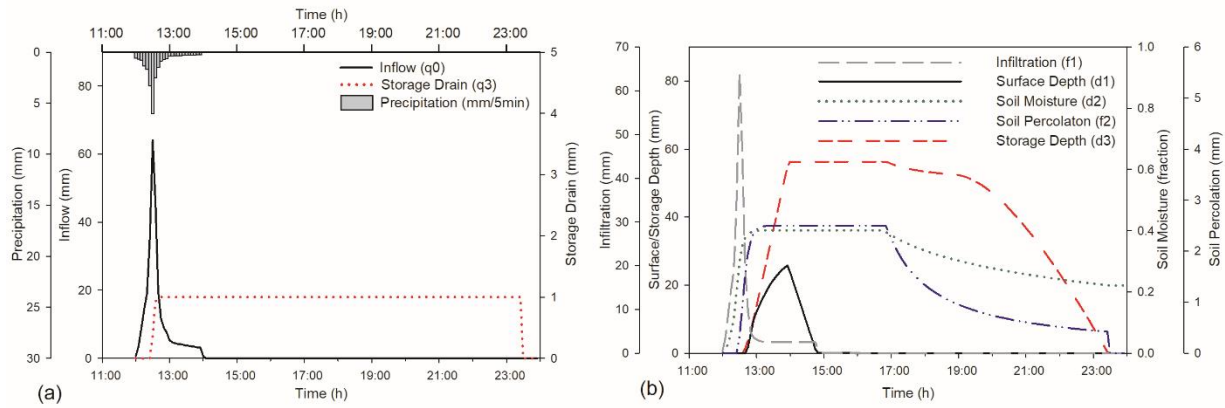
Figure 37 (Figure 8): The detailed results of the simulating the permeable pavement GI using the i-Tree Hydro model for 12 hours. Panel (a) shows the precipitation, as well as the inflow and the storage drain and panel (b) shows the active features of the GI device (except the pave percolation and pave depth – see Fig. S5b) during and after the rainfall.
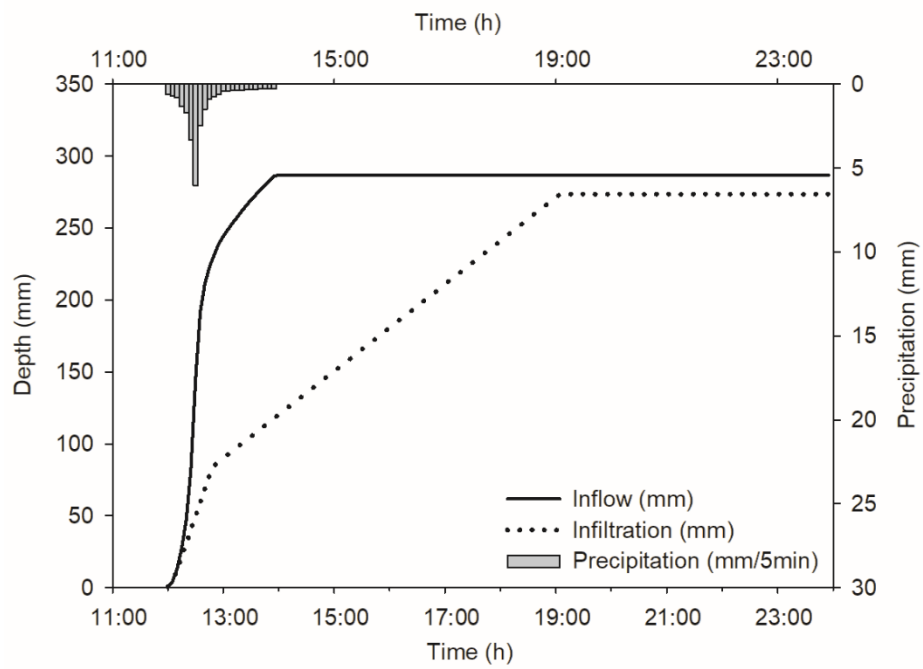
Figure 38 (Figure S1): The variation of the accumulated inflow and infiltration in the bioretention GI scenario simulated by i-Tree Hydro.
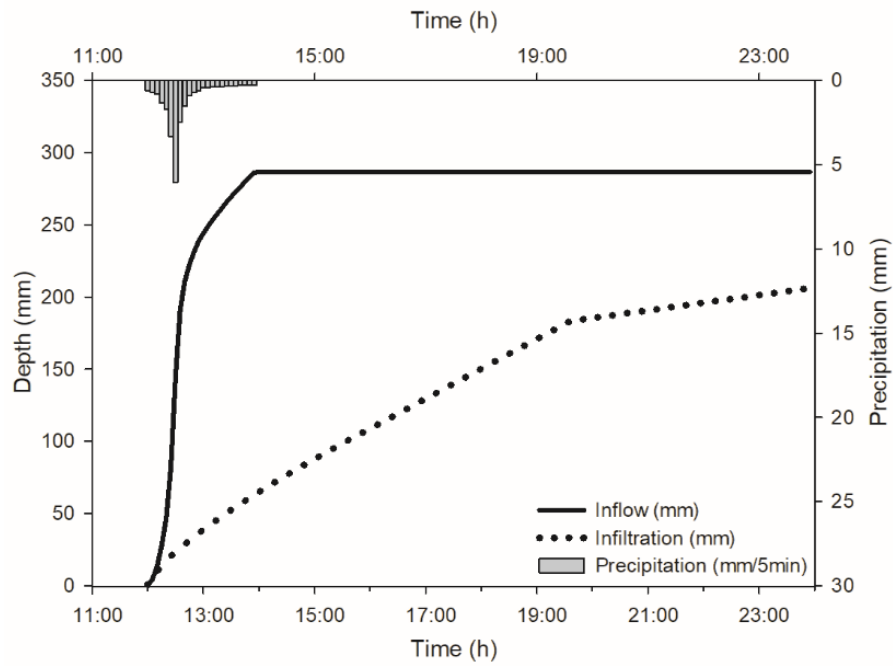
Figure 39 (Figure S2): The variation of the accumulated inflow and infiltration in the rain garden GI scenario simulated by i-Tree Hydro.
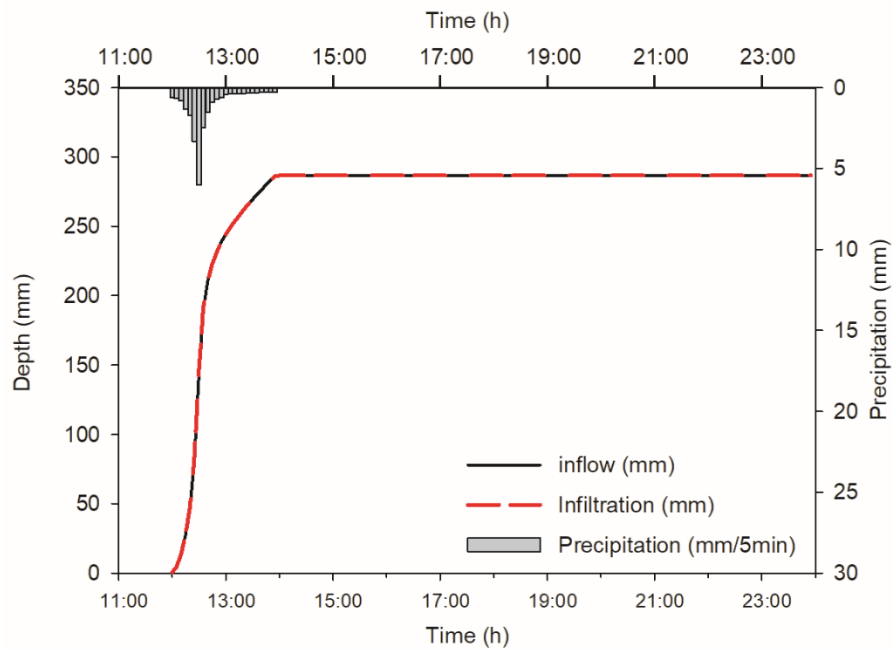
Figure 40 (Figure S3):   The variation of the accumulated inflow and infiltration in the infiltration trench GI scenario simulated by i-Tree Hydro.
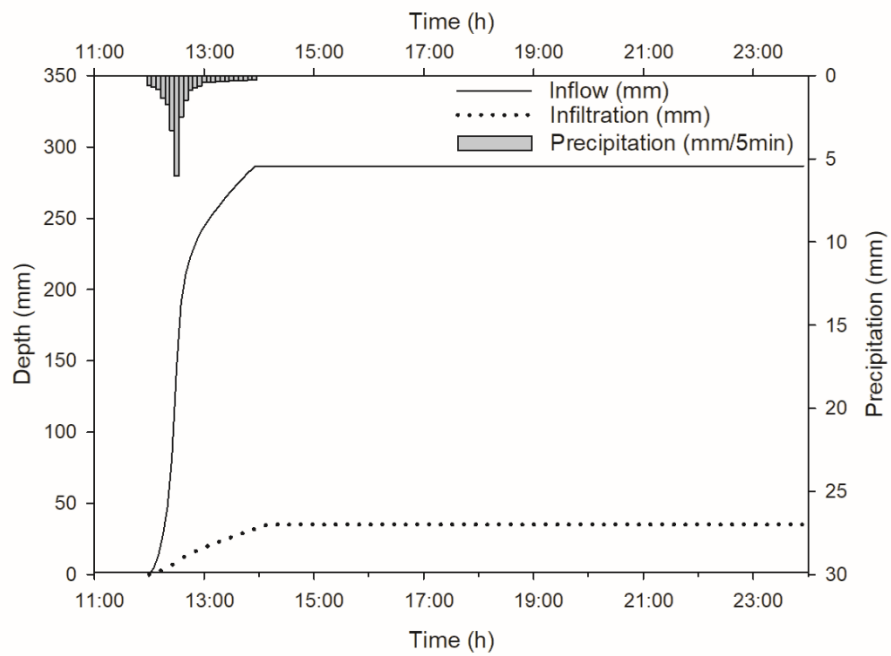
Figure 41 (Figure S4): The variation of the accumulated inflow and infiltration in the swale GI scenario simulated by i-Tree Hydro.
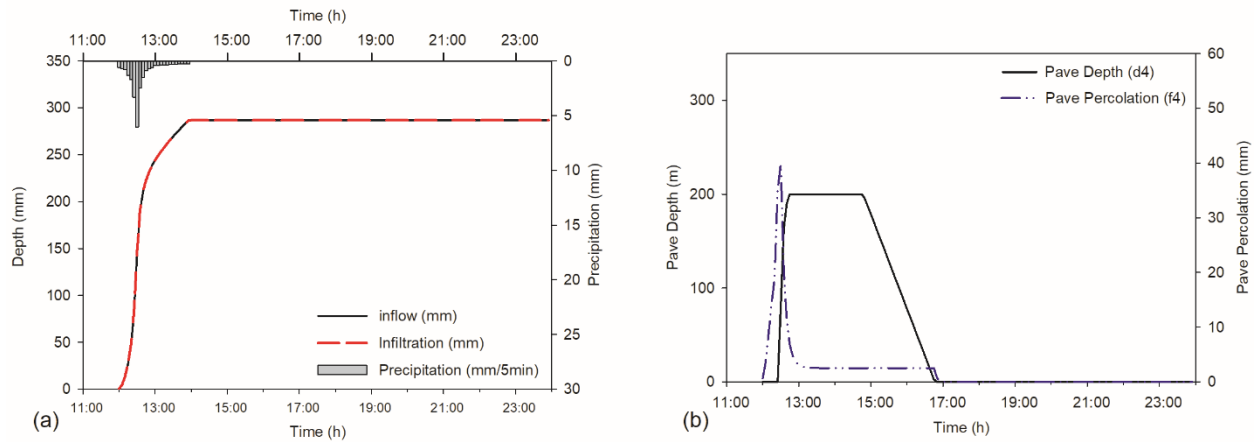
Figure 42 (Figure S5): (a) The variation of the accumulated inflow and infiltration in the permeable pavement GI scenario simulated by i-Tree Hydro. (b) The variation of the pavement percolation and pavement depth in the permeable pavement GI scenario simulated by i-Tree Hydro.
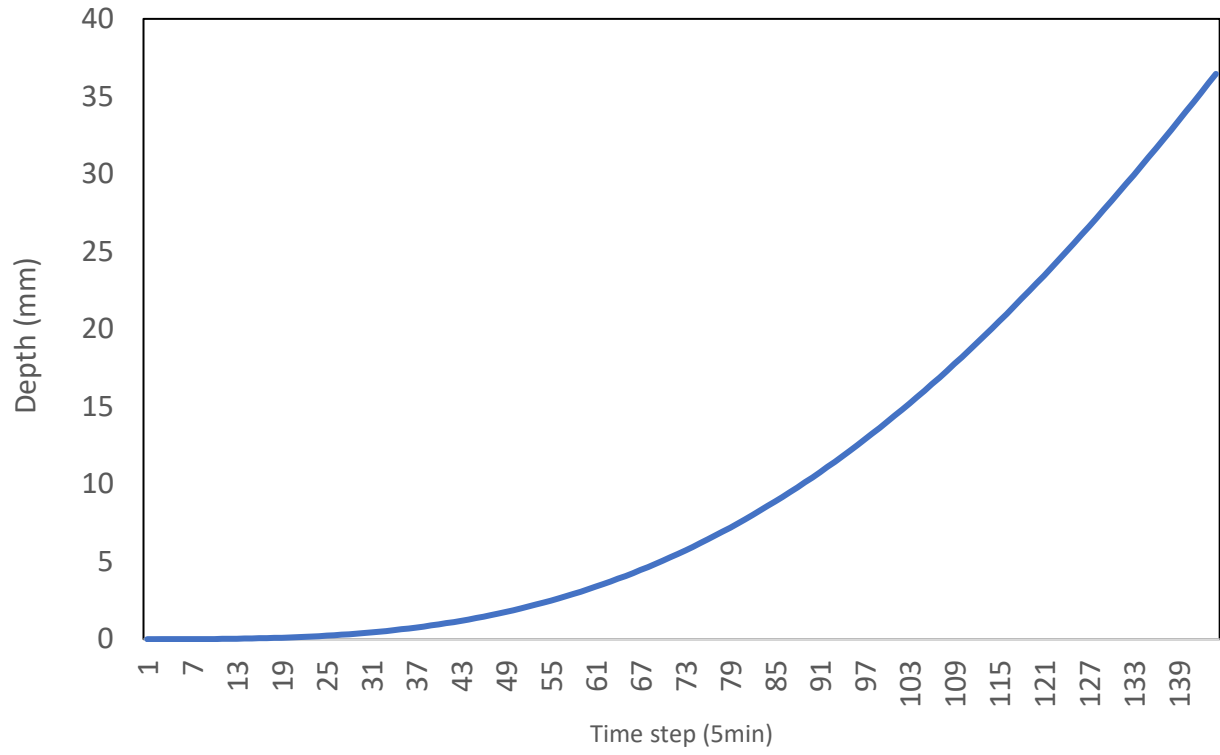
Figure 43 (Figure S6): The differences between average soil moisture deficit of the bulk area for two conditions of with and without green infrastructure linkage.

6   Synthesis and Future Work

This dissertation addresses the United Nations recommendations to implement nature-based solutions in achieving urban sustainability, with our focus on restoration of rivers and stormwater systems to improve water resources management, human wellbeing, and biodiversity. Based on the United Nations, the nature-based restoration approaches should be assessed to address the degradation in water quality and quantity caused by mismanagement in the urban systems where impervious cover decreases infiltration, warms runoff, and increases flooding. Two nature-based alternatives for addressing these concerns in water quality and quantity are riparian shading which provides shade effect and green infrastructure which increase the infiltration and evapotranspiration rates.

In this dissertation, C++ freeware computer algorithms were developed to simulate and design potential nature-based solutions. This research represented a) development of mechanistic computer models to simulate the thermal pollution in urban rivers and potential restoration alternatives to reduce the thermal pollution including riparian shade, stormwater infiltration, and mixing of river water and groundwater as hyporheic exchange; and b) development of mechanistic computer algorithms to simulate the impacts of permeable green infrastructure devices on urban stormwater runoff and the linking of stormwater infiltration with a catchment hydrology model simulating atmospheric, vegetation, and subsurface transfers of water. The newly developed i-Tree Cool River and updated i-Tree Hydro models were designed to bring

nature-based restoration alternatives to city planners and managers involved with urban systems.

The abstract of the 2nd chapter, A River Temperature Model to Assist Managers in Identifying Thermal Pollution Causes and Solutions, follows. Thermal pollution of rivers degrades water quality and ecosystem health, and cities can protect rivers by decreasing warmer impervious surface stormwater inflows and increasing cooler subsurface inflows and shading from riparian vegetation. This study develops the mechanistic i-Tree Cool River Model and tests if it can be used to identify likely causes and mitigation of thermal pollution. The model represents the impacts of external loads including solar radiation in the absence of riparian shade, multiple lateral storm sewer inflows, tributaries draining reservoirs, groundwater flow, and hyporheic exchange flow in dry weather steady flows and wet weather unsteady flows. The i-Tree Cool River Model estimates the shading effects of the riparian vegetation and other features as a function of heights and distances as well as solar geometry. The model was tested along 1500 m of a New York mountain river with a riparian forest and urban areas during 30 h with two summer storm events in 2007. The simulations were sensitive to the inflows of storm sewers, subsurface inflows, as well as riparian shading, and upstream boundary temperature inflows for steady and unsteady conditions. The model simulated hourly river temperature with an R^2 of 0.98; when shading was removed from the simulation the R^2 decreased 0.88, indicating the importance of riparian shading in river thermal modeling. When stormwater inflows were removed from the simulation, the R^2 decreased from 0.98 to 0.92, and when subsurface inflows were removed, the R^2

207

decreased to 0.94. The simulation of thermal loading is important to manage against pollution of rivers.

The abstract of the 3rd chapter, A model to Integrate Analysis of Urban River Thermal Cooling and Flood Risk in River Restoration, follows. River water quality and habitats are degraded by thermal pollution from urban areas caused by warm surface runoff, lack of riparian forests, and impervious channels that transfer heat and block cool subsurface flows. This study updates the i-Tree Cool River model to simulate restoration of these processes to reverse the urban river syndrome, while using the HEC-RAS model water surface profiles needed for flood hazard analysis in restoration planning. The new model was tested in a mountain river within the New York City drinking water supply area, and then used for base case and restoration scenarios on the 17.5 km reach of the Los Angeles (LA) River where a multi-million dollar riverine restoration project is planned. The model simulated the LA River average temperature in the base case decreased from 29.5°C by 0.3℃ when warm surface inflows were converted to cooler groundwater inflows by green infrastructure; by 0.7°C when subsurface hyporheic exchange was increased by removal of armoring and installation of riffle-pool bedforms; by 3.6℃ when riparian forests shaded the river; and by 6.4°C when floodplain forests were added to riparian forests to cool surface reservoirs and local air temperatures. The simulated decreases in river temperature lead to increased saturated dissolved oxygen levels, reaching 8.7 mg/L, up from the 7.6 mg/L in the base case scenario, providing improved fish habitat and reducing eutrophication and hypoxic zones.

The abstract of the 4th chapter, Comparison of Urban Stormwater Runoff

Modeling Performance By i-Tree Hydro and EPA SWMM, follows. Impervious landcover

in urban watersheds have long been implicated in the decline of watershed integrity,

due to its effects on stormwater runoff quantity and quality. To facilitate urban

watershed management, hydrologic models are used to assess how stormwater runoff

will respond to different management and land cover scenarios. This study aims to

compare the runoff quantity estimates of two hydrologic models, the i-Tree Hydro model

and the Environmental Protection Agency's Stormwater Management Model (EPA

SWMM), each using similar methods to represent impervious depression storage and

infiltration, but different methods to represent pervious depression storage, canopy

interception, evaporation, subsurface flow, and hydrograph routing. The models

simulated a 2-hr design storm event at a 5-min time step for six distinct sub-basins

totaling 11.7 ha in size, each with distinct land cover characteristics affecting runoff. To

reduce differences in model predictions of runoff, inputs for both models set potential

canopy interception and pervious depression to 0. The i-Tree Hydro model estimated a

total effective runoff of 15.4 mm, 3% higher than SWMM. The i-Tree Hydro model

simulated a peak effective runoff of 3.6 mm, 5% higher than SWMM. Both models

estimated the same time to peak runoff, with SWMM using a kinematic wave algorithm

and the i-Tree Hydro model using 2 calibrated parameters in a diffusive wave algorithm.

The i-Tree Hydro model estimated a total infiltration of 8.5 mm, 1% higher than SWMM

and total evaporation of 0.8 mm, 40% less than the SWMM. Based on this study, the

two models are equivalent in estimating total runoff, and can be adjusted to represent the same peak runoff characteristics.

The abstract of the 5th chapter, Development of Permeable Green Infrastructure Algorithms with Water-table and Vegetation Linkages in the i-Tree Hydro Model, follows. The United Nations advocates the use of green infrastructure devices in stormwater management to address the needs of urban sustainability, noting the devices can utilize stormwater for natural irrigation of urban greening projects, reduce pollution of receiving waters, and address water scarcity. Computer models that simulate green infrastructure within the catchment water balance are called for by the National Academy of Sciences. In this study, we update the urban runoff model, i-Tree Hydro, to represent the permeable green infrastructure water balance of ponding, infiltration, percolation, evaporation, and surface and subsurface drainage, and then link that balance with the catchment redistribution of subsurface water and water interception and evapotranspiration by vegetation. The green infrastructure devices modeled were bioretention basin, rain garden, infiltration trench, swale, and permeable pavement, with their design taken from the US Environmental Protection Agency's Storm Water Management Model (SWMM). Each green infrastructure device was simulated within the i-Tree Hydro model, comparing its water balance against that of SWMM, for a 2-yr return interval, 2-hr duration design storm, on a 2.7 ha urban area, simulated for 12-hr at a 5-min time step. The updated model was then used to estimate how a bioretention device changes the catchment water balance for a 1-yr simulation. Results showed that for the five green infrastructure devices, the two models estimated infiltration within

10%, percolation within 5%, evaporation within 2%, surface outflow within 15%, subsurface outflow within 13%, and exfiltration to native soils within 4%. On average total runoff volume reduction estimated by the i-Tree Hydro model was 28%, 1.6% less than SWMM. The differences in the water balance of the two models are attributed to different soil moisture algorithms, with slightly different code structure for infiltration and percolation. The new i-Tree Hydro model helps advance nature-based design by connecting the permeable green infrastructure devices with the catchment redistribution of subsurface water and the vegetation processes of interception and evapotranspiration.

Future work to advance this research could include updates to the i-Tree Cool River and i-Tree Hydro models that make them more accessible for users, and thereby advance the United Nations goals for nature-based solutions. The i-Tree Cool River model currently requires users to obtain: 1) upstream boundary condition inflow rate and temperature data, 2) lateral inflow rate and temperature data for any storm sewer or tributary, 3) groundwater inflow rate and temperature data at each cross-section, 4) average air temperature data representative of the riparian tree cover, and 5) shade factor data representing the riparian cover influence on the river, as well as inputs of solar radiation, river channel geometry and morphology. If the i-Tree Cool River model were coupled with the i-Tree Cool Air model and an updated i-Tree Hydro model, within a Unified Hydro framework, it is likely to auto-generate for the i-Tree Cool River model the first 4 inputs listed above.

The riparian land cover inputs used in i-Tree Cool River model would be used by i-Tree Cool Air model to predict air temperatures associated with the riparian land cover. An updated i-Tree Hydro model would include the non-linear regression equation for estimating river water based on air temperature, used in Chapter 2 and 3 of this dissertation, and this would allow the i-Tree Hydro model to predict upstream and lateral inflow rates and temperatures for the i-Tree Cool River model. The i-Tree Hydro model could also provide groundwater inflow and temperature to the i-Tree Cool River model, based on i-Tree Hydro model estimate of subsurface flow, proportioned to the contributing area adjacent to each river bank, where contributing area is computed in the topographic index equations of the i-Tree Hydro model. Further, the i-Tree tools could be expanded to replicate the TTools algorithm used by Heat Source, described in Chapter 2, to predict the shade factor as an input for the i-Tree Cool River model.

The i-Tree Hydro model green infrastructure algorithms could be updated to include more advanced water quantity, transport, and water quality routines. The water quantity routines for green infrastructure are limited to permeable green infrastructure devices that allow for infiltration into the catchment subsurface aquifer and generate increased subsurface flow. The additional water quantity routines should include non-permeable green infrastructure devices, such as green roofs, roof top disconnects, and cisterns (e.g., rain barrels) used in the Storm Water Management Model, which do not connect to the catchment subsurface aquifer. The transport of the water in green infrastructure devices should be enhanced to allow for linking green infrastructure devices in a series, expanding the current default of sending device surface outflow to

212

the catchment outlet. This would allow simulation of any connections, such as a roof disconnect sending outflow water to a swale which then sends surface output to a bioretention basin.

Finally, the water quality routines should be expanded to simulate the build-up and wash-off processes, and water quality treatment within green infrastructure, which are algorithms within the Storm Water Management Model. The build-up would allow for simulation of water quality constituents, i.e., pollutants, within precipitation, dry deposition, and groundwater, as well as removal due to processes such as street sweeping. The wash-off of pollutants would be set to transport the built-up loads to green infrastructure devices, and the model should simulate the percent reduction or mass removal of pollutants. The International Stormwater BMP (best management practices) databased provides some estimates of pollutant removal rates by various green infrastructure devices.

These updates to the models would require new coding and refactoring for this Unified Hydro model framework, to provide the flexibility for the users to connect the related hydrological and energy balances and processes and represent the urban systems we are trying to sustain.

Reza Abdi

reabdi@syr.edu | *650-350-8783* | *Syracuse, NY 13210*

HYDROLOGIST & WATER RESOURCES ENGINEER

Scholarship winner, organized, efficient, reliable, and passionate water engineer. Highly knowledgeable with 5+ years in urban watersheds, environmental flows, and complex environmental systems with professional experience in model development, data processing, and data visualization. Strong background in math, statistics, and experience in problem-solving and critical thinking. Involved with several USDA funded projects and highly interested to learn more about multidisciplinary fields in agriculture and food security.

CORE COMPETENCIES

- Water resources management
- Ecohydrology
- Physical processes
- Climate change

- C++ programming
- Data Visualization
- Python developing
- Machine learning

- Statistical Analysis
- R programming
- Algorithm Design
- Data Mining

EDUCATION

- *Ph.D., Water Resource Engineering* — *July. 2019*
  SUNY-ESF, Syracuse, NY
- *M.Sc., Water Resources Engineering* — *Dec. 2018*
  SUNY-ESF, Syracuse, NY
- *M.Sc., Hydraulic Structures* — *Sept. 2013*
  Islamic Azad University, Science and Research Branch, Tehran, Iran
- *B.S., Water Engineering* — *Jan. 2010*
  Urmia University, Urmia, Iran

RESEARCH INTERESTS

Water resources engineering, climate change, Hydrologic and eco-hydrologic modeling, Complex environmental systems

RESEARCH EXPERIANCE

SUNY ESF, Dept. of Environmental Resources Engineering (PhD), Syracuse, NY — 2015 – Present
Title of thesis: Development of Algorithms to Simulate Tree Effects on River Hydraulics and Thermal Loads.
Supervised by: Professor Ted Endreny.
- Developed numerical solver and routines of i-Tree Cool River tool (in C++), USDA Forest Services funded projects, for analyzing the tree effect on water quality collaborated with a multi-disciplinary team with more than 20 engineers and researchers.
- Developed the green infrastructure (GI) module of the i-Tree Hydro Modal for computing the performance of the GIs in reducing the urban storm sewer and water temperature.
- Combined the i-Tree Cool River, Air, and Hydro models to generate model based pre-processed input data for analyzing the urban areas impact on river thermal pollution.
- Developed a C++ function for Gaussian elimination linear interpolation for matrix operations.

SUNY ESF, Dept. of Environmental Resources Engineering (MS), Syracuse, NY — 2017 – 2018
Title of thesis: Simulating Impact of Urban Forests and Green Infrastructure on Thermal Pollution in Rivers.

Supervised by: Professor Ted Endreny.

- Developed new modules for the i-Tree Cool River Model to simulate river restoration scenarios in steady state.
- Coupled the i-Tree Cool River Model with the one-dimensional (1D) river analysis system model, HEC-RAS, to feed the model with pre-processed data form HEC-RAS for the adverse longitudinal slopes in finer resolutions.
- Implemented impact of applying pool and riffle system effect on thermal pollution in rivers.

   Islamic Azad University, Science and Research Branch (MS), Tehran, Iran

2010 – 2013

Title of thesis: Evaluation of Environmental Flows in Rivers Using Hydrological and Hydraulic Methods.

   Supervised by: Professor Mehdi Yasi

- Studied different eco-hydrologic and eco-hydraulic methods for estimating the environmental flows in the second largest perennial river of Iran.
- Compared the ecohydrological based estimated environmental flows with the proposed numbers of the environmental flows in the technical reports of three dams on the river.
- Wrote an R code for calculating 7-day, 2-year (7Q2) and 10-year (7Q10) for long-term hydrologic datasets of five weather stations in the case study (Zab River) watershed.

   Additional Research Achievement: Information School, Syracuse University, Syracuse, NY

2017 – 2018

- Performed net promoter score (NPS) analysis framework for hotels in R and evaluated key attributes affecting hotels net promote for the Applied Data Science course.
- Developed a blood bank management system using SQL/Access and created a user-friendly platform for the front-end user for the Data Administration Concepts & Database Management course.
- Developed model for predicting likelihood of permanent residency approval in United States for applicants holding H-1B visa in PySpark and got more than 95% accuracy in inquiries for the Advanced Information Analytics course.

TEACHING EXPERIENCE

- Led discussion sections, graded, explained, and held office hours for several courses as teaching assistant such as Fate and Transport of Contaminants in Environment, Mechanics of Materials, River Form and Processes, Senior Capstone Design, and Water, an Incredible Journey.   2015 – 2018
- Performed as structural analysis tutor for five undergrad students of Engineering Department in Urmia University which improved their grades by at least 25%.   2011 – 2012
- Taught the Arc-GIS basic and intermediate levels in Bagh – Bonyan Azerbaijan NGO privately.   2010 – 2014

WORK EXPERIENCE

Keyhan Abrah Asia Consulting Engineers Company, Tehran, Iran   2013 – 2015

   Engineer IV - V

- Developed a MATLAB code for estimating and evaluating environmental flows of Urmia Lake basin and eight major rivers in the watershed and authorized the hydraulic and hydrology reports of the project.
- Applied the environmental assessment tools, PHABSIM and GEFC for the Urmia Lake basin.
- Performed statistical analysis for long-term time series datasets of weather data in Urmia Lake basin in R platform and provided data visualizations for the reports.
- Designed drip and sprinkler irrigation systems as an Agricultural and Natural Resources Engineering Organization certified designer in Urmia Lake basin for more than 1000 hectares.

Sadrab Niroo Consulting Engineers Company, Urmia, Iran   2010 – 2012

   Engineer I - III

- Collaborated with a team of five engineers and data scientists to analyze wastewater distribution data using R and reduced data analysis annual cost by 20 %.

- Led a wastewater network designing project in water and wastewater company, Iran, in engineering division and performed communication with employer company and finished project nine months sooner than the scheduled time.
- Involved with several river restoration projects by designing and reporting the possible restoration alternatives in the rivers.
- Collaborated on two large projects for estimating the floodplain of the rivers for more than 900 km 2nd to 4th order rivers in North-West Iran using HEC-RAS and HEC-GeoRAS and spent more than 1 month for completing fieldwork.

Additional Professional Achievements, Urmia, Iran   2011 – 2014
- Led a volunteer team of engineers for designing water distribution systems for villages and got funding for five small-scale networks from donors in Bagh – Bonyan Azerbaijan NGO.

SKILLS

Technical Skills
Programming*: C++, R, MATLAB, SAS, Python, Spark, PySpark*
Software*: Arc-GIS, WMS, HEC-RAS, HEC-GeoRAS, HEC-HMS, SMADA, Auto CAD, Water CAD, Sewer CAD*
Modeling*: SWMM, DRM, GEFC, IHA, PHABSIM*

Languages: English (fluent), Persian (Native), Azerbaijani (Fluent), Turkish (Intermediate)

PUBLICATIONS

Book

- *Yasi, M.* **Abdi, R.** *(2018). "Evaluation of Environmental Requirement Assessment in Rivers", Urmia university publishing (in Persian – in review).*

Selected Articles

- **Abdi, R.,** *Endreny, T. (2018). "River temperature response modeling to unsteady stormwater inflows and riparian shading in an urban forest landscape", Water, 11*(5), 1060.
- **Abdi, R.,** Endreny, T., Nowak, D., Crispel, J. (2018). "A model to Integrate Analysis of Urban River Thermal Cooling and Flood Risk in River Restoration", *Journal of Environmental Management (in review).*
- **Abdi, R.,** Endreny, T., Ianniruberto, M., Filizola, N., Gualtieri, C. (2018). "A 3D analysis of hydraulic complexity about the confluence of Negro and Solimoes rivers, Brazil", *Ecohydrology (in review).*
- **Abdi, R.***, Yasi, M. (2015). "Evaluation of environmental flow requirements using eco-hydrologic and hydraulic methods in perennial rivers", Journal of Water Science & Technology. 72 (3) 354-363.*
- **Abdi, R.***, Yasi, M., Sedghi H. (2014). "Evaluation of environmental flows in perennial rivers with eco-hydrological methods (case study: Zab transboundary river)", Journal of water and soil science, University of Tabriz-Iran. 37 (366), 81-102 (in Persian).*
- **Abdi, R.***, Yasi, M., Sedghi H. (2013). "Evaluation of environmental flows in rivers with ecologichydraulic-hydrologic Methods", Journal of water and wastewater. 26 (296), 71-81 (in Persian).*
- **Abdi, R.***, Yasi, M., Sokooti, S.R., Mohammadi, E. (2013). "Environmental requirement assessment in Zarrinehrood river by hydrological methods", Journal of watershed engineering and management. 6 (3), 211-223 (in Persian).*

PRESENTATIONS

- **Abdi, R.,** Endreny, T. (2018). "Dynamic River Temperature Simulation of Urban Stormwater Inflows and Riparian Shading in an Urban Forest Landscape". *AGU Fall meeting, Washington DC, USA (Dec. 2018).*
- Endreny, T., **Abdi, R.,** Ianniruberto, M., Filizola, N., Gualtieri, C. (2018) "Is hydraulic complexity at a river confluence needing a 3D approach?" *AGU Fall meeting, Washington DC, USA (Dec. 2018).*

- **Abdi, R.,** Endreny, T. (2018). "Simulating riparian forest and green infrastructure impacts on river temperature quantifies benefits of urban greening in reducing thermal pollution". *World Forum Urban Forest (WFUF), Mantova, Italy (Nov. 2018).*
- Endreny, T., Gualtieri, C., **Abdi, R.** (2018) "Hydraulic complexity as a driver of biological niches and richness in Amazon River". *8th International Symposium on Environmental Hydraulics, University of Notre Dame, Indiana, USA.*
- **Abdi, R**., Endreny, T., (2017). *"Balancing energy budget in a river, for simulating heat pollution and benefits of shade from riparian vegetation". Spotlight 2017, SUNY-ESF, Syracuse, NY.*
- **Abdi, R**., Endreny, T. A., Bodnaruk, E. (2016). *"Sensitivity of urban air temperature predictions to heat Storage parameters of impervious, short vegetation, and tree land cover". Spotlight 2016, SUNY-ESF, Syracuse, NY.*

HONORS & AWARDS

- Ph.D. research assistantship full funding scholarship from SUNY Research Foundation (SUNY-RF) and USDA, SUNY-ESF (2018 - 2019, Summers 2016, 2017, 2018, and 2019).
- Awarded merit funding as a graduate teaching assistantship scholarship from the Department of Environmental Resource Engineering (ERE), SUNY-ESF (Fall 2015 to Spring 2018).
- Awarded "O'Brien & Gere scholarship" from (Fall 2018 and Spring 2016).
- Awarded "Graduate Fellow Award" scholarship (Fall 2016).
- Awarded "Dean's graduate scholarship", SUNY-ESF (Fall 2015 and Fall 2017).
- Ranked 31th in 2014 Iran nationwide entrance exam for water resource engineering Ph.D. program.

MEMBERSHIPS

- American Geophysical Union (AGU)	2016 – Present
- American Society of Civil Engineers (ASCE)	2015 – Present
- Iranian National Committee on Large Dams (IRCOLD)	2013 – Present
- Iranian Water Resources Association (IR-WRA)	2013 – Present
- Iranian National Committee on Irrigation & Drainage (IRNCID)	2013 – Present